Feras A. Alshehri

Ancillary services from Hydrogen Based Technologies to Support Power System Frequency Stability

TU Delft

Ancillary services from Hydrogen Based Technologies to Support Power System Frequency Stability

By

Feras A. Alshehri

in partial fulfilment of the requirements for the degree of

Master of Science
in Electrical Engineering

at the Delft University of Technology,
to be defended publicly on Wednesday September 5, 2018 at 10:00 AM.

Supervisor:	Dr. ir. J.L. Rueda Torres	
Thesis committee:	Prof. ir. M. van der Meijden	TU Delft
	Dr. ir. J.L. Rueda Torres	TU Delft
	Dr. A. Rodrigo Mor	TU Delft

TU Delft

Abstract

The share of renewable energy sources in the electricity generation is expected to maintain a steady growth in the future driven by economic and environmental reasons. However, these renewable sources such as wind and solar have fluctuating power output. This fluctuation causes strain on the power system and can cause imbalances between generation and load which may result in frequency instability. In the current liberalized energy market, the system operator uses ancillary services market to procure frequency containment reserve (FCR) which arrests undesirable frequency excursions within the first few seconds after the occurrence of an imbalance and ensures satisfactory primary frequency control. The system operator also procures frequency restoration reserve (FRR) which helps restore the frequency to its nominal value.

Electrolyzers can manage their demand of electrical energy for production of hydrogen (i.e. power-to-gas conversion) and it is possible to store that generated hydrogen for long periods which is an advantage compared to battery storage. This hydrogen can be used for several applications (e.g. transportation), and part of it can be used by fuel cells to provide electrical power back to the power system when needed. One of the technologies used in electrolyzers and fuel cells is the proton exchange membrane (PEM). Fuel cells and electrolyzers based on PEM technology are capable of rapidly changing the power set point to increase or decrease the power demand or supply, respectively.

This thesis studies the PEM electrolyzers and fuel cells and their ability to support the frequency stability through participation in the ancillary services market. Based on DIgSILENT PowerFactory software package, this thesis develops generic dynamic models for PEM fuel cell and electrolyzer for frequency stability studies and uses these models to assess their effectiveness in providing frequency support and participation in the FCR market. Numerical simulations are performed on two dynamic test systems: The North Netherlands 380 kV transmission and its extension to include a reduced size representation of the transmission systems covering the North-West Germany and South Denmark. Both dynamic test systems are developed in PowerFactory based on the detailed model of continental Europe built in PSS®E software package.

The developed model for the fuel cell shows close resemblance to the literature data for both dynamic and static performance especially in the linear operating range. The simulation results show that PEM devices can provide frequency support in the FCR market and results in improved frequency nadir and reduced oscillations during the post-disturbance period which is considerably better than what can be achieved by using the currently in operation primary frequency control of the conventional power plants with synchronous generators.

The numerical simulations also include sensitivity analysis to changing system operating conditions such as network size, location of PEM devices and system inertia. It is found that changing the location of the PEM devices or the size of the network does not affect the performance in supporting the frequency. Also, it is found that PEM devices provide significantly improved frequency response compared with synchronous generators at lower system inertia levels. Sensitivity analysis to changing control parameters for PEM devices such as the bid size and frequency droop showed that increasing the bid size or droop results in improved frequency response in the form of lower nadir.

Some confidential information within this thesis have been removed. To request the full version please contact Dr. Ir. Jose L. Rueda Torres

---

This work has received funding from the European Union's Connecting Europe Facility (CEF) programme under the grant agreement Nº INEA/CEF/SYN/A2016/1336043 – TSO2020 Project (Electric "Transmission and Storage Options" along TEN-E and TEN T corridors for 2020). This thesis reflects only the author's views and the European Commission is not responsible for any use that may be made of the information it contains.

Co-financed by the European Union
Connecting Europe Facility

Contents

List of Tables

List of Figures

1. Introduction

Renewable energy sources (RES) will continue to grow driven by the need for energy security against a volatile oil and gas market, their environmental benefits and reduction of CO_2 emissions, the need for increased access to energy for rural areas, and their cost competitiveness and affordability especially for fossil fuel importing countries[1]. In addition to these reasons, the Paris Agreement of 2015 within the United Nations Framework Convention on Climate Change (UNFCCC) requires significant reduction in greenhouse gases in order to limit the increase in global temperature [2]. This reduction will be mainly achieved through replacement of fossil-fuel based generation with RES.

The increase in RES on the other hand poses its own challenges and one of the main challenges is the increase in volatility of generation. The two fastest growing technologies are solar photovoltaic (PV) and wind energy. Both are characterized by variability and low availability and this rises the need for storage to balance daily and seasonal variations in generation. The most common methods to manage the fluctuations are reserve generation, demand side response and energy storage. With no technology proven to be effective for grid scale storage, researchers keep exploring the potential for several technologies such as batteries, pumped hydro, gas compression, and fly wheels. The research in use of hydrogen as storage

Also, the liberalization and the horizontal restructuring of the energy market forces The Transmission System Operator (TSO) to rely on the ancillary services market to help support the system specially to balance supply and demand and maintain frequency stability.

On the other hand, the use of hydrogen as an energy vector is growing and gaining more attention. Hydrogen is not considered a source of energy since it is not naturally available. Instead, it is considered as an energy carrier that must be generated, transported or stored and later converted into another form of energy [3]. in this hydrogen is similar to electricity and it has the potential to work as a parallel and complement to the electrical system.

Gas reforming is the most common method to generate hydrogen. It uses steam to partially oxidize hydrocarbons such as natural gas, petroleum, or coal and produce carbon dioxide and hydrogen gases [3]. The second method is water electrolysis which uses electrolyzers that use electrical energy to split water molecules into hydrogen and oxygen molecules. A more detailed description of electrolyzers will be presented in chapter 3. Other methods that are in research stage include splitting water direct thermal heat and by directs sunlight known also as photocatalysis [3]. The majority of hydrogen produced is used in the production of ammonia, the commonly used fertilizer. The second most common use of hydrogen is in refining followed by chemicals and metals processing while he use of hydrogen in energy is less than 1% [4].

The use of hydrogen as a carrier of energy is associated with the use of hydrogen fuel cells that have demonstrated reliable operation in specific application areas such as transportation, stationary power and portable power. In the transportation sector, Fuel cell powered buses and fuel cell electric vehicles (FCV) or fuel cell electric vehicles (FCEV) have demonstrated the maturity of the technology and its readiness to be implemented at a larger scale. However, the widespread of FCVs remains limited by the availability of hydrogen fuelling stations [5] which in turn require larger number of vehicles to spread further making the spread of both at a standstill unless significant investment is takin in fuelling station or a coordinated investment in both.[gangi]. Toyota for example is heavely investing in FCVs and have taken the unusual step of making around 5700 patents available without royalties in an effort to support further developments in fuel cell technologies [6]. In portable applications, fuel cells are used in Portable communication devices for military applications due to their light weight and smaller size compared to batteries [7]. In stationary applications, fuel cells are used as backup power for critical loads such as telecommunication infrastructure, utility networks and government facilities. Gives an advantage of high reliability, low maintenance and longer independent operation compared to battery or diesel backup [5].

Advantages of using h2 for energy storage. Hydrogen can be used efficiently in energy storage applications since it can be stored for prolonged periods, which means that hydrogen can be used as an energy storage to overcome both seasonal and daily variations in RES generation [7, 8]. Hydrogen transportation also is considered cheap and efficient and does not result in significant losses. Some research suggested that hydrogen can be transported using existing natural gas grid which means no new infrastructure is needed to transport it. Salt caverns also make a viable and cost-effective solution for long term storage of hydrogen as mentioned above [3].

1.1. Summary of current state-of-the-art and research gaps

Hydrogen is considered as an energy carrier as it does not exist in its pure form in nature. In that regard it is comparable to electricity as both have to be produced and both of them can be efficiently transported for long distances. In the case of hydrogen, it can be transported using pipelines with minimum losses [9]. Fuel cells which use hydrogen as fuel to generate electricity have successfully demonstrated their ability to be used in off-grid installations either as primary supply or as back-up with performance that is comparable to traditional set-ups [10, 11]. However, the use of hydrogen fuel cell generation remains limited to small installations and isolated demonstrations projects.

Electrolyzers represent the concept of power-to-gas conversion which means exploiting the synergy/interplay between consumption of electrical energy, predominantly produced by variable renewable energy based power plants, and the production of hydrogen. It was shown by [12] that the production of hydrogen through electrolysis can provide two advantages which are flexibility in hydrogen production based on price of the electricity and the demand side response to support the power system dynamic performance.

Power-to-gas and gas-to-power have the potential to manage excess/deficit power generation resulting from the variable nature of renewable power generation. It can also store energy to overcome RES daily and seasonal variations. Hydrogen or syngas generated by power-to-gas can carry energy to locations where the grid is inaccessible or inadequate and it can provide hydrogen feedstock to chemical industries[13].

There are few studies on the potential for electrolyzers or power-to-gas to support the network stability through demand side response. For example, [14] demonstrates through simulations that electrolyzers provide faster power injection compared to combined cycle gas turbines (CCGT) which translates into frequency oscillations of smaller magnitude and improved frequency nadir. However, there is not enough research on fuel cells and their potential to perform similar support of frequency stability in the power system. The study in [15] shows that there is potential for fuel cells to participate in frequency support in combination with wind turbines. However, the study focuses more on the optimal ratio of fuel cell to wind turbine capacity.

So far, there is lack of understanding of the impact of PEM fuel cells alone or in combination with PEM electrolyzers on the power system frequency stability and how they can participate in the current ancillary services market. It is important to address this topic now because as more renewable sources are added to the power system and more traditional synchronous generators are decommissioned, the need increases for alternative methods to maintain generation-load balance and support the system frequency stability.

To study the impact of PEM fuel cells on the power system frequency stability, an appropriate model is needed. The model must provide frequency control, emulate the dynamic behavior of the fuel cell, controls power output and appropriate for grid-connection. Unfortunately, such model is does exist in literature. Since PEM fuel cells and electrolyzers are still in early commercialization phase, most modeling efforts are geared towards small scale applications and are focused on identifying modeling parameters or increasing efficiency.

1.2. Research goal & Research Question

The main goal of this thesis is to study how beneficial power-to-gas and gas-to-power conversion can be to support the frequency stability of electrical power systems. Concretely, this thesis addresses the following research questions:

1. How can hydrogen PEM fuel cells and electrolyzers be represented in frequency stability studies?

There are numerous mathematical models for PEM fuel cells and electrolyzers in literature that reflect different study requirements. For this thesis, a generic model that reflects the necessary features (fast response, separate P & Q control) for the study of frequency stability is developed in PowerFactory based on widely accepted assumptions in existing literature.

2. How do hydrogen PEM fuel cells and electrolyzers perform when providing ancillary services for active power frequency support?

Using the proposed models, the capability of PEM fuel cells and electrolyzers in providing ancillary services is assessed. In particular, their performance is assessed in terms of active power control and primary frequency support. Several operational scenarios are simulated to evaluate the capability of PEM fuel cells and electrolyzers to meet the requirements of the power system.

3. How can changes in the transmission network and the control parameters affect the performance of PEM hydrogen technologies.

An assessment will address the sensitivity of PEM fuel cells and electrolyzers performance to changes in network layout, setup, inertia levels etc. Also, sensitivity to changes in the controls of the devices on the performance and the ability to support the frequency stability.

4. What are the technical and other challenges that limit the use of hydrogen based ancillary services for active power frequency support?

The simulations above will highlight any issues that limit the use of PEM fuel cells and electrolyzers in providing frequency support ancillary services. These issues will be analysed to achieve a deeper understanding of limitations of grid-connected hydrogen fuel cells and electrolyzers. Further, other factors that may limit the wide use of PEM hydrogen technologies to provide ancillary services to the system.

1.3. Research approach

This study starts with a literature review on modeling of PEM fuel cells and electrolyzers. The different approaches to dynamic modeling are reviewed and common modeling assumptions are identified. Also, a review of the methods of power control for grid connected renewable resources is done in order to create a generic model for the grid-connected fuel cell and electrolyzer. The generic model is developed in DIgSILENT PowerFactory by using standard components (e.g. static generator for the fuel cell) and DIgSILENT Simulation Language (DSL) to develop the frequency and power control for the models.

The test network model is based on reduced size model of the North Netherlands, North-West Germany and South Denmark 380-400 kV transmission network and is also built using DIgSILENT PowerFactory. The model is based on network layout and the dynamic data from the PSS®E model of the European Network of Transmission System Operators (ENTSO-E). The incomplete PSS®E model is first completed and all the substations and network components are properly identified, then a systematic translation of the model from

PSS®E to PowerFactory is done including the dynamic data of the network components (e.g. synchronous generators). Afterwards, the developed generic models for PEM fuel cell and electrolyzer are added to the network model.

The test grid is subjected to different disturbances in order to assess the effectiveness of PEM fuel cells and electrolyzers in supporting frequency stability. Then, sensitivity analysis is performed by changing the test network or its parameters and by changing the control parameters in the model for the PEM fuel cell and electrolyzers. The frequency response data are collected and analyzed to evaluate how sensitive the models are to these changes. The generic model for the fuel cell is modified to enable secondary frequency support and the model is tested for to assess its effectiveness in providing both the primary and secondary frequency support.

1.4. Outline

The brief outline of this thesis report is as follows:

1.4.1. Chapter 1: Introduction

This chapter provides the necessary background and introduction into the topic of hydrogen technologies and their potential for supporting the electrical system. The current state of literature is presented and the scientific gap is identified. Then the motivation, the research questions and the research approach are introduced.

1.4.2. Chapter 2: Frequency Stability & Ancillary Services

The concept of frequency stability is introduced. Then an overview of the ancillary services is presented with focus on active power frequency support services and their current regulation scheme.

1.4.3. Chapter 3: Hydrogen PEM Fuel Cell & Electrolyzer

The operating principles of hydrogen PEM fuel cell and PEM electrolyzer are introduced. Generic dynamic models are developed to represent these devices in frequency stability studies.

1.4.4. Chapter 4: Test Network Development

A part of the European interconnected gird is used for testing. The translation and reduction of the test transmission network will be discussed as well as the dynamic modeling of the synchronous generators connected to the network.

1.4.5. Chapter 5: Assessment of The Impact of Different Types of Disturbances

Different types of disturbances will be applied to the test system to assess the effectiveness of PEM technologies in providing primary frequency support as a participant in the FCR market.

1.4.6. Chapter 6: Sensitivity Analysis

Several changes will be applied to the test system and the control parameters of PEM devices in order to measure the sensitivity of PEM technologies to variations in the network conditions and the control parameters and how the frequency response will be affected.

1.4.7. Chapter 7: Potential for Frequency Restoration Reserve

The model for PEM fuel cell will be slightly change to allow for secondary frequency support as part of the FRR market. A disturbance will be applied to the system and the effectiveness of the PEM fuel cell in restoring the frequency will be assessed

1.4.8. Chapter 8: Limitations and Challenges for PEM Hydrogen Technologies

There are limitations that prevent the widespread use of PEM technologies and their use in the power ancillary services market. These limitations will be discussed and future outlook will be presented.

1.4.9. Chapter 9: Conclusions

The main conclusions of the research will be presented and future research work is suggested.

2. Frequency Stability and Ancillary Services

Ancillary services are defined as “Services that assist the network operator in maintaining system balance” [16] These include Frequency control, Voltage control, Spinning reserve, Standing reserve, Black start capability, Remote automatic generation control, Grid loss compensation, Emergency control actions [17]. The main focus of this thesis is on frequency control services which will be detailed in the following sections with focus on the Dutch market structure.

2.1. Power System Frequency Stability

Power system stability is defined as “ the ability of an electric power system, for a given initial operating condition, to regain a state of operating equilibrium after being subjected to a physical disturbance, with most system variables bounded so that practically the entire system remains intact” [18]. Power system stability can be categorized into three categories which are rotor angle stability, frequency stability and voltage stability. A summary of this classification is shown in Figure 2.1.

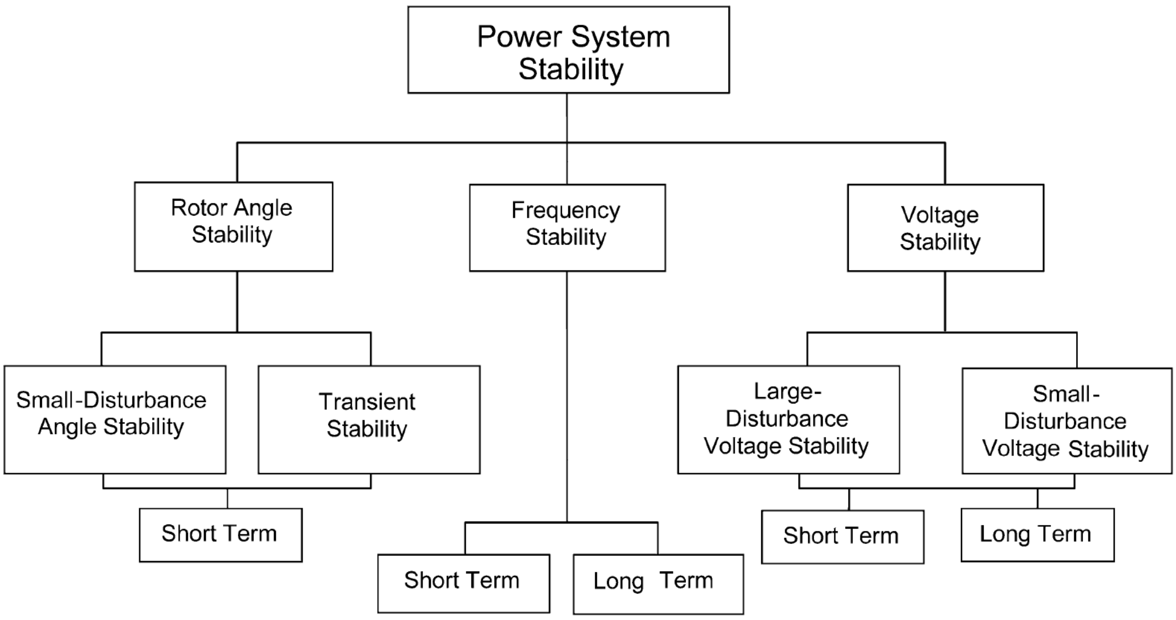

Figure 2.1. Classifications of power system stability[18]

More specifically, frequency stability is defined as ability of a power system to maintain steady frequency following a severe system upset resulting in a significant imbalance between generation and load [18]. The instability in such case will result in increasing frequency deviation or sustained frequency oscillations.

In the case of a severe disturbance that results in a sudden generation load imbalance frequency will start to deviate and the power system response to such deviation is defined into three classifications: inertial response, primary frequency response and secondary frequency response as shown in Figure 2.2. The details of these responses will be detailed in the following sections.

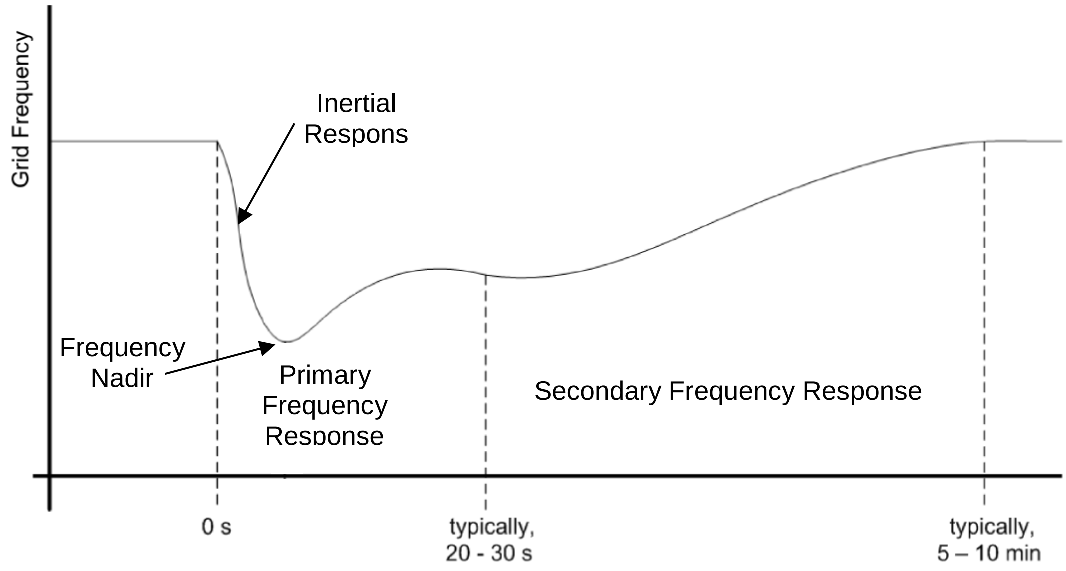

Figure 2.2. Classifications of frequency response[19]

2.2. Inertial Response

The basic definition of rotational inertia is the resistance of a rotating object to change in speed and direction of rotation. When applied to power system it means the resistance of the power system to sudden changes in frequency. The inertial response is typically present for the first 5-10 seconds after the disturbance and is dependent on the amount of rotating mass within the system which are traditionally present in the synchronous generators and rotating loads. The inertia of the power system contains the sudden power imbalance and causes the frequency deviation to be gradual. In the future, synchronous generators will decrease in numbers and will be replaced with more devices that are interfaced through power electronics. This will mean that the inertia in the system will decrease and the frequency deviation will become more sudden and the damping of oscillations will be smaller. A measure for this initial deviation is called Rate of Change of Frequency (RoCoF) and is defined as the frequency deviation within the first 500 ms. The lower the inertia in the system, the higher the RoCoF and the more sudden the change in frequency will be. Frequency nadir is another important value in the evaluation of the frequency response and it is defined as the maximum value of frequency deviation it is dependent on both the inertial response and the primary frequency response.

2.3. Primary Frequency Response and Frequency Containment Reserve (FCR)

Primary frequency control are actions to arrest and stabilize frequency following a disturbance and it functions in the first 30 seconds, overlapping with the inertial response, to automatically stabilize the frequency in the entire connected synchronous area after a disruption.

The conventional method for providing the frequency containment is automatically performed through the Governor droop control for synchronous generators. The droop characteristic is described by equation (2.1) [20].

$$\Delta P = \frac{f - f_0}{R} \tag{2.1}$$

Where ΔP is the change in generator power in MW, f is the measured frequency in Hz, f_0 is the reference frequency in Hz, and R is the droop in Hz/MW.

In the current Dutch power system, the primary frequency is manged through Frequency Containment Reserve (FCR) Market. The support is not only limited to synchronous generators but can be provided by any technically prequalified generator or load, known as supplier, after signing the framework agreement and gaining access to the auction platform. The TSO identifies the required reserve capacity based on the total generation capacity in the managed area. Suppliers submit their bids and the lowest bids are chosen until the required reserve capacity is achieved. The technical requirements of bids are the following [21]:

- Bid must be symmetrical for both upward and downward support.
- Minimum bid size is 1 MW.
- Full activation frequency deviation of ±200 mHz.
- Auctions is done weekly and the bids are for a duration of one week.
- The activation of the full bid must be within 30 seconds.
- Sources with limited energy such as batteries, must continuously supply the full bid for at least 30 minutes.

The relation between the generation reserve bid and the droop described by equation (2.2) [21]

$$\frac{P_{bid}}{P_{nom}} = \frac{100}{x}\frac{|f - f_0|}{f_0} \tag{2.2}$$

Where P_{bid} is the bid value in MW, P_{nom} is the nominal power in MW, f is the measured frequency in Hz, f_0 is the reference frequency in Hz, and x is the droop in %. While the actual power generated due to disturbance is defined by equation (2.3)

$$\Delta P = P_{bid}\frac{|f - f_0|}{\Delta f_{max}} \tag{2.3}$$

Where ΔP is the change in generator power in MW, P_{bid} is the bid value in MW, f is the measured frequency in Hz, f_0 is the reference frequency in Hz, and Δf_{max} is the full activation frequency deviation. The change in power output of the supplier or ΔP is a linear function of the deviation of frequency however, here ΔP is limited to a maximum value of P_{bid} and does not increase further even if the frequency deviation is beyond the full activation frequency deviation as shown in Figure 2.3. A Typical power output of an FCR supplier due to a step increase in loads that causes frequency deviation and automatic bid activation is shown in Figure 2.4.

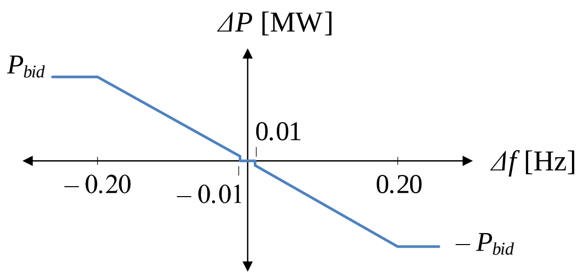

Figure 2.3. Droop control for FCR supplier

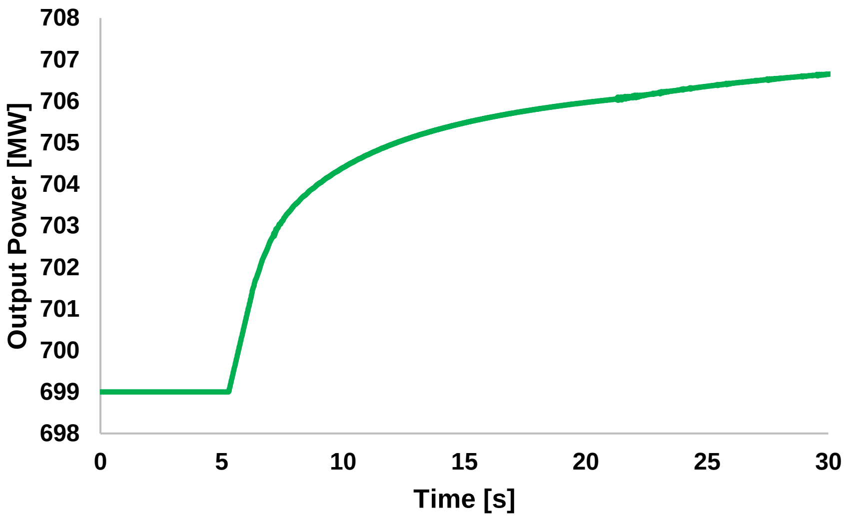

Figure 2.4. Typical FCR supplier power output due to automatic bid activation

The ability of the hydrogen PEM fuel cells and electrolyzers in providing primary frequency support and participation in the FCR market is the main focus of this research thesis.

2.4. Secondary Frequency Response and Automatic Frequency Restoration Reserve (aFRR)

The secondary frequency response usually takes up to several minutes and it functions through changing the power set point for the generators mainly to restore the frequency to the nominal value, release primary frequency reserves and reduce the area control error and provide the prearranged interchange with neighbouring areas[22]. In the current Dutch power system this function is managed through Automatic Frequency Restoration Reserve (aFRR). Suppliers submit their bids and the bids will be selected in a ladder starting with lowest cost based on the active power imbalance. The main requirements for aFRR bids are [22]:

- Bid must be controllable by the TSO.
- Minimum bid size of 1 MW.
- Bids can be activated partially or in full.
- Observable power change within 30 seconds of bid activation.
- Ramp rate must be at least 7% per minute.

A Typical power output of an aFRR supplier due to a bid activation signal by the TSO is shown in Figure 2.5.

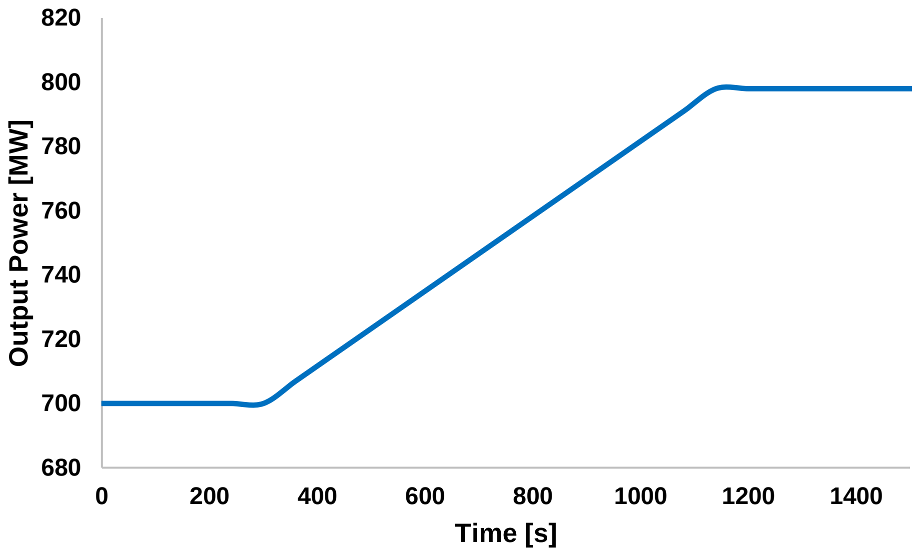

Figure 2.5. Typical aFRR supplier power output due to bid activation signal

This research thesis will address at a basic level the ability of PEM fuel cells and electrolyzers to provide secondary frequency support and participate in the aFRR market.

The other type of frequency restoration is Manual Frequency Restoration Reserve (mFRR) which is also known as tertiary frequency control. In the current Dutch market, mFRR bids are usually used for large or long-lasting imbalance. Here the change in set point is done manually by the TSO to the full bid value and the activation is usually after 15 minutes[22]. This type of frequency support is not of concern to this research thesis due to the high capacity and slow response requirements from participants.

2.5. Future changes in power system and ancillary services market

In the future the inertia of the power system is expected to decrease gradually due to the decrease of synchronous generators which operate mainly on fossil fuel or nuclear energy. These generators will be replaced with renewable energy sources that will mainly be interfaced with the grid through power electronic converters that do not provide inertial support to the system.

Another aspect that will change in the future power system is the change in regulations and procurement process of the FCR market. Some of these changes will be in the near future and include increasing the auction frequency to be daily instead of weekly and reducing the bid duration to be 4 hours time slots instead of full week [23]. Also, in order to produce better price signals, the settlement rule will be changed from as-bid to marginal pricing which means that every unit is paid the same price as the highest accepted overall offer which is expected to result 8% price increase [24].These changes will result in more flexibility in the bidding process and procurement of the FCR service and are expected to reduce the cost of procurement in the FCR market. Other possible changes further in the future may include allowing asymmetric bids and changing the minimum bid size from 1 MW. The effect of these changes on the participation of PEM technologies in the FCR market will be discussed in detail in Chapter 8.

3. Hydrogen PEM Technologies

The conversion of energy between electricity and hydrogen is done through fuel cells and electrolyzers. Electrolyzers convert electricity to hydrogen and fuel cells convert hydrogen to electricity. There are several technologies that enable this electro-chemical conversion and one of the most promising technologies is the Proton Exchange Membrane (PEM) which is used in both fuel cells and electrolyzers. In this chapter the working principle of these devices will be explained and accurate models will be developed in order to properly represent these devices in frequency stability studies.

3.1. The Fuel Cell

3.1.1. Working principle

Fuel cells are static energy conversion devices that extract the chemical energy of fuels through electrochemical process into electrical and thermal energy. The fuel cell’s basic structure composes of a porous anode and a porous cathode with an electrolyte layer separating them and a very thin layer of catalyst between the electrolyte and the electrodes. The fuel, usually hydrogen, is fed to the anode and the oxygen, or air, is fed to the cathode. Energy is extracted from the fuel cell through connecting an external circuit between the anode and the cathode [25]. Figure 3.1 shows a schematic of the fuel cell.

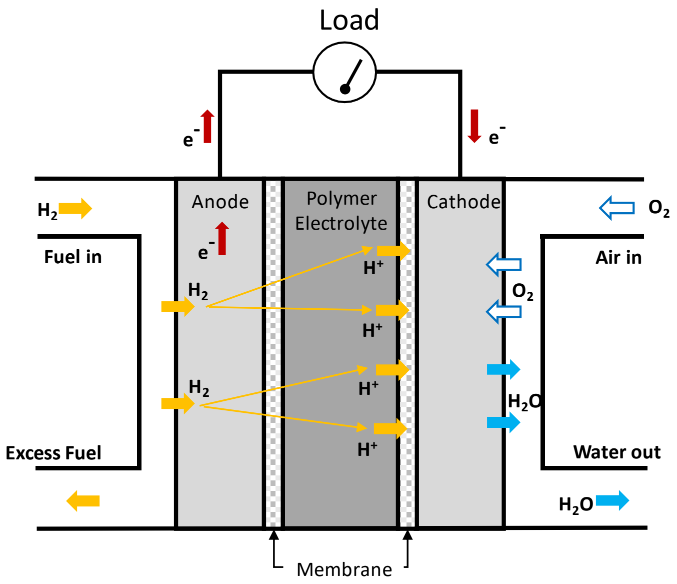

Figure 3.1. Typical section of fuel cell

The working principle for all fuel cells is based on supplying the porous electrodes with fuel and air. The hydrogen is supplied to the anode and the oxygen is supplied to the cathode. The hydrogen flow is absorbed into a platinum catalyst layer at that separates the anode and the electrolyser. The hydrogen molecule separates into individual atoms and then into a free electron and a proton that passes through the membrane as show in equation (3.1) [26].

Anode reaction:

$$2H_2 = 4H^+ + 4e^- \tag{3.1}$$

On the other side the membrane, the oxygen molecule separates into individual atoms and each combine with two electrons coming from the external circuit to form a negative oxygen ion as shown in equation (3.2)

Cathode reaction:

$$O_2 + 4e^- = 2O^{2-} \tag{3.2}$$

These ions combines with two protons that passed through the membrane to form water molecules as shown in equation (3.3) [26].

Cathode reaction:

$$2O^{2-} + 4H^+ = 2H_2O \tag{3.3}$$

The summarized equation of the fuel cell is

$$2H_2 + O_2 = 2H_2O + \text{energy} \tag{3.4}$$

3.1.2. Fuel Cell Types

Fuel cells are usually categorized by the type of electrolyte used. The most common types of fuel cells are polymer electrolyte fuel cell (PEFC) commonly known as Proton Exchange Membrane fuel cell (PEMFC), alkaline fuel cell (AFC), phosphoric acid fuel cell (PAFC), molten carbonate fuel cell (MCFC), and solid oxide fuel cell (SOFC).

Proton Exchange Membrane (PEM) Fuel Cells

Known also as Polymer Electrolyte fuel cell (PEFC) features a solid membrane such as fluorinated sulfonic acid polymer. The electrodes are made of carbon and platinum is used as a catalyst in the electrodes. The fuel cell works on pure hydrogen and considered to be low temperature where the temperature is usually less than 100 °C. It is also considered to have high current density, rapid-start up and fast response. However, it is very sensitive to contaminants in hydrogen[27].

Alkaline Fuel Cells (AFC)

This type of fuel cell uses a concentrated alkaline electrolyte solution instead of an acid. The higher reactivity of the alkaline allows the separation of oxygen molecules without the need for precious metals such as platinum. Instead, a variety of material can be used as catalysts in the electrodes including nickel however these metals are susceptible to oxidation at the air electrode as well as poisoning by CO and CO_2 in the air. The alkaline fuel cell can be operated at higher temperatures than up to 200°C.[27, 28]

Phosphoric Acid Fuel Cells (PAFC)

This type of fuel cell uses a concentrated phosphoric acid as an electrolyte. It operates between 150-220°C and is less vulnerable to poisoning by CO compared to PEMFC and AFC. PAFC fuel cells are used for stationary applications in combination with a natural gas reformer that converts natural gas to hydrogen.

These fuel cells require platinum catalyst and special construction material due to the corrosivity of the phosphoric acid.[27, 29]

Molten Carbonate Fuel Cells (MCFC)

This fuel cell uses an electrolyte of alkali carbonates that form highly conductive molten salt at the operating temperatures of 600-700°C. It uses nickel and nickel oxide for electrodes instead of noble metals. It used mainly in large stationary and marine applications and has a slow start up time. However, this type of fuel cell requires CO_2 recycling to form the carbonate ions and the high temperatures require special material impacts the mechanical stability as well as stack life.[27, 30]

Solid Oxide Fuel Cells (SOFC)

Solid oxide fuel cells operate at very high temperatures 600-1000°C and have a solid electrolyte that conducts oxygen ions which is the opposite mechanism of other types of fuel cells that conduct hydrogen ions through the electrolyte. The solid electrolyte makes these fuel cells very rugged and enable them to have longer life times. SOFC is used for stationary and mobile power applications. However, the high operating temperature creates issues related to material selection and the mismatch between thermal expansion of the material. [27, 31]

The fuel cell type used for this thesis project is the Proton Exchange Membrane (PEM) fuel cell due to its popularity in the research development especially in new fields such as stationary and mobile applications as well as its demonstrated use in Fuel Cell Electric Vehicles (FCEV). From a technical standpoint PEM fuel cells are suitable for frequency support applications due to its fast start up time, fast response and its high current density.

3.1.3. Fuel Cell Model

In literature, several approaches have been adopted to develop the model and characterization of the steady state and dynamic behaviour of PEM fuel cells. For example, models based on electrochemical equations [32-35], provide valuable insight into the reactions that happen within the stack, yet they are very complex and require the knowledge of technical parameters that are not publicly available. On the other hand, models based on mathematical approximations, semi-empirical or empirical data and model fitting [36-41], are generally simpler, but they represent specific commercial fuel cells, and thus may not be generalized to all existing units.

For this thesis, a complete depiction of a PEM fuel cell is developed, which covers the dynamics of the stack, the power conditioning system (i.e. DC-AC inverter) and the balance of plant. The presented model is built upon previous research [42], that estimates physical parameters through experimentation and empirical data collection from the 1.2 kW Nexa PEM fuel cell, a frequently studied unit in this field. An advantage of using the Nexa model is the inclusion of an air compressor, a cooling fan and fully automated control [43], making it possible to incorporate the description of the balance of plant within the stack model.

The modelling of the fuel cell relates the fuel cell stack voltage to the current drawn and it can be divided into two types: static model that relates current and voltage at each operating point and a dynamic model that represents electrochemical and thermodynamics of the fuel cell. The voltage of the fuel cell stack is dependent on the drawn current and the stack temperature. While the current is determined by the load, the temperature can be defined through a thermodynamic model. The following assumptions are made for developing the model of the PEM fuel cell:

1. Supplied hydrogen and air are ideal and uniformly distributed gases. They are supplied at a constant pressure to the fuel cell’s gas flow channels.

2. Constant ambient temperature of 25°C.

3. Thermodynamic properties are evaluated at the average stack temperature, temperature variations across the stack are neglected, and the overall specific heat capacity of the stack is assumed to be a constant.

4. Parameters for individual cells can be lumped together to represent a fuel-cell stack and the individual fuel-cell stacks can be lumped together to represent the fuel-cell array.

5. The hydrogen storage capacity is sufficiently large to supply hydrogen to the fuel cells and absorb any hydrogen produced by the electrolyzers.

3.1.3.1. Thermodynamic model

The stack temperature is determined by the heat generation rate $\dot{\boldsymbol{Q}}$ and heat dissipation rate towards ambient temperature. As shown in the following equation

$$mc_p \frac{dT}{dt} = \dot{Q} - H_t(T - T_\infty) \tag{3.5}$$

Where mc_p is the thermal capacitance ($\mathrm{J/°C}$) and H_t is the heat transfer coefficient ($\mathrm{W/°C}$). The equation shows that the stack temperature increases with heat generation rate and decrease with heat dissipation. Further, the heat generation within the fuel cell is defined by

$$\dot{Q} = (E_h - V)I \tag{3.6}$$

Where E_h ,defined by equation (3.7), is an imaginary potential (V) obtained by converting all the enthalpy of water into electricity.

$$E_h = \frac{\Delta h^{\mathrm{o}}_{\mathrm{f,H_2O}}}{2F} \times 47 \tag{3.7}$$

Here $\Delta h^{\mathrm{o}}_{\mathrm{f,H_2O}}$ = -285.83 $\mathrm{kJ/mol}$ at 25 ℃ and it is he formation of enthalpy of water vapor at 25 ℃. F is Faraday number 96,654 $\mathrm{C/mol}$. Here it is assumed that these values will remain constant and $E_h = 69.654\ \mathrm{V}$. In order to simplify equation (3.5), the current is assumed to be steady for a long enough time that the temperature does not change and $\frac{dT}{dt}$ becomes zero and the simplified equation becomes

$$H_t = \frac{(E_h - V)I}{T - T_\infty} \tag{3.8}$$

The dynamic model for temperature change can be represented by the following equation

$$T(t) = T_2 + (T_1 - T_2) \times \exp\left(-\frac{\mathrm{H_t}}{mc_p} t\right) \tag{3.9}$$

Here T_1 is the initial temperature and T_2 is the final steady state asymptotic temperature.

3.1.3.2. Dynamic Model

The Dynamic model developed in [42] will be used to model the transient and static response of the PEM fuel cell. The advantage of using this model is that it is less computationally extensive compared with the previously mentioned models. Also, the parameters of the fuel cell are estimated using empirical data which results in a very close fit to the experimental measurements.

The fuel cell output voltage as a function of current is empirically defined by the following equation[44]

$$V = E_0 - IR - A\ln\left(\frac{I}{I_{ex}}\right) \tag{3.10}$$

Where $\boldsymbol{E_0}$ here is the Nernst potential, $\boldsymbol{R}$ is the resistance in ohms, $\boldsymbol{A}$ is the Tafel Slope in Volts and $\boldsymbol{I_{ex}}$ is the exchange current which is considered a constant.

The Nernst potential and it is calculated by the equation[45]

$$E_0 = 47 \times \left[1.482 - 0.000845T_K + 0.0000431T_K \ln\left(p_{\mathrm{H}_2} p_{\mathrm{O}_2}^{0.5}\right)\right] \tag{3.11}$$

Where T_K is the stack temperature in Kelvin and $p_{\mathrm{H}_2}, p_{\mathrm{O}_2}$ are the hydrogen and oxygen pressures in atm, respectively. Multiplication by 47 is to account for the 47 individual cells within the stack.

The other parameters are estimated using empirical data fitting. The resistance is dependent on the temperature and is defined as

$$R(T) = R_0 \times \exp\left(\frac{E_{a,R}}{R_g T_K}\right) \tag{3.12}$$

Where R_0 (Ω) is the pre-exponential factor and $E_{a,R}$ $(\mathrm{J/mol})$ is the activation energy.

The Tafel slope is also dependent on temperature and is defined as

$$A(T) = A_0 \times \exp\left(\frac{E_{a,A}}{R_g T_K}\right) \tag{3.13}$$

Where A_0 (V) is the pre-exponential factor and $E_{a,A}$ $(\mathrm{J/mol})$ is the activation energy.

With these equations the dynamic model of the fuel cell stack voltage is defined. The output power from the fuel cell is simply the multiplication of the output current and the stack voltage. Table 3.1 below gives the parameters for the fuel cell dynamic model equations.

Table 3.1. Parameters for fuel cell dynamic model equations

Parameter	Value	Equation
mc_p	$4304\ \mathrm{J/^\circ C}$	3.9
$\mathrm{H_t}$	$15.07 \times I^{0.2358}\ \mathrm{W/^\circ C}$	3.9
I_{ex}	$1 \times 10^{-6}\mathrm{A}$	3.10
R_0	$0.1537\ \Omega$	3.12
$E_{a,R}$	$1800\ \mathrm{J/mol}$	3.12
A_0	$0.1591\ \mathrm{V}$	3.13
$E_{a,A}$	$5344\ \mathrm{J/mol}$	3.13

3.1.4. Model implementation in PowerFactory

The fuel cell is represented in power factory as an externally controlled current source static generator. In PowerFactory, the static generator is used to represent any type of non-rotating generator that is connected to the grid via a converter. In this model the static generator's output power is controlled via the input currents in the synchronous domain I_d and I_q, hence it is considered as a current source [46]. The control of the static generator is developed using DIgSILENT Simulation Language (DSL) which can be programmed using visual structures such as frames and blocks [46]. The basic block diagram for the fuel cell model is shown in Figure 3.2.

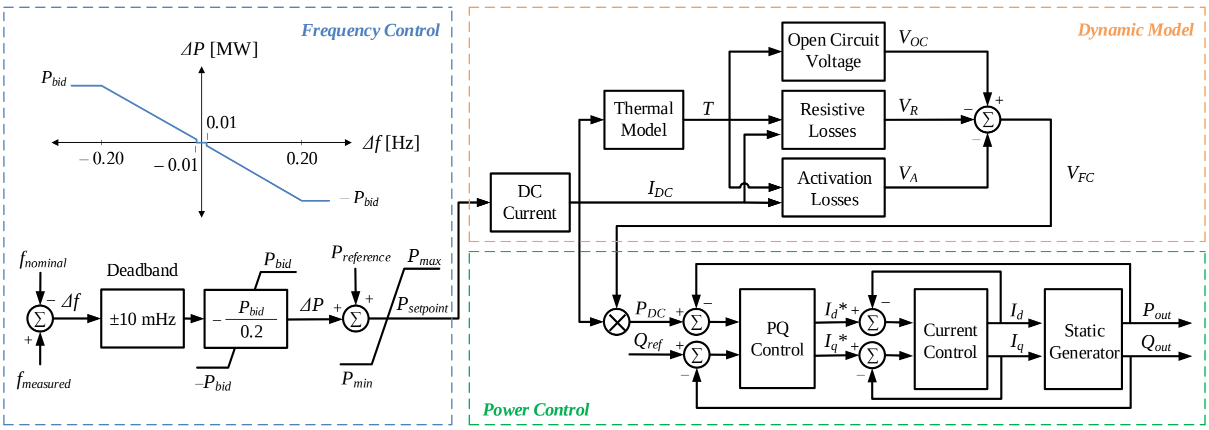

Figure 3.2. Dynamic model, control block diagram and droop characteristic of the modelled PEM fuel cell.

The PowerFactory model can be divided into three components: frequency control, fuel cell dynamic model and power control. The following sections provide a detailed description of each of these parts.

3.1.4.1. Frequency control

The frequency control diagram in Figure 3.2 and the PowerFactory block diagram in Figure 3.3 show the details of the frequency control.

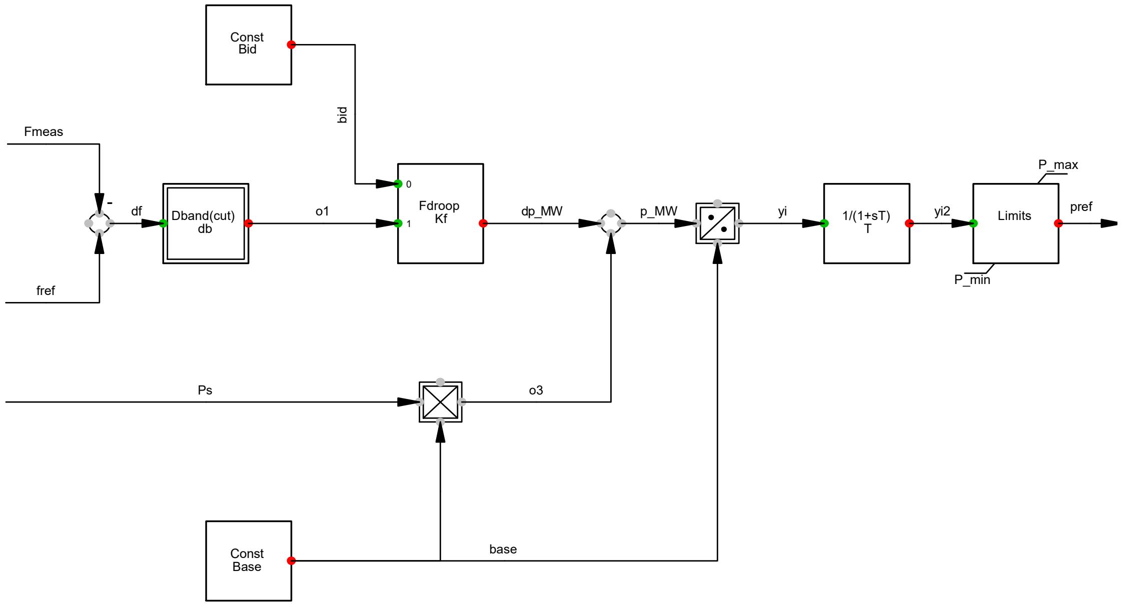

Figure 3.3. Fuel cell frequency control block diagram

First, the frequency deviation is measured. Then a dead band of 10 mHz is applied to the frequency deviation in order to avoid action on low magnitude noise signals. Then the signal is run through a droop control block which is defined by the following equation

$$\Delta P = -P_{bid} \frac{(f - f_{nominal})}{\text{Full Bid Frequency Deviation}} \tag{3.14}$$

P_{bid} is the bid value as decided by the FCR market, f is the measured frequency in Hz, $f_{nominal}$ is the reference frequency in Hz and Full Bid Frequency Deviation is decided by the system operator, e.g.200 mHz for the Dutch system, and is the frequency at which the generator shall supply the full bid value. The power output of this block (ΔP) is limited by the value of the bid (P_{bid}) and does not exceed it even if the frequency deviation goes beyond the full bid frequency deviation. The power reference is then added in order to give the power set point for the fuel cell. Limits are applied to the power set point in order to ensure the fuel cell plant operates within the allowable limits which are 20%-100% for the fuel cell plant rated power.

3.1.4.2. Fuel cell dynamic model

The dynamic model of the fuel cell is primarily a translation of the dynamic model described in section 3.1.3.2 into DSL. Figure 3.4 shows the block diagram for the PowerFactory dynamic model.

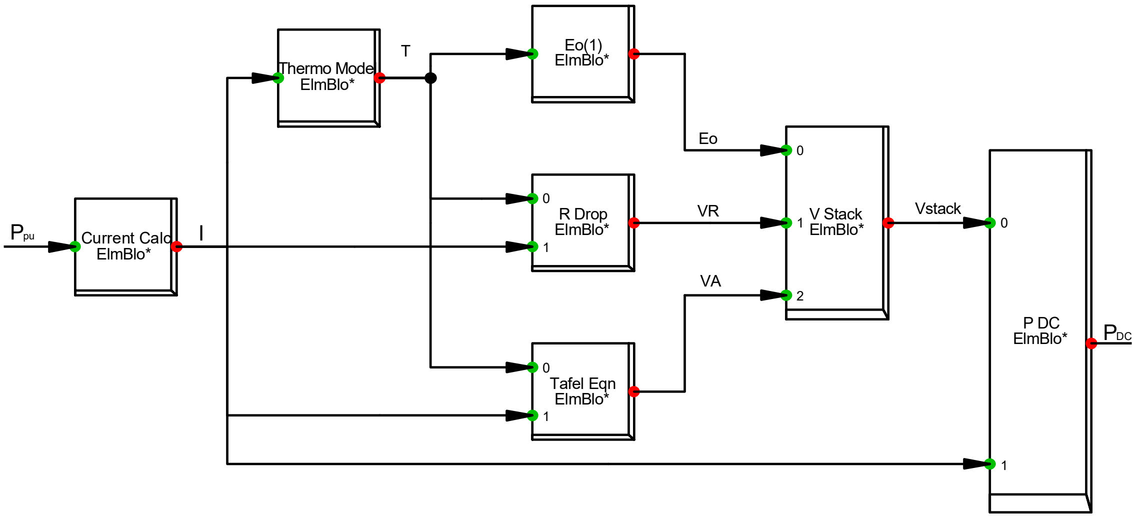

Figure 3.4. Block diagram for fuel cell dynamic model

The first block "Current Calc" translates the incoming power set point from the frequency control first from per units to watts by multiplying by the rated power of the Nexa Fuel cell. Then current drawn, DC current in Amperes, is calculated using empirical data from [43] which is implemented as a look-up table.

The current is fed into the next block "Thermo Model" which represents the thermal model from equation (3.9). In the equation, the initial and final asymptotic temperatures are calculated using empirical data from [42] which is implemented as a look-up table. The fuel cell's first response to change in current is almost instantaneous but suffers from overshoot or undershoot of voltage. This exponential function in this block is the main driver for that and it also controls the settling of the stack voltage.

The current and temperature signals are then fed into the next three parallel blocks "Eo(1)" which represent the Open circuit voltage from equation (3.11), "R Drop" which represents the resistive losses from equation (3.12) and "Tafel Eqn" which represents the activation losses from equation (3.13). The outputs of these blocks are added in the block "V Stack" to give the instantaneous stack voltage. Then, the stack voltage is multiplied by the current in block "P DC" to give the DC power output in watts then it is divided by the fuel cell rated power to give the power reference for the power control in per units.

Since the there is a slight deviation between the model of the fuel cell and the actual output of the studied fuel cell stack, the output of the dynamic model gives output power slightly less than the power measured by experimental results. In order to correct that, a new look up table is developed to relate the current drawn to the power output in order to establish a new relationship between the drawn current and the output power. This change does not affect the other parts of the model since the dynamic model input and output are in per unit power.

3.1.4.3. Power Control

From the system point of view, the fuel cell is modelled as a current source static generator controlled by external current signals. The power control part is consistent of two loops; an outer power control loop and an inner current control loop that sets the static generator current signals.

The power control block shown in Figure 3.5 controls both active power P and reactive power Q. For active power control, the model compares the actual power output of the static generator to the reference power signal coming from the dynamic model. The power deviation is filtered for noise signals through a dead band block then fed to a Proportional and Integral (PI) controller. Then a reference signal is added to the output signal from the PI controller which gives the set setpoint for the value of Id for the current loop. An identical control mechanism is applied for Q control except that Q reference is constant in order for the static generator to supply constant reactive power.

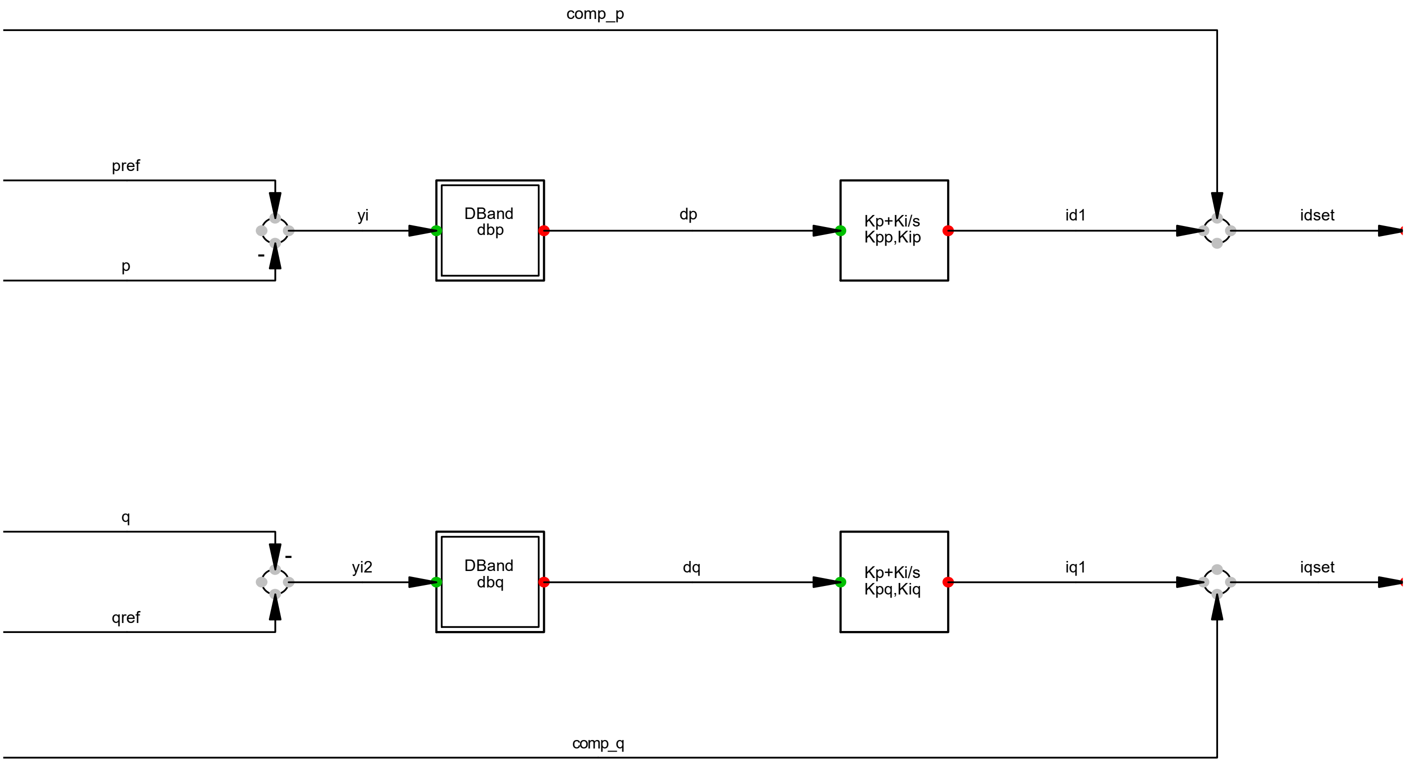

Figure 3.5. Fuel cell power control loop

The second part of the power control is the current control loop which takes Id and Iq current reference points from the P and Q control block and sets the I_d and I_q for the static generator. Figure 3.6 shows the current control block. For I_d control, first the actual Id value is compared to the Id value reference from the power control block and the difference is run through a dead band to eliminate low level noise. The filtered signal is then run through a load-lag filter and then to PI controller. A reference compensating signal is added then a limit is applied which is between 0.2 and 1.0 per unit. Finally, a first order delay is applied to represent the delay in the power control unit. The output is then fed into the static generator as the I_d reference. The control for I_q is done in a similar method with the exception of the dead band as there is no issue with low level noise.

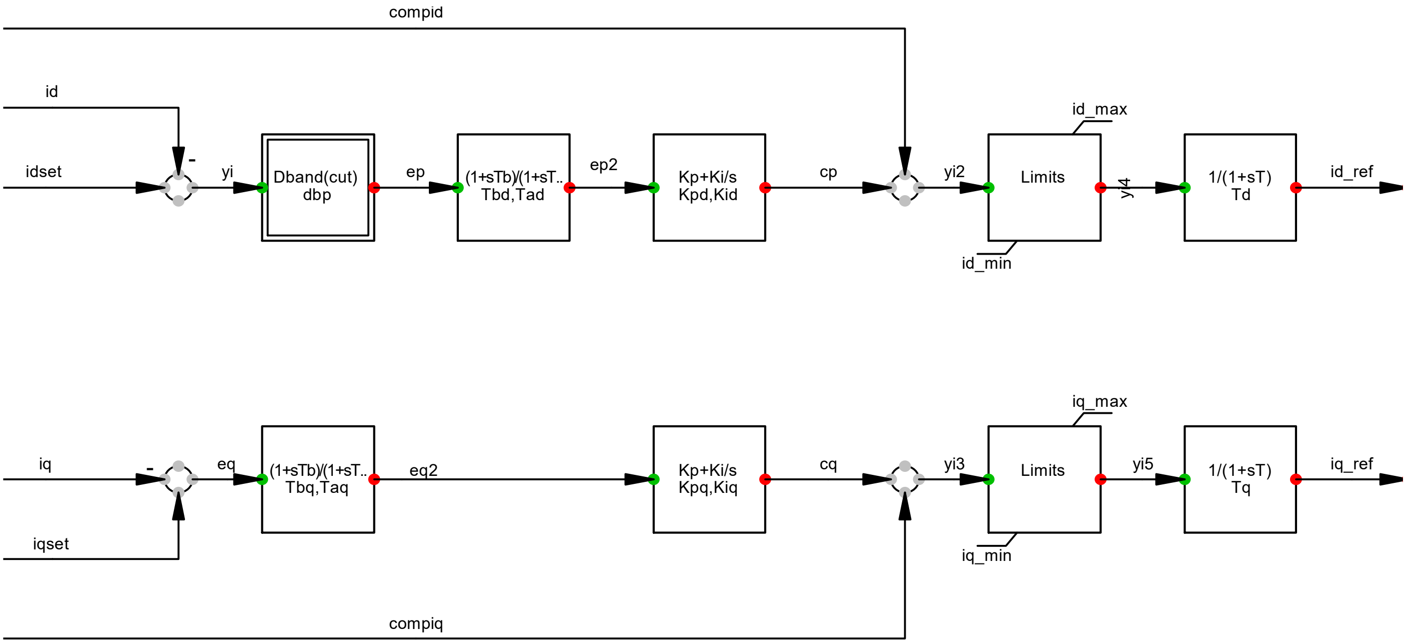

Figure 3.6. Fuel cell current control loop

The control parameters for the fuel cell model are listed in Appendix I.

3.1.5. Model Validation

In order to verify the model developed in PowerFactory, it is compared to other models and experimental data in literature. First, the static output of the model is tested by calculating, using MATLAB, the fuel cell stack voltage for each steady state value of current over the complete range of the Nexa fuel cell (0-45 A) using the equations (3.9-3.13) and comparing it with literature data. Figure 3.7 compares the static output of the model equations with the experimental data from [40]. The data shows close resemblance for static operation. There is some offset for low values of current however since the fuel cell will be operated at minimum 20% this offset is not of concern as long as the model shows resemblance of linear behaviour at higher current values. This shows that the PowerFactory model can represent the steady state operation of the PEM fuel cell.

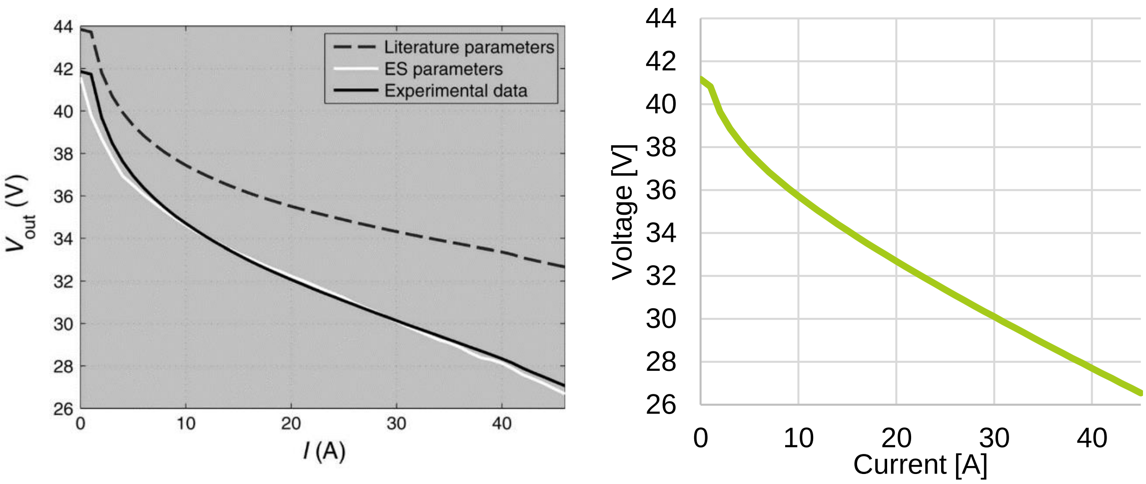

(a) Literature Data [40]   (b) Model Data from MATLAB

Figure 3.7. Static Model Validation

In order to validate the PowerFactory dynamic model, the performance of the model is compared to dynamic data from the literature. The drawn current from the fuel cell will be changed in several steps over time and the stack voltage will be measured. Figure 3.8 shows the current profile and the compares the dynamic output of the PowerFactory dynamic model with the experimental data from [39]. As shown in the figure, the data from the model is almost identical to the data from literature. The exception is that at low current levels, the voltage is less than the experimental data. This issue could be due to some approximations taken in the model equations. However, this issue does not affect the reliability of the dynamic model because the fuel cell does not operate at that power level which is outside the fuel cell operating range of 20-100%.

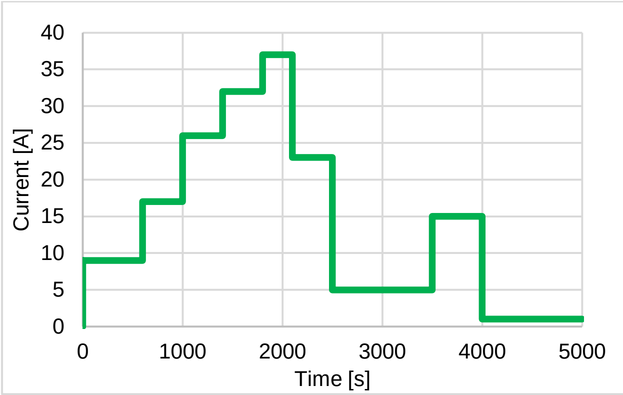

(a) Current Profile [39]

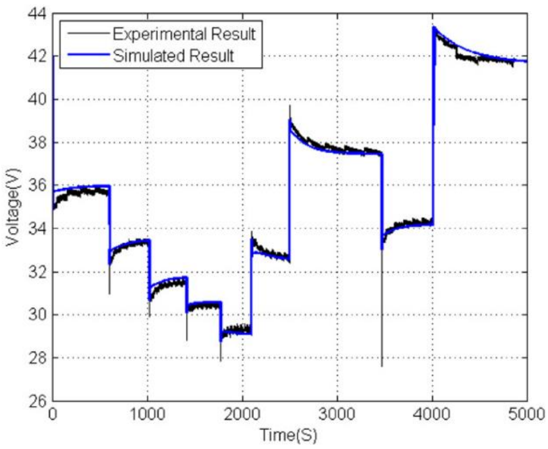

(b) Literature Data [39]

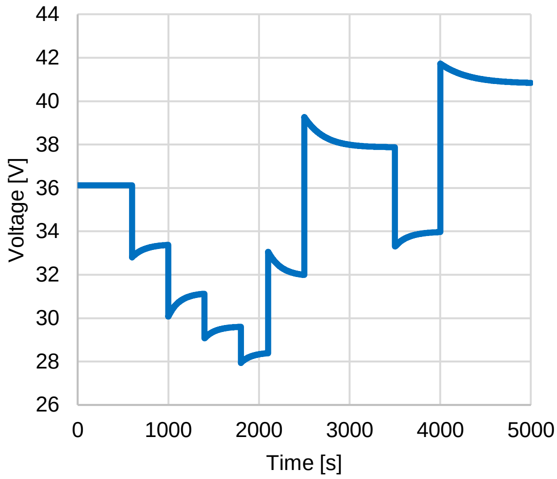

(c) Model Data from PowerFactory

Figure 3.8. Dynamic Model Validation

3.2. The Electrolyzer

The electrolyzer is a device that is capable of electrolysis which is the electrochemical decomposition of water to produce hydrogen and oxygen gases. The basic structure of the electrolyzer is similar to the fuel cell as shown in Figure 3.9.

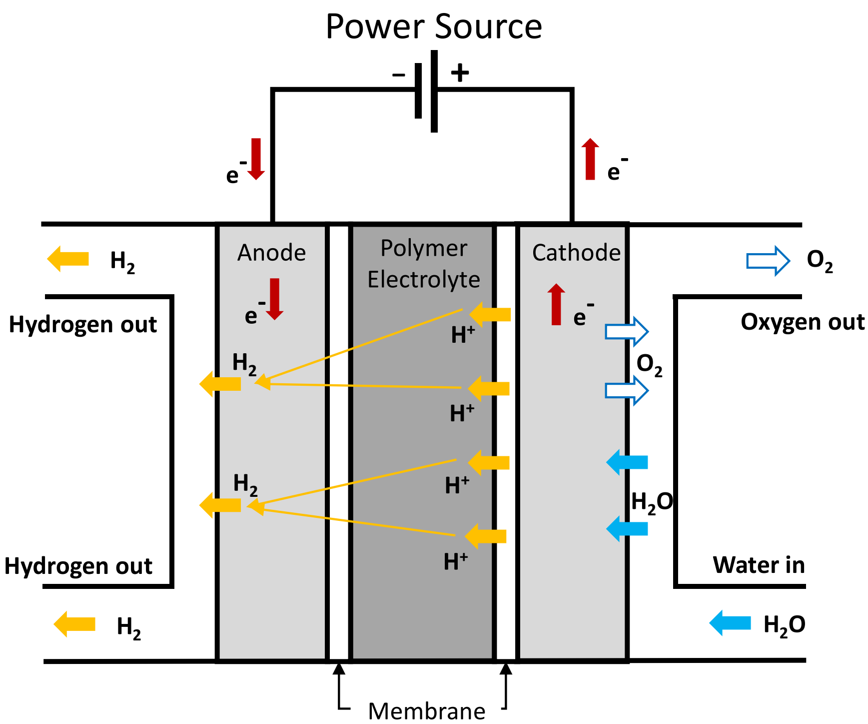

Figure 3.9. Cross section of hydrogen electrolyzer

The electrolyzer is made of two electrodes: anode and cathode separated by a membrane and an electrolyte while an external source provides electrical voltage across the electrolyzer. The water is fed to the electrolyzer where it reacts at the anode where it is separated into oxygen and hydrogen ions as shown in equation (3.15)

$$2H_2O \rightarrow O_2 + 4H^+ + 4e^- \tag{3.15}$$

The hydrogen ions pass through the membrane and electrolyzer to the cathode while the electrons travel through the electrical circuit to the cathode where it combines with the hydrogen protons to create hydrogen molecules as shown in equation (3.16).

$$4H^+ + 4e^- \rightarrow 2H_2 \tag{3.16}$$

The oxygen and hydrogen gases can then be collected and utilized. The overall equation for the electrolyzer is the same as equation (3.4) for the fuel cell except in the opposite direction

$$2H_2O + \text{energy} = 2H_2 + O_2 \tag{3.17}$$

3.2.1. Electrolyzer Types

Similar to the fuel cells, the electrolyzers are categorize by the type of electrolyzer used. The main types of electrolyzers are Proton Exchange Membrane (PEM) electrolyzers, alkaline electrolyzers and solid oxide electrolyzers.

Proton Exchange Membrane (PEM) Electrolyzer

This electrolyzer uses the same solid acid polymer membrane used in the PEM fuel cell. It operates at lower temperatures where the temperature is usually less than 100 °C. It is also considered to have high current density, rapid-start up and fast response. [47, 48]

Alkaline Electrolyzer

This type of electrolyzer uses a concentrated alkaline electrolyte solution instead of an acid. It uses electrodes made from nickel and nickel alloys. Alkaline electrolyzer technology is quite mature however it is considered to have low power densities and long start up time.[47]

Solid Oxide Electrolyzer

This type is known also as high temperature electrolyzer. It uses a combination of thermal and electrical energy to split the water molecules. It has low current density and the high operating temperature creates issues related to material selection and the mismatch between thermal expansion of the material. [47]

The electrolyzer type used for this thesis project is the Proton Exchange Membrane (PEM) electrolyzer due to its popularity in the research development especially in the new field of power-to-gas and the possibility for it to provide ancillary services to the system. From a technical standpoint, the PEM electrolyzer are suitable for frequency support applications due to its fast start up time, fast response and its high current density.

3.2.2. PEM Electrolyzer Model

There are several models that are proposed to represent the dynamics of the PEM electrolyzer. Some models are based on the electrochemical and thermal equations [49-51] while other are based on mathematical approximation and optimization [41, 52]. These are helpful in understanding the mechanism of hydrogen generation inside the electrolyzer stack. However, the concern of this thesis is on the electrical performance of the electrolyzer which is mainly the relationship between the drawn current and the stack voltage which is detailed in [53]. An Electromagnetic Transient (EMT) model for Real-Time Digital Simulator (RTDS) that is capable of providing ancillary services was developed in [54]. The model developed in this thesis is a simplified generic model for stability studies in DIgSILENT PowerFactory simulation package.

PEM electrolyzers are run in one of two modes; a voltage mode or a current mode. In voltage mode, the voltage is constant and the current drawn varies by the operating point. In current mode, the current is controlled to have constant hydrogen production and the voltage is held constant through varying the input power[53]. The voltage of the electrolyzer is described by equation (3.18) [53].

$$V = V_{oc} + V_{act} + V_{ohm} + V_{conc} \tag{3.18}$$

Here, V is the operating voltage, V_{oc} is the open circuit voltage, V_{act} is the activation voltage losses, V_{ohm} is the ohmic losses and V_{conc} is the concentration losses.

The open circuit voltage is dependent on the is dependent on the stack temperature and is defined by the Nernst potential as shown in equation (3.19) [53].

$$V_{oc} = E_o + \frac{RT}{2F}\left[\ln\left(\frac{p_{H_2}\sqrt{p_{O_2}}}{a_{H_2O}}\right)\right] \quad (3.19)$$

Where E_o is the constant reversible cell voltage, R is the universal gas constant, T is the temperature in Kelvin, F is Faraday constant, p_{H_2} and p_{O_2} are the hydrogen and oxygen pressures in atmospheres and a_{H_2O} is water activity between electrode and membrane.

The activation overpotential is dependent on both the current density and the stack temperature and is defined by equation (3.20) which is based on the Butler-Volmer equation[53].

$$V_{act} = \frac{RT}{\alpha_{an}F}\sinh^{-1}\left(\frac{i}{2i_{0,an}}\right) + \frac{RT}{\alpha_{cat}F}\sinh^{-1}\left(\frac{i}{2i_{0,cat}}\right) \quad (3.20)$$

Where i is the current density, α_{an} and α_{cat} are the anodic and cathodic charge transfer coefficient, $i_{0,an}$ and $i_{0,cat}$ are the exchange currents at anode and cathode R is the universal gas constant, T is the temperature in Kelvin and F is Faraday constant.

The ohmic overpotential is dependent on the current and the temperature and is described by equation (3.21) [53].

$$V_{ohm} = I\left(R_{el} + R_{pl} + R_{mem}\right) \quad (3.21)$$

Where R_{el} is the resistance of the electrodes, R_{pl} is the resistance of the bipolar plates and R_{mem} is the resistance of the membrane. Here, R_{el} and R_{pl} are dependent on the geometry of the components while R_{mem} is dependent on both the geometry and the temperature.

The concentration overpotential is dependent on the temperature and is caused by high current values. The calculation of the concentration overpotential is shown in equation (3.22) where it is a combination of the overpotential in anode and cathode [53].

$$V_{conc} = \frac{RT}{4F}\ln\left(\frac{C_{O_2}^{mem}}{C_{O_2,0}^{mem}}\right) + \frac{RT}{2F}\ln\left(\frac{C_{H_2}^{mem}}{C_{H_2,0}^{mem}}\right) \quad (3.22)$$

Where $C_{O_2}^{mem}$ and $C_{H_2}^{mem}$ are the oxygen and hydrogen concentrations are the membrane-electrode interface, $C_{O_2,0}^{mem}$ and $C_{H_2,0}^{mem}$ are the concentrations at a reference operating point, R is the universal gas constant and T is the temperature in Kelvin.

The above model shows that the increase in current drawn by the electrolyzer increases the operating voltage. Figure 3.10 shows the current density voltage relationship for different operation conditions.

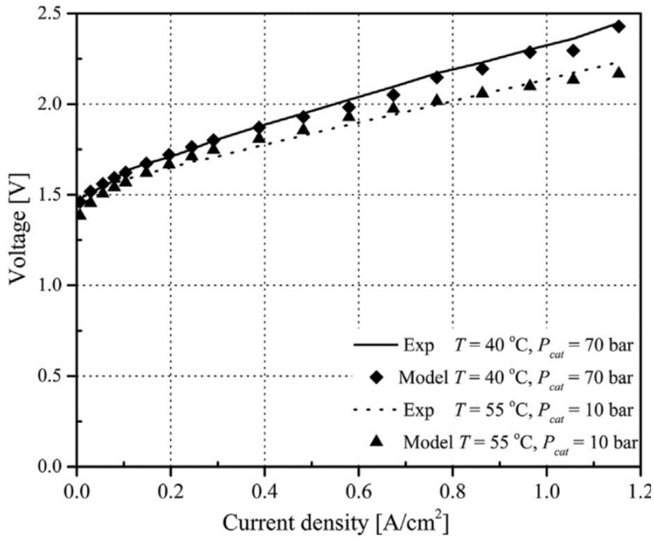

Figure 3.10. Electrolyzer current density and voltage relationship for different operating conditions[53]

3.2.3. Power Factory Model

The electrolyzer is modelled in PowerFactory as an externally controlled general load. The control of the load is developed using DSL. The basic block diagram for the fuel cell model is shown in Figure 3.11.

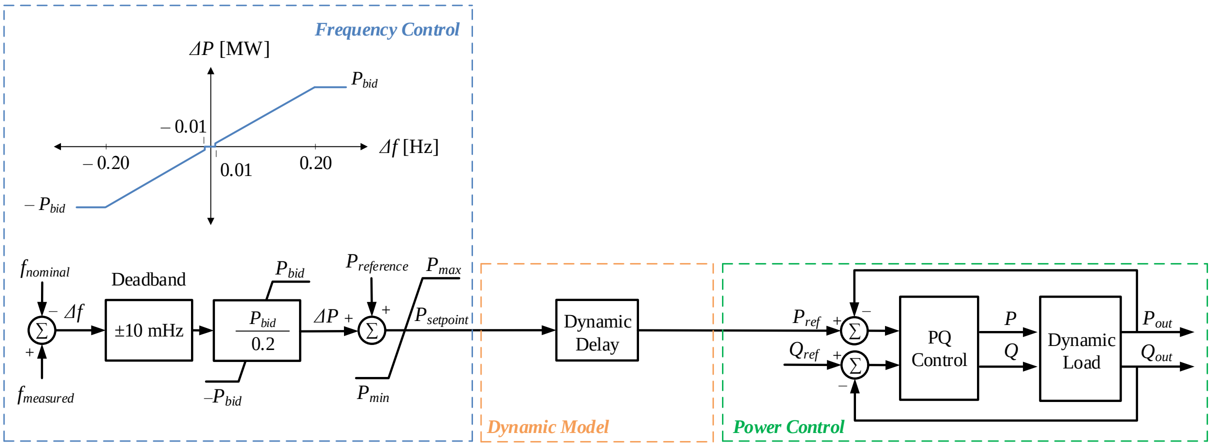

Figure 3.11. Dynamic model, power control block diagram and droop characteristic of the modelled PEM fuel cell.

The PowerFactory model can be divided into three components: frequency control, electrolyzer dynamic model and power control. The frequency control and the dynamic model have been combined into one block diagram.

3.2.4. Frequency control & Dynamic model

The frequency control diagram in Figure 3.11 and the PowerFactory block diagram in Figure 3.12 show the details of the frequency control.

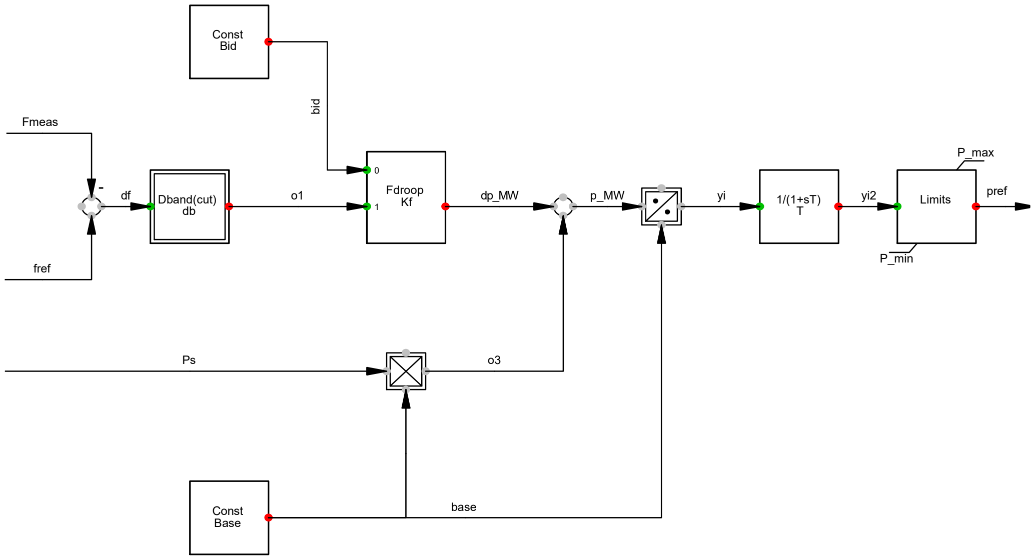

Figure 3.12. PEM Electrolyzer frequency control and dynamics block diagram

First, the frequency deviation is measured. Then a dead band of 10 mHz is applied to the frequency deviation in order to avoid action on low magnitude noise signals. Then the signal is run through an inverse droop control block which is defined by the following equation

$$\Delta P = P_{bid} \frac{(f - f_{nominal})}{\text{Full Bid Frequency Deviation}} \tag{3.23}$$

P_{bid} is the bid value as decided by the FCR market, f is the measured frequency in Hz, $f_{nominal}$ is the reference frequency in Hz and Full Bid Frequency Deviation is decided by the system operator, 200 mHz for the Dutch system, and is the frequency at which the generator shall supply the full bid value. The power output of this block (ΔP) is limited by the value of the bid (P_{bid}) and does not exceed it even if the frequency deviation goes beyond the full bid frequency deviation. The power reference is then added in order to give the power set point for the electrolyzer. Afterwards, a first order delay is applied to represent the dynamics of the electrolyzer. Finally, Limits are applied to the power set point in order to ensure the electrolyzer plant operates within the allowable limits which are 20%-100% for the electrolyzer plant rated power.

3.2.5. Power Control

From the system point of view, the electrolyzer is modelled as a general load controlled by external current signals. The power control part is a power control loop that sets the load's active and reactive power signals.

The power control block shown in Figure 3.13 controls only the active power (P). The model compares the actual power output of the static generator to the reference power signal coming from the frequency and dynamics block. The power deviation is filtered using a lead-lag filter then fed to a Proportional and Integral (PI) controller. Then a reference signal is added to the signal from the PI controller which gives the P set setpoint. Limits are applied to ensure the operation limits of the electrolyzer 0.2-1.0 p.u. are maintained. Finally, the per unit power is multiplied by the rated value of the electrolyzer plant to give the input control signal for the general load.

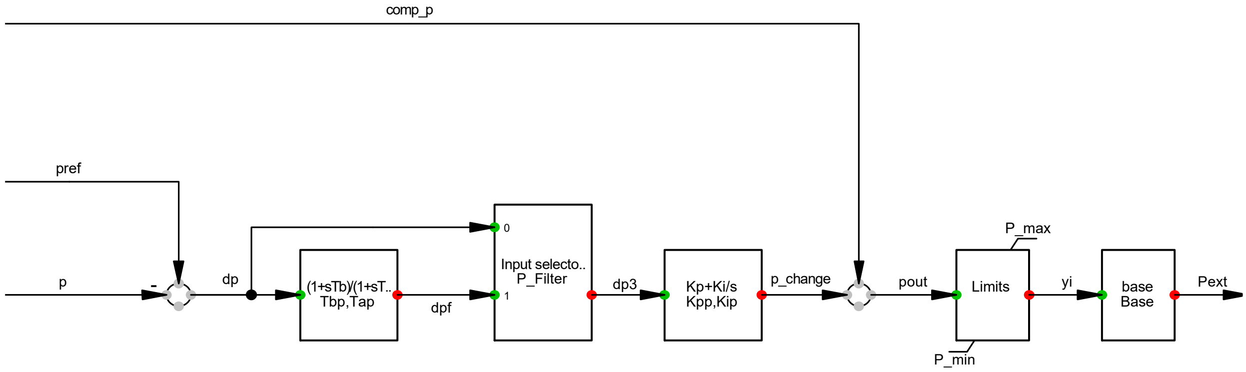

Figure 3.13. Electrolyzer power control loop

For the electrolyzer load, the reactive power (Q) control is not needed because compared to the static generator, the used general load is capable of maintaining a constant Q without the need for external control.

The control parameters for the electrolyzer model are listed in appendix I.

4. Test Network Development

The test network represents a reduced size model of the high voltage transmission network (380-400 kV) for North Netherlands, North-West Germany and South Denmark. This network, shown in Figure 4.1, is part of the interconnected transmission network of continental Europe. This chapter will discuss in detail the development of the network model in DIgSILENT PowerFactory and its components.

Figure 4.1. Map of the represented part of the European high voltage transmission network [55]

4.1. Power Network Identification

The power network representation is based on the PSS®E model of the European Network of Transmission System Operators (ENTSO-E) shown in Figure 4.2. This model is used as the basis for the network layout, power flow and dynamic data of system components.

This PSS®E model includes the complete the connected European transmission network however it cannot be used directly as-is because the single line diagram only shows the transmission network of North Netherlands while the rest of the network is hidden. A hidden bus is embedded in the model but does not show in the single line diagram which means that the load flow to the bus, the connected transmission lines, generators and loads are also hidden. In addition, the visible buses and other system components are not labeled or identified in the model. In order to translate this model into DIgSILENT PowerFactory, the model must show (unhide) and identify in the single line diagram all the buses, transmission lines, generators and loads in North Netherlands, North-West Germany and South Denmark. This process is done in three stages as explained in the next paragraphs.

First stage is correctly identifying the transmission network for North Netherlands. For this purpose, the maps in [55, 56] are used to identify the network buses, lines and generators. These maps show the connections between the substations and the distance between them. The different substations in the model can be identified by comparing the data from the maps with the length of transmission lines between buses in the

PSS®E model. Each substation in this part of the network is represented by a single bus and the buses had a naming convention that uses abbreviations of the substations (e.g. EEM380 is the 380 kV bus at Eemshaven) which simplifies the process of the transmission network identification.

The second stage is unhiding and Identifying the North-West German network. This process is more complex because the buses have to be unhidden individually and in sequence starting from the cross-border connection with the Netherlands. Other complexities include the naming convention for German buses which only uses numbers in the model (e.g. DE915348) and the representation of one substation using multiple buses. To overcome these complexities, the following approach is used:

1. The network layout, topology and locations of generators are identified using the maps in [55, 57-60].
2. Starting from the cross-border connection with the Netherlands, the first German bus is unhidden and the first substation at Diele is identified.
3. Measuring the distance between Diele and the next substations in the map and comparing it with the length of the transmission lines connected to the Diele bus in the model. the transmission line that matches the length in the map is the one connecting Diele to the next substation. Here buses with distance of 1 km or less are considered in the same substation.
4. The bus in the other end of the transmission line is unhidden and the new substation is identified and labeled.
5. The process is repeated at the new substation until the cross-border connection between Germany and Denmark is reached.

The third stage is unhiding and identifying the South Denmark transmission network. This network also uses numbers to identify the buses similar to the North-West German network. Therefore, the same approach above is used to unhide and identify the different buses and substations using the network map from [55] and system data from [61].

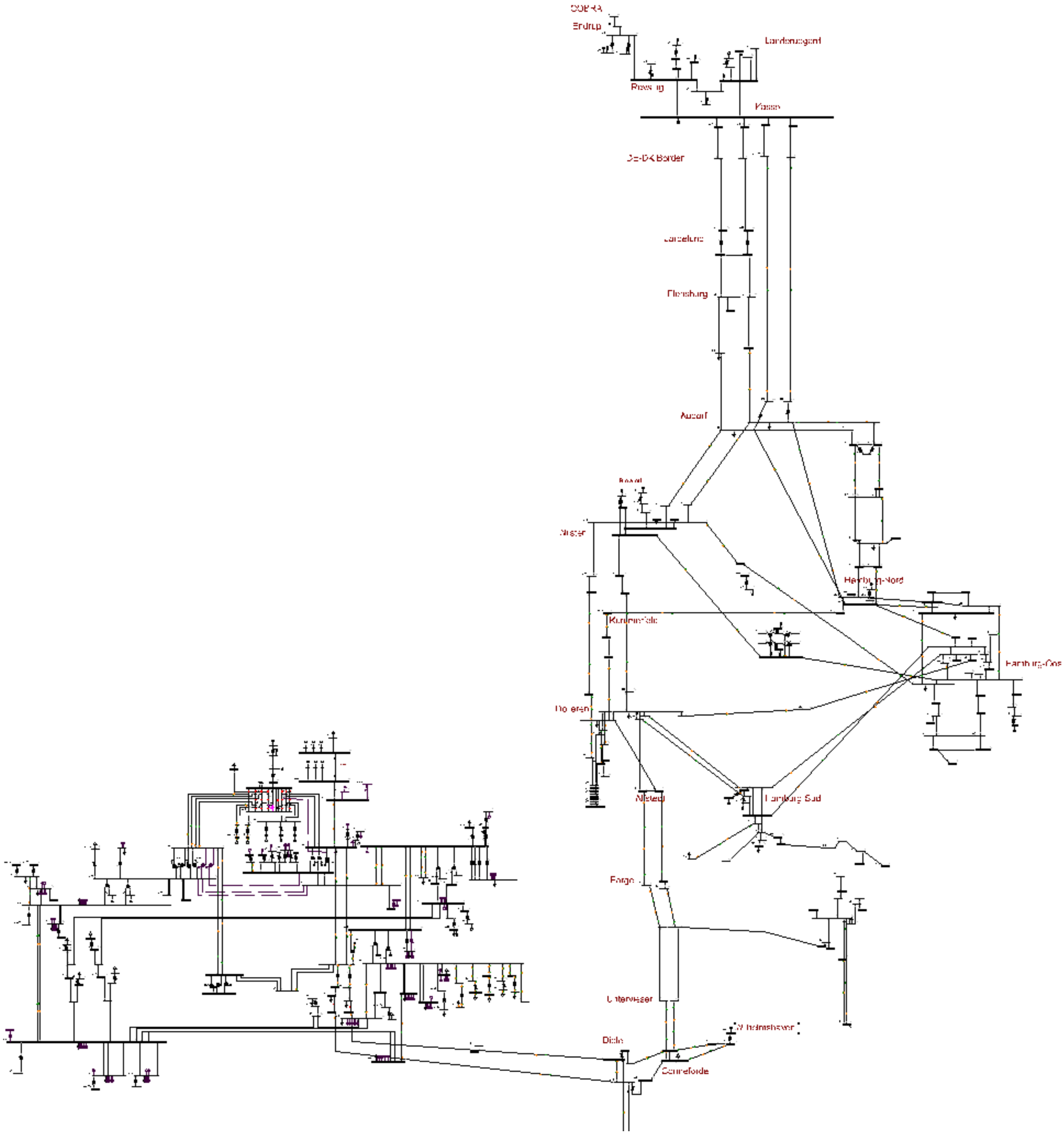

Figure 4.2. PSS®E model of the represented transmission network

4.2. Translation and Reduction into PowerFactory

The purpose of translation and reduction is to represent the power system in another modeling program while minimizing the changes in power flow and dynamic behavior. For this purpose, the following reduction rules are applied to the model translation from PSS®E to PowerFactory:

- Buses within the same substation are combined into one bus.
- Buses that divide transmission lines between substations are removed.
- Parallel generators with identical parameters are aggregated into one generator which is scaled up to their combined rated power.
- Parallel transformers with identical parameters are aggregated into one transformer which is scaled up to their combined rated power.
- Load flow to/from outside the modeled part is represented by constant load which is positive for power outflow or negative for power inflow. These loads are labeled in the single line diagram as "EndLoad Bus_name"

The resulting PowerFactory network is shown in Figure 4.3. The network layout and the location of the buses reflects the relative geographic location of the substations which improves the readability of the single line diagram.

4.3. Improvement to the PowerFactory Network Model

The PowerFactory model is further improved to reflect a more accurate representation of the modeled power system. This is achieved by adding the connected renewable sources, HVDC links and additional loads.

The first HVDC links NORNED (700 MW) between Netherlands and Norway is added at the bus Eemshaven and represented by a constant negative load of 700 MW. The second HVDC link is COBRAcable (700 MW) between Netherlands and Denmark is represented from both sides as a constant load. A positive Load of 700 MW is added to the bus Endrup in Denmark and a negative load of 700 MW is added to Eemshaven Oudschip in the Netherlands. These HVDC links are assumed to be working at rated capacity so they do not participate in frequency support.

In the North Netherlands power system, there is around 3058 MW of onshore wind capacity at the 110 kV level. This capacity is represented in the model by aggregating the distributed windfarms into one large equivalent windfarm at the nearest 380 kV bus. Table 4.1 shows a summary of the onshore wind generation in North Netherlands.

Table 4.1 Onshore wind capacity in North Netherlands

380 kV substation	Capacity [MW]
Vierverlaten	929.50
Meeden	490.40
Eemshaven	986.50
Zwolle	168.50
Ens	483.90
TOTAL	**3058.80**

In North-West Germany, there is around 6846 MW of offshore wind generation capacity [62]. This capacity is aggregated at three buses as shown in Table 4.2.

Table 4.2 Offshore wind generation in North-West Germany [62]

Substation	Wind Farm	Capacity
Diele	BorWin1	400.00
	BorWin2	800.00
	BorWin3	900.00
	Total	**2100.00**
Dorpen West	DolWin1	800.00
	DolWin2	916.00
	DolWin3	900.00
	Total	**2616.00**
Wilster	HelWin1	576.00
	HelWin2	690.00
	SylWin1	864.00
	Total	**2130.00**
Total offshore wind capacity		**6846.00**

All the wind capacity added to the model provide constant P at 60% of the rated power and constant Q at 20% of the rated power. The wind generation will remain constant during disturbances and it does not contribute to frequency support.

Also, to reflect the higher industrial demand to the south of Germany [63] two constant loads of 5000 MW each are added to the system at the buses in Dorpen-West and Hamburg-Sud which represent the south most substations in the system.

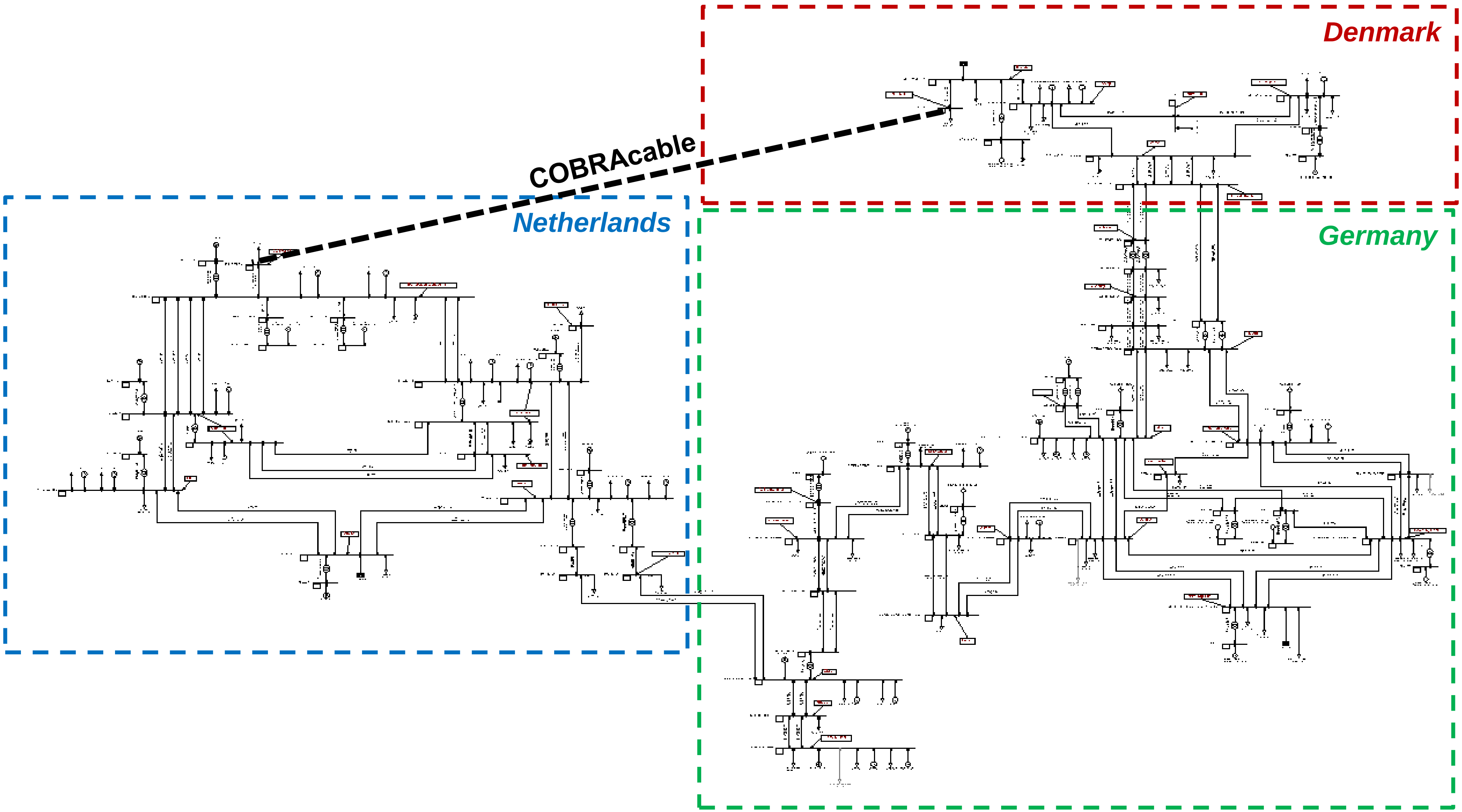

Figure 4.3. PowerFactory reduced model of the transmission network

4.4. Power System Dynamic Representation

After representing the layout of the network's buses and transmission lines, the next step is to develop the dynamic model of the power network and the connected elements. First, the buses in the model use the generic ***ElmTerm*** terminal model while the transmission lines use the generic ***ElmLne*** line model [46]. Since each line in the PSS®E model has different rating, resistance and reactance, a new line type is developed for each line in PowerFactory. The line type defines the line rating, resistance and inductance in ohm/km which are converted from per unit lumped parameters in PSS®E. All line types in the PowerFactory model are 3-phase overhead lines.

4.4.1. Dynamic model for synchronous generators

The system model has 14 synchronous generators repressed by 6th order (subtransient). These generators are spread in the network as follows: 2 in Netherlands, 10 in Germany and 2 in Denmark. In order to simply the network development and reduce the computational demand, all these generators will have the same dynamic model that is developed using PowerFactory DSL. The frame for this model is shown in Figure 4.4. This model includes the synchronous generator which is represented by ***ElmSym*** model [46]. The synchronous generator has two inputs: turbine power (pt) and excitation voltage (ve) and provides two feedback signals which are the speed (w) and terminal voltage magnitude (ut). All the inputs and outputs of the synchronous generator are in per units.

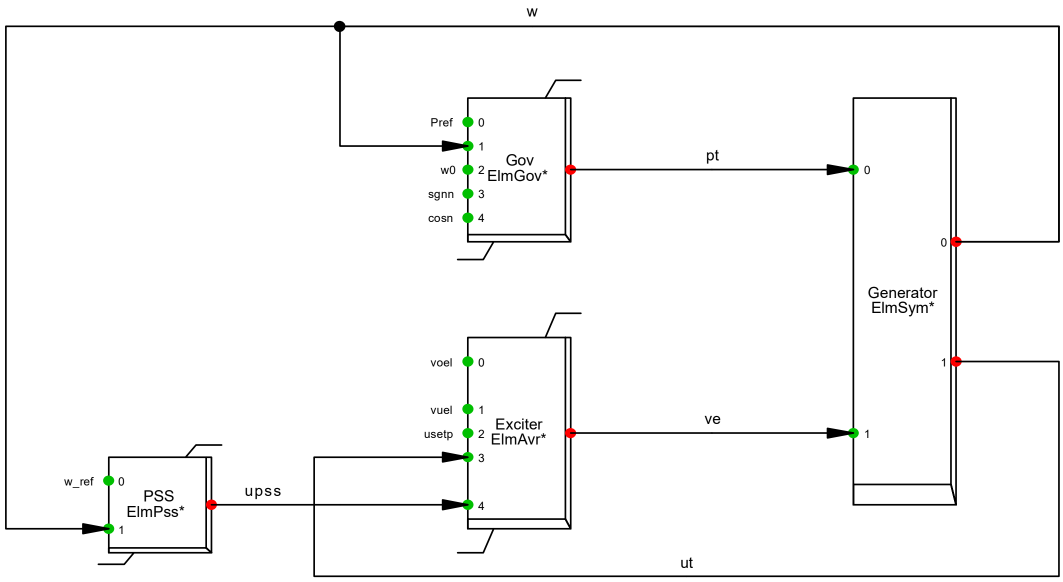

Figure 4.4. DSL Frame for synchronous generator model

4.4.2. Governor Model

The governor model implemented for synchronous generators is based on the model used in PSS®E which is a steam turbine governor (TGOV1). This same model is also available in PowerFactory's ENTSO-E Dynamics library under the name (Gov_Steam0). The used governor model is a modified version of this model as shown in Figure 4.5.

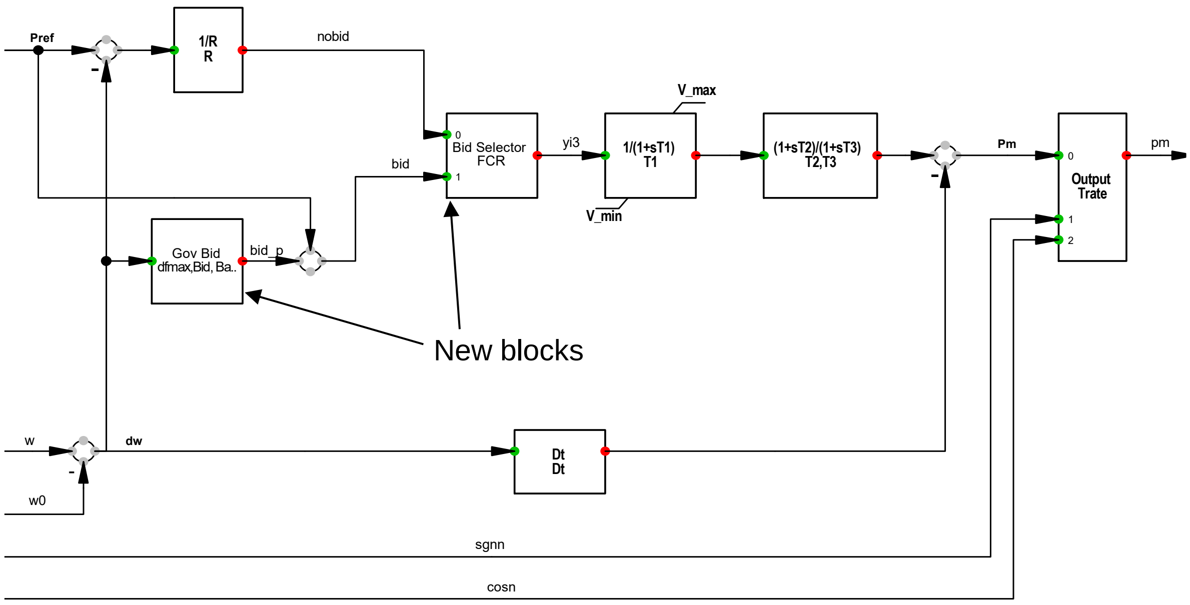

Figure 4.5. Synchronous generator governor model

As seen in Figure 4.5, the governor can be operated with conventional configuration or as a participant in the FCR market. The new block "Gov Bid" defines the droop function of the governor according to Equation (4.1) which is developed based on the droop definition in the FCR market specification in [21]. The equation relates the change in power output in p.u. to the bid value in MW, frequency deviation and market specifications.

$$\Delta P = -\frac{P_{bid}}{MVA\ base}\frac{(w - w_0)f_{nominal}}{\text{Full Bid Frequency Deviation}} \tag{4.1}$$

P_{bid} is the bid value as decided by the FCR market, w is the measured speed in p.u., w_0 is the reference speed in p.u., and $f_{nominal}$ is the system nominal frequency of 50 Hz. The Full Bid Frequency Deviation is decided by the system operator and is the frequency at which the generator shall supply the full bid value. For this thesis, this value is 200 mHz which is the value for the Netherlands FCR market. The power output of this block (ΔP) is limited by the value of the bid (P_{bid}) and does not exceed it even if the frequency deviation goes beyond the full bid frequency deviation.

The other block "Bid Selector", specifies whether the governor works in direct conventional support or in FCR market. The block receives the power signal from both the conventional support and the FCR market support then selects and outputs one of them based on the value of the control parameter called (FCR). If FCR = 0 the block outputs the conventional support power and if FCR = 1, the block outputs the power in accordance with FCR market rules.

The control parameters for this governor model are taken from the PSS®E dynamic data and are shown in Appendix I.

4.4.3. Exciter Model

The exciter model used in PSS®E is Simplified Excitation System (SEXS) and the same is available in PowerFactory as part of the Standard Models library under the name (avr_SEXS). The used model shown in Figure 4.6 is slightly modified by adding a gain block for the Power System Stabilizer (PSS) signal. This will enable the generator control to activate and deactivate the PSS. The control parameters for this exciter model are taken from the PSS®E dynamic data and are shown in Appendix I.

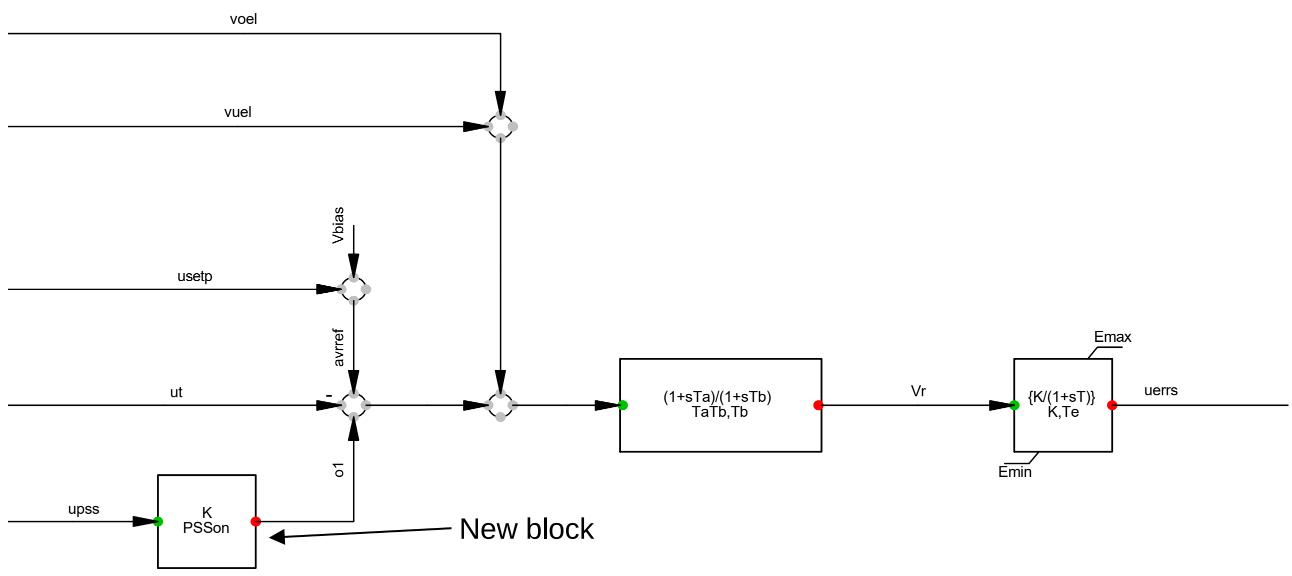

Figure 4.6. Synchronous generator exciter model

4.4.4. Power System Stabilizer (PSS) Model

The stabilizer model used PSS®E is IEEE Dual-Input Stabilizer Model (PSS2A) which is also available in PowerFactory model library. However, this model is not used due to its intensive computational requirements and the difficulty in initializing and stabilizing the signal using the same control parameters from PSS®E. Instead a simpler PSS model is used based on the PSS design in [64] as shown in Figure 4.7. The control parameters for this stabilizer model are chosen in accordance with the recommended values in [64] chapter 17 and are shown in Appendix I.

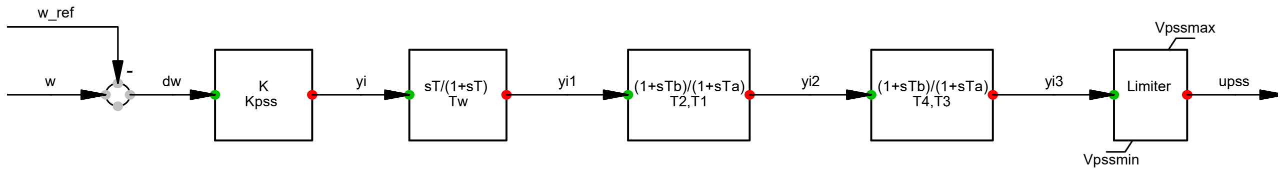

Figure 4.7. Synchronous generator stabilizer model

4.4.5. Dynamic Representation of Other Components

Simple generic models are used to represent the other components in the system. Wind parks are represented by static generators with constant P and Q. COBRAcable and NorNed DC Links are represented by generic loads with constant P and Q as well. The power flow of these components will remain constant during the simulation period and they will not contribute to the frequency stability or the dynamic behavior of the system. The connected external grids are only providing external inertia and oscillation damping and do not contribute to primary and secondary frequency support. In PowerFactory, the external grid is based on a simplified model of synchronous generator with predefined parameters [46]. For the frequency stability study in this thesis, there are four parameters that need to be defined. First, the grid is operated as ***PQ Bus Type*** which means the output is according to set values of P and Q and it does not function as a reference bus.

The power flow setting for the grid is $P = 0$ and $Q = 0$ in order not to interfere with the initial load flow. The second parameters is the inertia constant H and it is chosen to be $H = 5\ s$ which is a value higher than the synchronous generators in the system in order to provide additional oscillation damping. The other parameters are primary and secondary frequency bias. These define the reaction of the external grid to frequency deviation and both values are set to 0 since the contribution of the external grid in frequency support is not desired.

4.5. Dynamic Model Verification

In order to test the accuracy of PowerFactory representation of the network, the developed system is tested for a symmetrical three phase to ground fault at the bus in Eemshaven Oudeschip as shown in Figure 4.8 and the results are tested against the PSS®E model. The simulation is run for a fault at $(t = 3\ s)$ and for three different fault durations of $10\ ms$, $100\ ms$ and $200\ ms$ and it is performed in both PSS®E and PowerFactory for 15 seconds. The simulation in PSS®E is done for only the Netherlands section while the PowerFactory simulation is done twice; once for only the Netherlands Section and once with the full network.

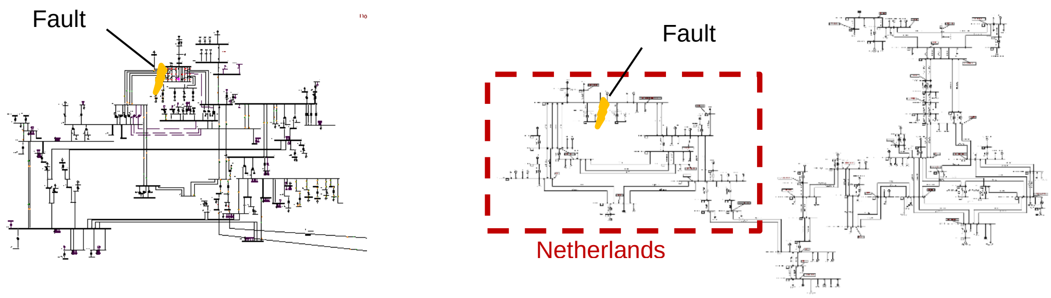

(a) PSS®E simulation setup (b) PowerFactory simulation setup

Figure 4.8. Test grids for Fault Simulation

By comparing the results of the simulations shown in Figure 4.9, it can be observed that the dynamic behavior of the both models is very similar. The difference in the steady state voltage magnitude is due to the difference in the initial load flow and the location of the swing bus between the models. While the post disturbance voltage profile is due to the difference in settings and control parameters of the AVR controllers of the synchronous machines.

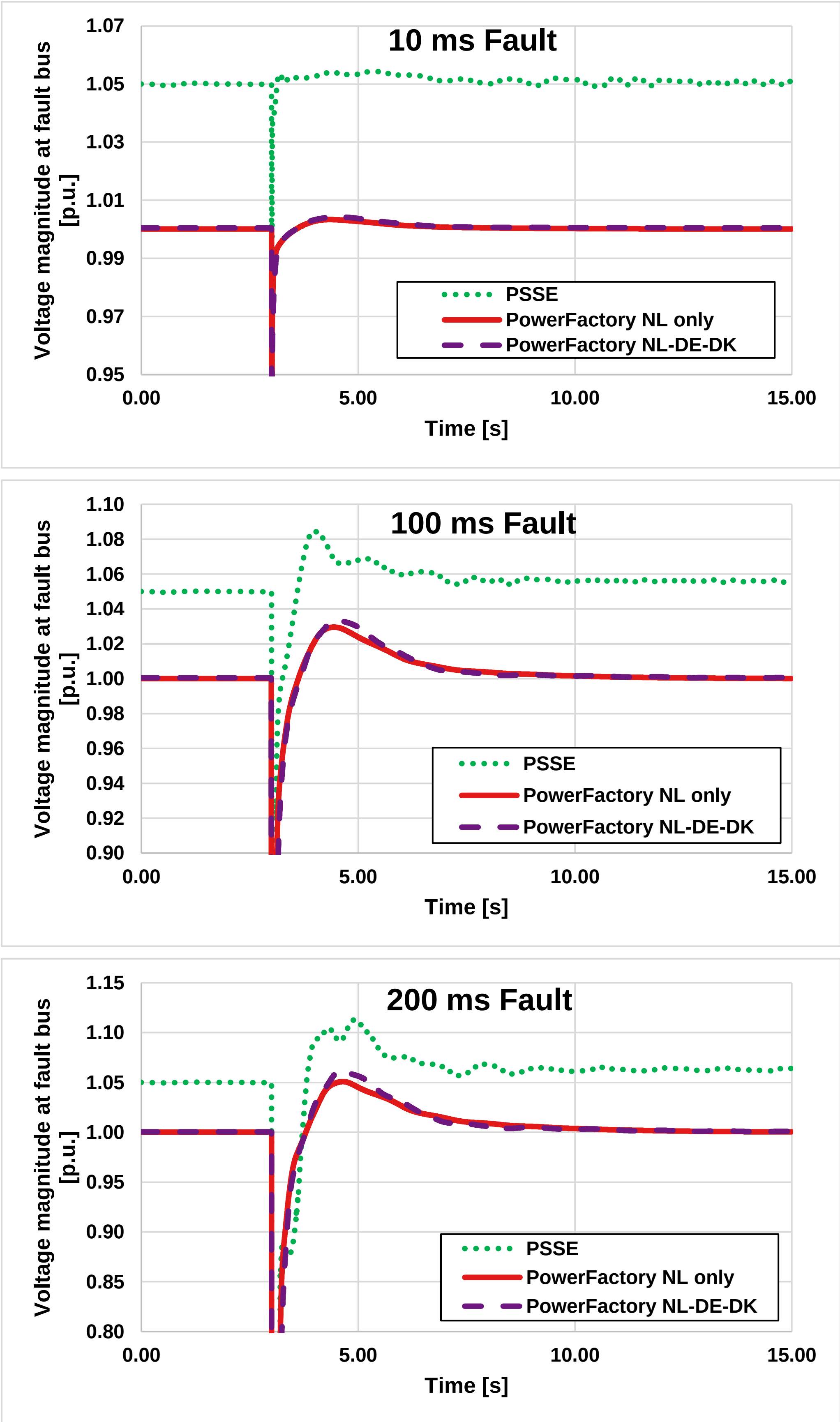

Figure 4.9. Comparison of voltage magnitude evolution for a three phase to ground fault for PSS®E and PowerFactory

4.6. Addition of PEM Fuel Cells and Electrolyzers

The dynamic model for the test system is complete and the fuel cell and electrolyzers are added to the system as shown in Figure 4.10. The locations for the PEM devices are chosen in buses where wind energy is connected such as Diele and Dorpen West in Germany or near industrial areas such as Hamburg-Nord.

There are two different capacity levels (20 MW and 150 MW) for both the fuel cells and electrolyzers which are added with identical power rating to the same bus with the same initial power flow. This will ensure that the generation of the fuel cell is absorbed by the electrolyzer and the addition of the PEM devices does not affect the power flow in the network in normal operating conditions. The dispersion of the allow for different operational scenarios such as changing the location of the FCR support by PEM fuel cells and electrolyzers or distributing the FCR support over multiple PEM devices.

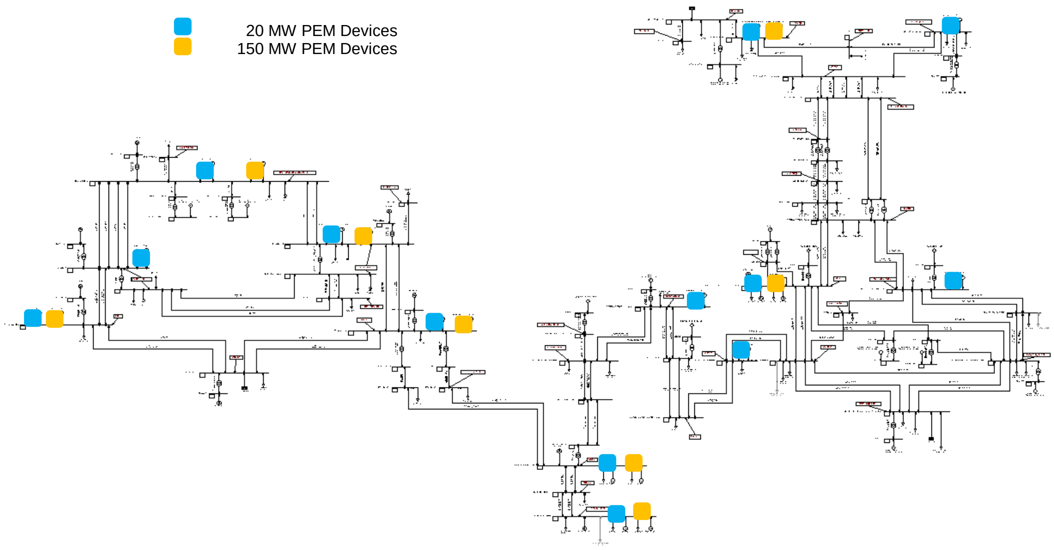

Figure 4.10. Distribution of PEM devices

5. Assessment of the Impact of Different Types of Disturbances

In order to test the performance of the implemented models of the fuel cells and electrolyzers, the developed models will be tested in a simulation against a variety of scenarios where frequency will be disturbed. First, the hydrogen technologies will be tested for frequency support during generation-load demand imbalances in a limited area of the network. Afterwards, other system disturbances, line disconnections and Islanding, will be applied on the full-sized network. In these simulations, the performance of PEM technologies will be compared to the performance of the synchronous generators. It is important to note the following conditions that will apply to all disturbances and scenarios as indicated above:

1. The initial load flow in the network remains constant.
2. Inertia of the system remains constant.
3. Total FCR bid capacity in the system remains constant.
4. Generators and loads not participating in the FCR market will remain constant.

5.1. Generation Load Imbalance

The imbalance between generation and loads occur due to changes in generation or changes in loads but when generation exceeds the load demand, frequency will increase and when load demand exceeds generation, frequency decreases. Four study cases will be simulated to test the performance of the fuel cells and electrolyzers to generation-load demand imbalance. These cases are summarized below:

- Increase of 30 MW of wind generation
- Decrease of 30 MW of wind generation
- Increase of 30 MW in active power load demand.
- Decrease of 30 MW in active power load demand.

The value of the disturbance is chosen to be 30 MW because this value causes sufficient frequency deviation that allows to study the primary frequency response in the FCR market, but the deviation remains within the 200 mHz full bid activation frequency deviation.

For these simulations, only the Netherlands part of the network will be tested. The network has been reduced and the model for Germany and Denmark is reduced to a constant load in order to limit the inertia and reduce the system size and variables. As shown in Figure 5.1, two synchronous generators, one electrolyzer and one fuel cell are connected to the 380 kV bus in Eemshaven Oudeschip. The wind generator connected to Eemshaven 380 kV bus which will be adjusted to reflect generation changes (i.e. sudden increase/decrease of 30 MW wind generation). Also, the load connected to the same bus will be adjusted to reflect the change in active power load demand (i.e. sudden increase/decrease of 30 MW load demand). The synchronous generators and the hydrogen technologies will be compared with respect to provision of FCR under three scenarios: only synchronous generators, only PEM electrolyzer, only PEM fuel cell, a combination of 50%

electrolyzer and 50% fuel cell and a mixed support of 50% synchronous generators 25% fuel cell and 25% electrolyzer. In all scenarios there is 50 MW of FCR capacity. This value is chosen because it provides sufficient FCR capacity, so the frequency deviation remains within the 200 mHz full bid activation frequency deviation.

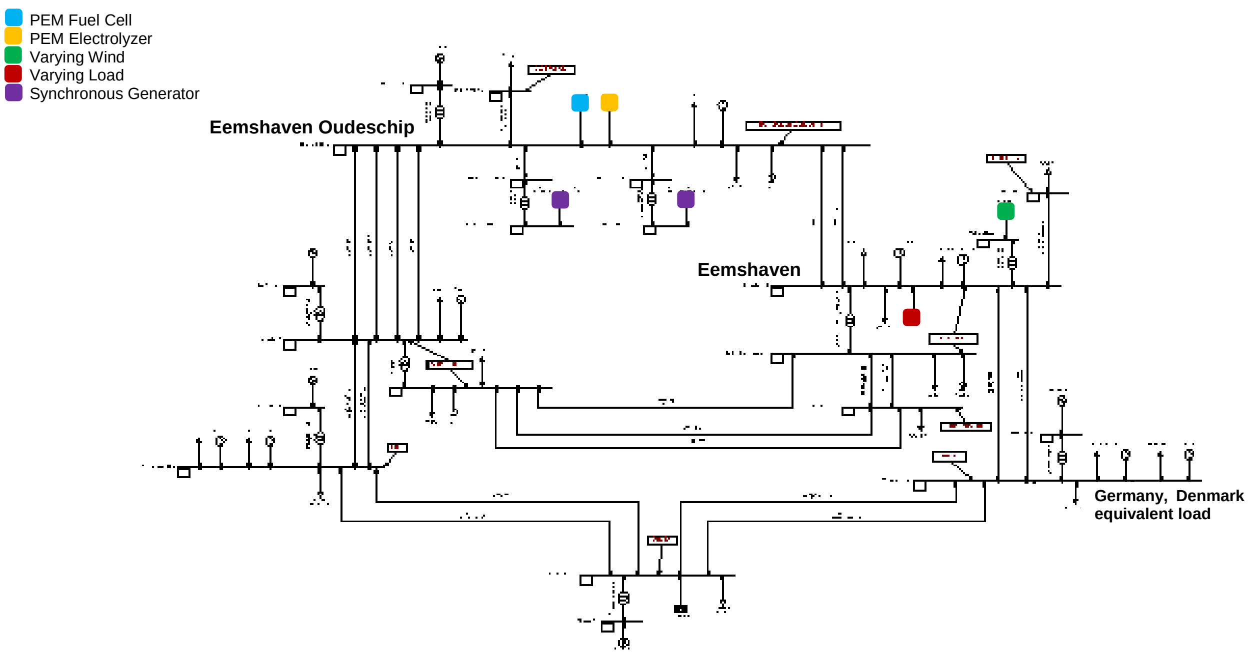

Figure 5.1. Network representation for generation-load imbalance

5.1.1. 30 MW increase in wind generation

This increase is represented by a step increase at $(t = 5\,s)$ in the wind generation connected to the Eemshaven 380 kV bus in Figure 5.1. The generation is increased from the default value of 600 MW to 630 MW. Table 5.1 below shows the details of the scenarios and a summary of the frequency response.

Table 5.1. Frequency response to increase in wind generation for different FCR support scenarios

Nº	Scenario	Sync. generators	PEM electrolyzer	PEM fuel cell	Nadir [Hz]	RoCoF [mHz/s]
(1)	Base case (Sync Gen)	2 x 25 MW FCR bid	No FCR support	No FCR support	50.17	49.88
(2)	Mixed Bid	2 x 12.5 MW FCR bid (50%)	12.5 MW FCR bid (25%)	12.5 MW FCR bid (25%)	50.12	47.74
(3)	PEM Electrolyzer	No FCR support	50 MW FCR bid	No FCR support	50.10	46.04
(4)	PEM Fuel Cell	No FCR support	No FCR support	50 MW FCR bid	50.10	47.43
(5)	H_2 PEM Devices	No FCR support	25 MW FCR bid (50%)	25 MW FCR bid (50%)	50.10	46.78

The simulated dynamic frequency responses shown in Figure 5.2 show that the faster active power injection by the PEM fuel cells and electrolyzers improves the frequency response by reducing the maximum frequency deviation (nadir) when compared with the base case when only synchronous generators are responsible for FCR support. Even in the case when FCR capacity is divided between synchronous generators and hydrogen technologies, the response is improved compared to the case with only the synchronous generators. In all scenarios, the Rate of Change of Frequency (RoCoF) does not change significantly because for the first 5 seconds the inertial response is most dominant.

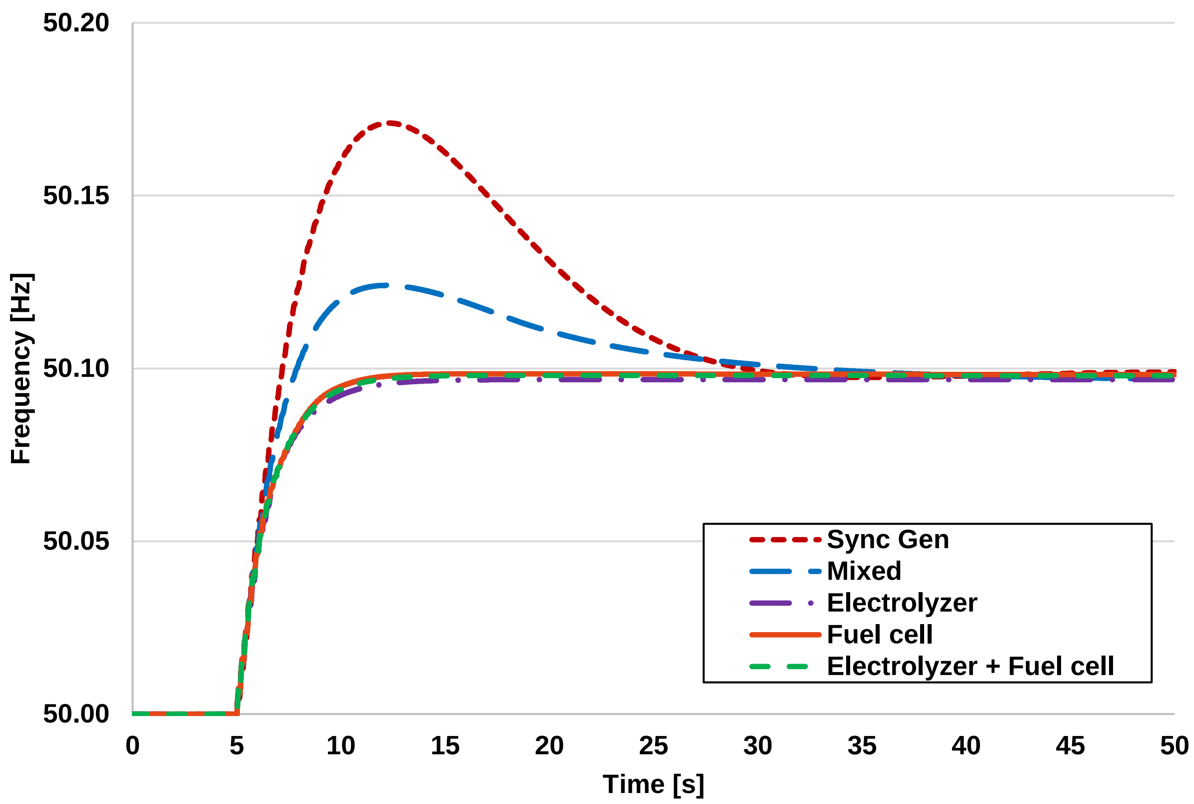

Figure 5.2. Frequency response for wind generation increase

5.1.2. 30 MW decrease in wind generation

The decrease is represented by a step decrease at $(t = 5\,s)$ in the wind generation connected to the Eemshaven 380 kV bus in Figure 5.1. The generation is decreased from the default generation of 600 MW to 570 MW. Table 5.2 below shows the details of the scenarios and a summary of the frequency response.

Table 5.2. Frequency response to decrease in wind generation for different FCR support scenarios

Nº	Scenario	Sync. generators	PEM electrolyzer	PEM fuel cell	Nadir [Hz]	RoCoF [mHz/s]
(1)	Base case (Sync Gen)	2 x 25 MW FCR bid	No FCR support	No FCR support	49.83	49.93
(2)	Mixed Bid	2 x 12.5 MW FCR bid (50%)	12.5 MW FCR bid (25%)	12.5 MW FCR bid (25%)	49.88	47.74
(3)	PEM Electrolyzer	No FCR support	50 MW FCR bid	No FCR support	49.90	46.04
(4)	PEM Fuel Cell	No FCR support	No FCR support	50 MW FCR bid	49.90	47.44
(5)	H_2 PEM Devices	No FCR support	25 MW FCR bid (50%)	25 MW FCR bid (50%)	49.90	46.79

The simulated dynamic frequency responses shown in Figure 5.3 show that the faster active power injection by the PEM fuel cells and electrolyzers improves the frequency response by reducing the maximum frequency deviation (nadir) when compared with the base case when only synchronous generators are responsible for FCR support. Even in the case when FCR capacity is divided between synchronous generators and hydrogen technologies, the response is improved compared to the case with only the synchronous generators. In all scenarios, the RoCoF does not change significantly.

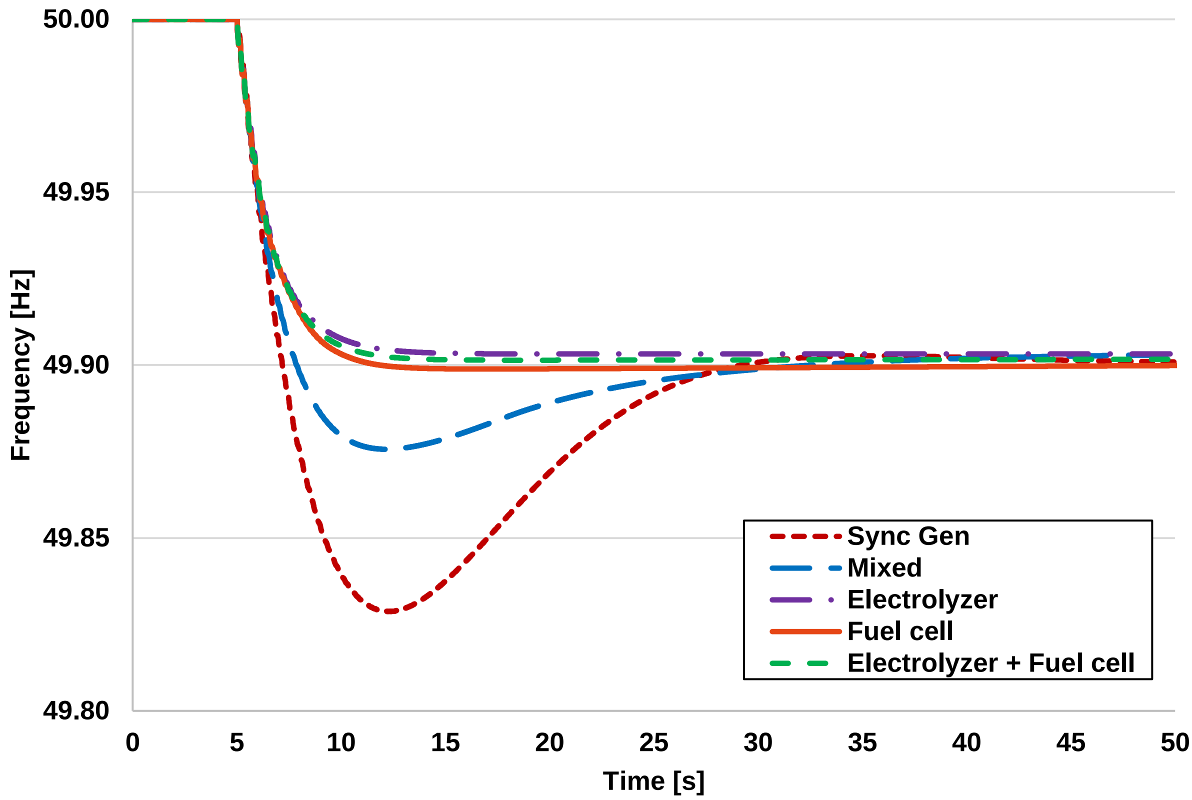

Figure 5.3. Frequency response for wind generation decrease

The difference in the frequency response is due to the difference in the internal dynamic between the synchronous generator and the PEM devices as shown in Figure 5.4. The PEM devices and the synchronous generator use the same frequency controller but the faster dynamics of the PEM fuel cell and electrolyzer result in faster power injection as shown in Figure 5.5. In the figure, the initial jump in the response of the synchronous generator is how PowerFactory represents the inertial response of the generator immediately after the disturbance. The difference in the speed of power injection can be seen starting 1.5 s after the disturbance where the power output of the fuel cell is higher than the output of the synchronous generator.

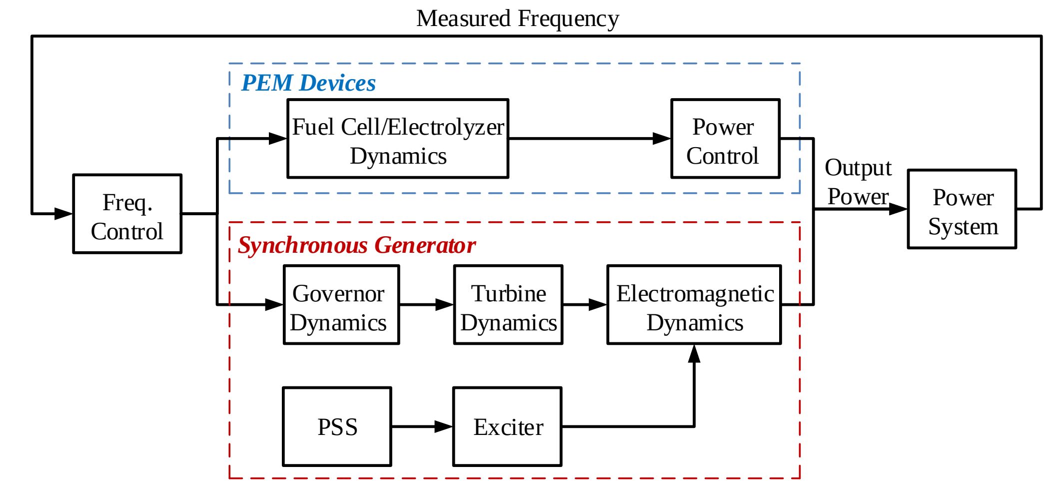

Figure 5.4. Difference in dynamics between PEM devices and synchronous generator

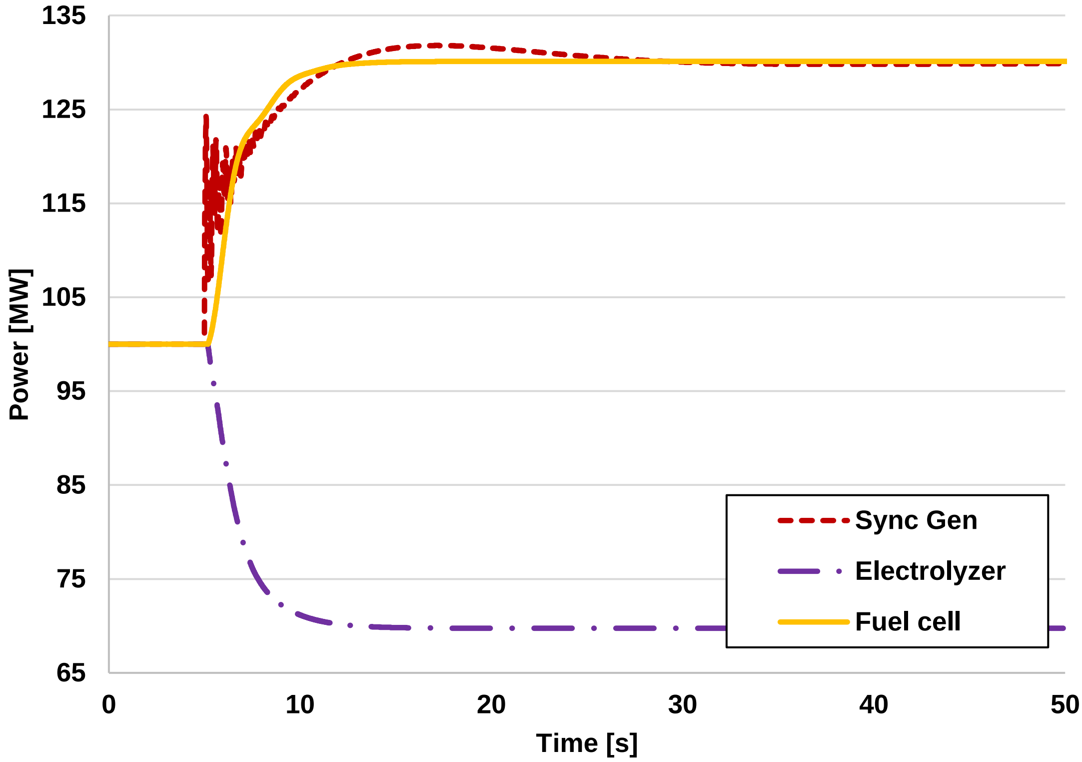

Figure 5.5. Power output for wind generation decrease

5.1.3. 30 MW increase in load demand

The decrease is represented by a step increase at $(t = 5\,s)$ in the load connected to the Eemshaven 380 kV bus in Figure 5.1. The load demand is increased from the default P value of 725.6 MW to 755.6 MW. The frequency response of the system is identical to the case of the decrease in wind generation as shown in Figure 5.6.

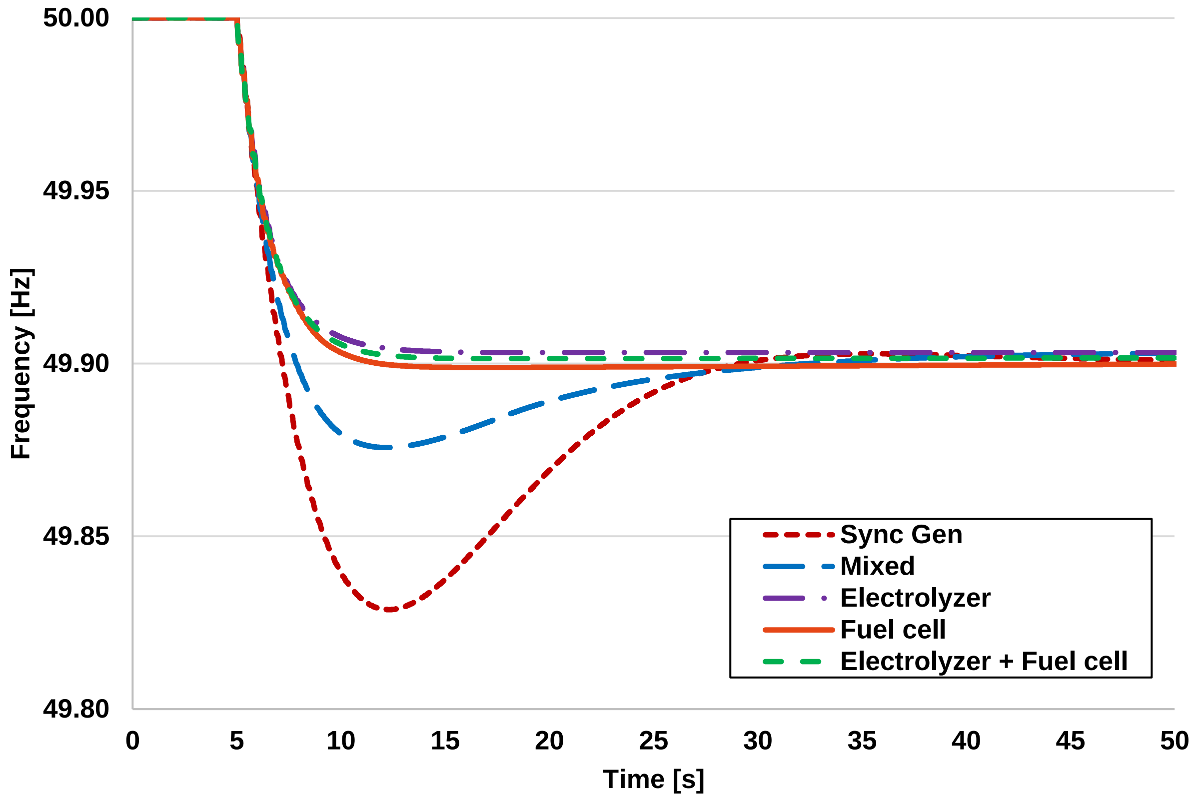

Figure 5.6. Frequency response for load demand increase

5.1.4. 30 MW decrease in load demand

The decrease is represented by a step decrease at $(t = 5\,s)$ in the load connected to the Eemshaven 380 kV bus in Figure 5.1. The load demand is decreased from the default P value of 725.6 MW to 695.6 MW. The frequency response of the system is identical to the case of the increase in wind generation as shown in Figure 5.7.

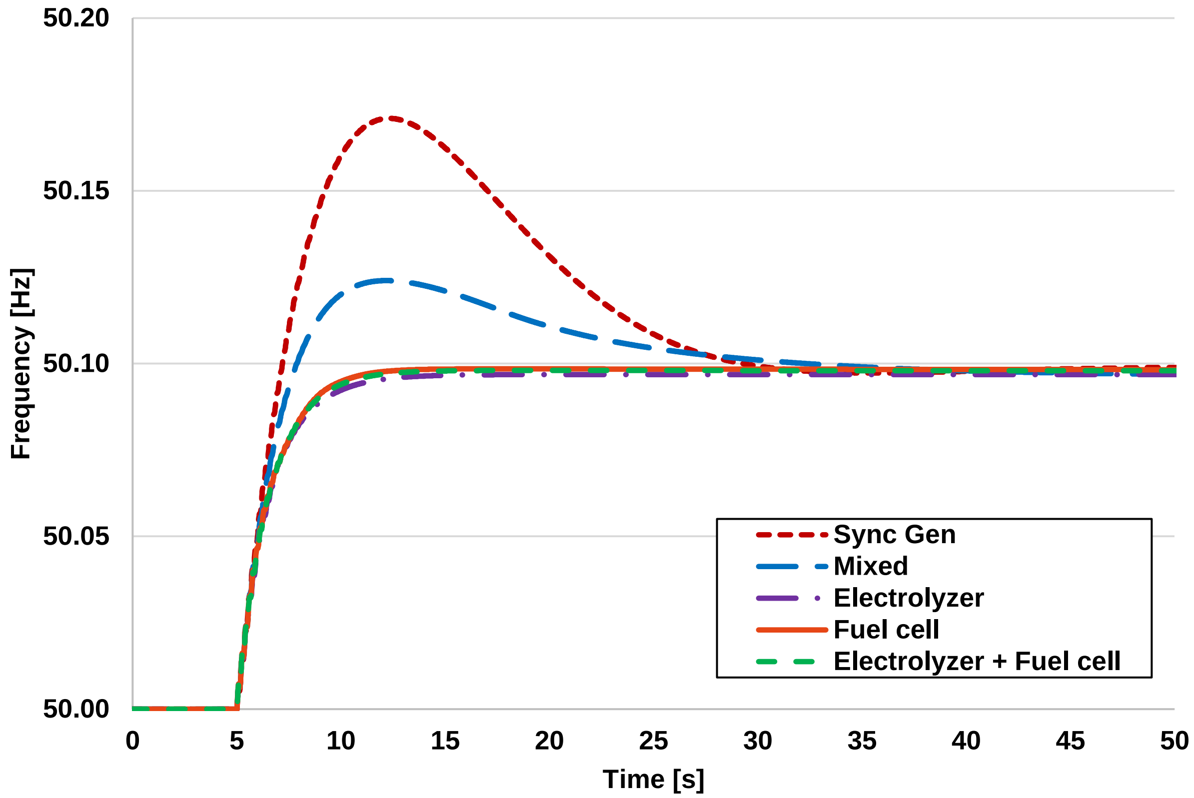

Figure 5.7. Frequency response for load demand decrease

In General, the PEM fuel cells and electrolyzers are capable of providing primary frequency support through an FCR bid. They are capable of providing upward and downward support according to the frequency deviation. Further, they are capable of improving the frequency response of the power system by reducing the frequency nadir due to their ability for faster active power injection when compared to traditional synchronous generators under the same operating conditions. Also, as expected the type of generation-load demand imbalance does not matter since the effect is the effect on frequency is the same.

5.2. Line Outage

The next type of disturbance to be studied is the outage of lines between the different area of the network. For this disturbance, there will be 100 MW of FCR support divided between the two sides of the line.

5.2.1. Outage of one line from Netherlands to Germany

One of the lines between Netherlands and Germany will be taken out of service at $(t = 5\,s)$ as shown in Figure 5.8. The FCR support will be once with 50 MW of synchronous generation on each side of the outage and once with Fuel cells and electrolyzers with the same 50 MW for FCR support.

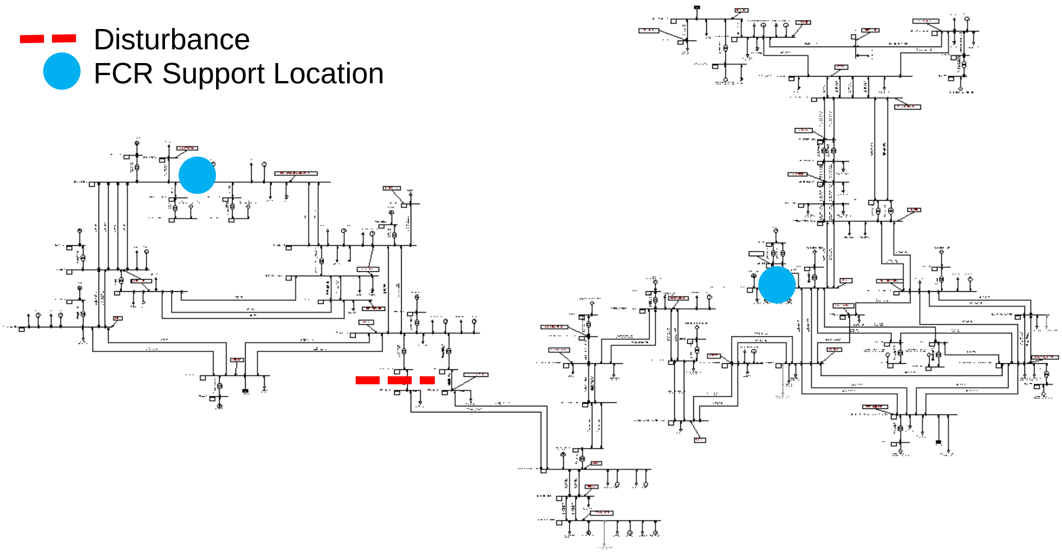

Figure 5.8. Location of line outage of NL-DE line and FCR support

The system response for both cases is shown in Figure 5.9. The disturbance due to the loss of one line does not cause significant change in the frequency. The dead band for the fuel cell and electrolyzers had to be disabled in order for the devices to react to the change in frequency. It is noticeable however that even with such a small disturbance the PEM devices provide an improved frequency response when compared to synchronous generators which is due to the PEM fuel cells and electrolyzers fast power injection.

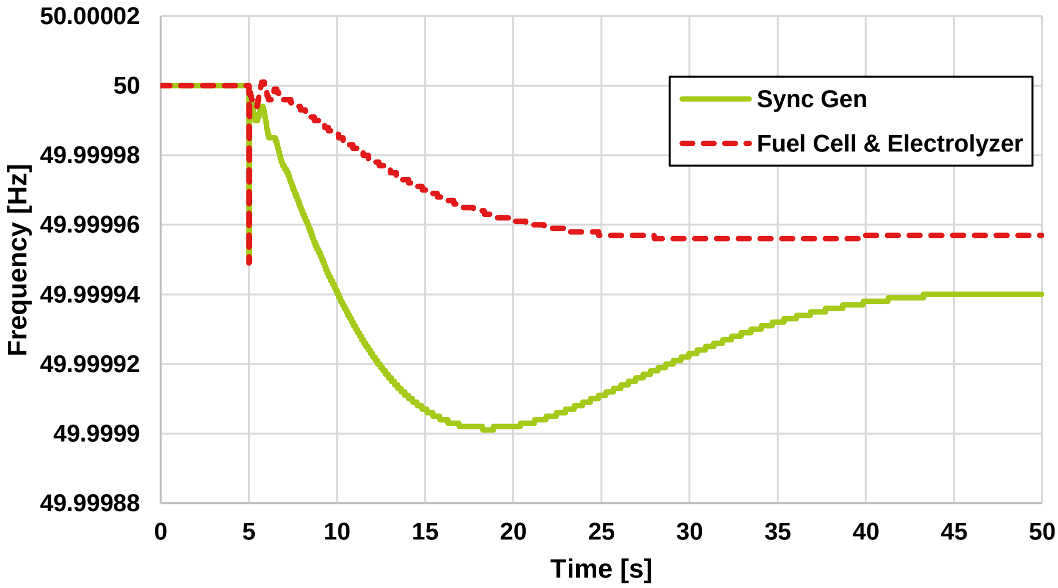

Figure 5.9. Frequency Response for line outage between Netherlands and Germany

5.2.2. Outage of lines from Germany to Denmark

Three of the four lines between Germany and Denmark will be taken out of service one by one at $(t = 5\,s)$ as shown in Figure 5.10. The FCR support will be once with 50 MW of synchronous generation on each side of the outage and once with Fuel cells and electrolyzers with the same 50 MW for FCR support.

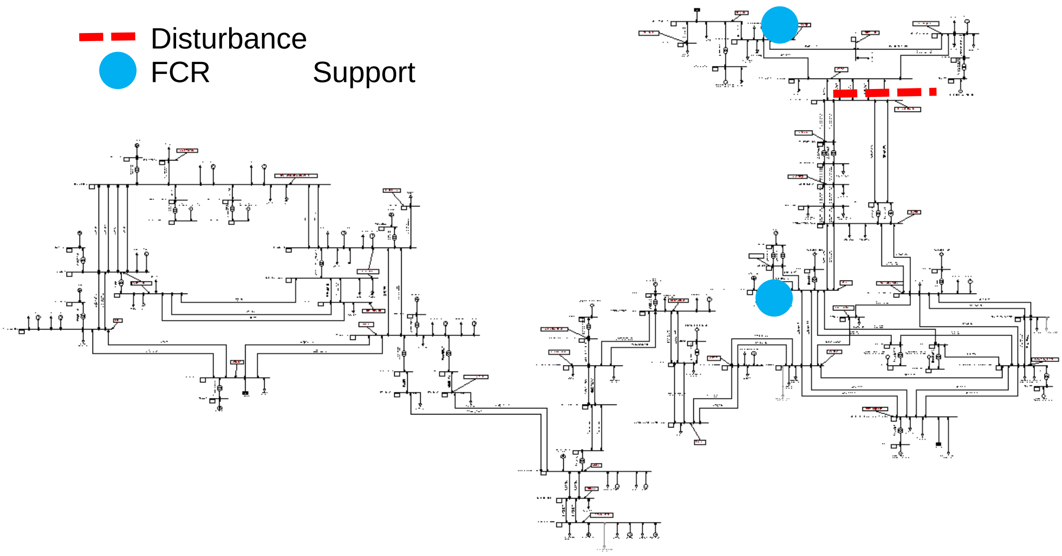

Figure 5.10. Location of line outages of DE-DK line and FCR support

The system response for both cases is shown in Figure 5.11. Similar to the previous case, the disturbance due to the loss of one line and up to three lines does not cause significant change in the frequency. The dead band for the fuel cell and electrolyzers also had to be disabled in order for the devices to react to the change in frequency. Contrary to the previous case, the synchronous generator support results in lower frequency deviation when compared to the PEM technologies. This is due to the power dead band used in the power controller for the PEM fuel cell as shown in Figure 3.5. Such small deviation in frequency results in a small power output that is partially filtered by the previously mentioned dead band. However, at such low frequency deviation values, the results are inconclusive which FCR support is more effective.

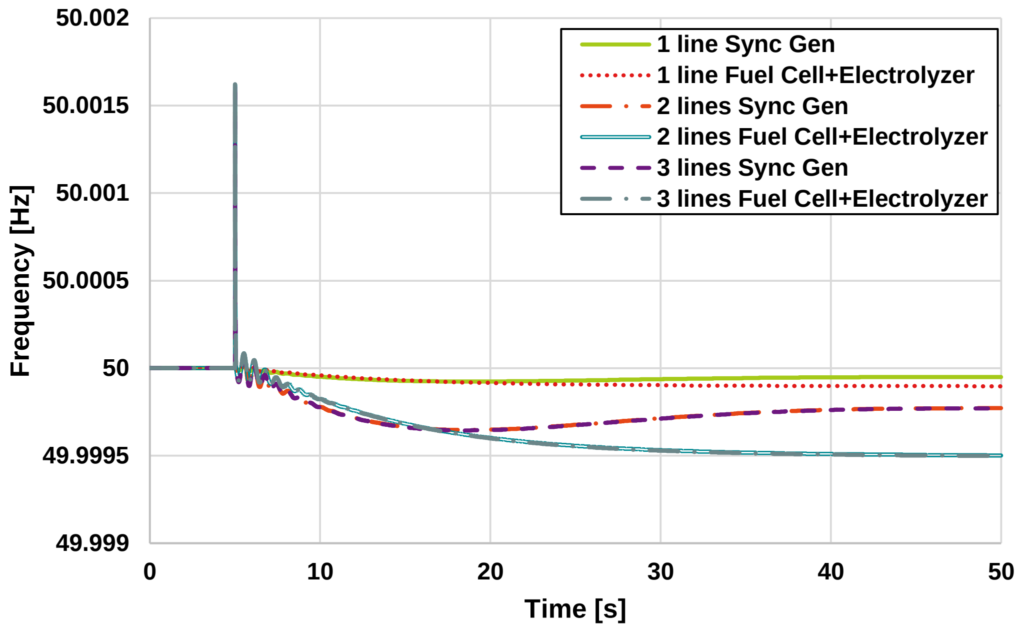

Figure 5.11. Frequency Response for line outage between Germany and Denmark

5.3. Disconnection Between Two Areas

5.3.1. Disconnection of the Netherlands

The power flow between Netherlands and Germany is the import of 67.6 MW of active power from Germany to the Netherlands and 559.4 of reactive power export from the Netherlands to Germany. At $(t = 5\,s)$ the lines between the Netherlands and Germany will be disconnected and there will be 100 MW of FCR support by electrolyzers and fuel cells on both sides as shown in Figure 5.12.

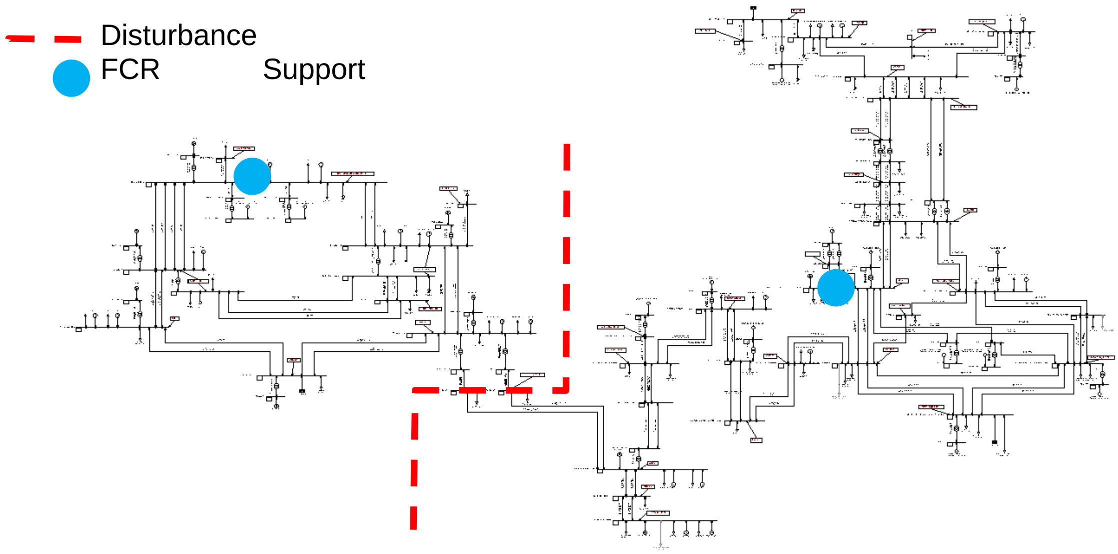

Figure 5.12. Location of the disconnection of the Netherlands and FCR support

The frequency response for the separated areas of the interconnected network are shown in Figure 5.13. Due to the disconnection, a power imbalance is created at the two separated areas. In Germany, the frequency increases due to the loss of load while in Netherlands the frequency decreases due to the loss of generation. The difference in inertia between the two areas causes the two areas to have different initial response in the first 10 seconds. Also, the difference in the steady state value frequency deviation is less than 10 mHz which is within frequency dead band.

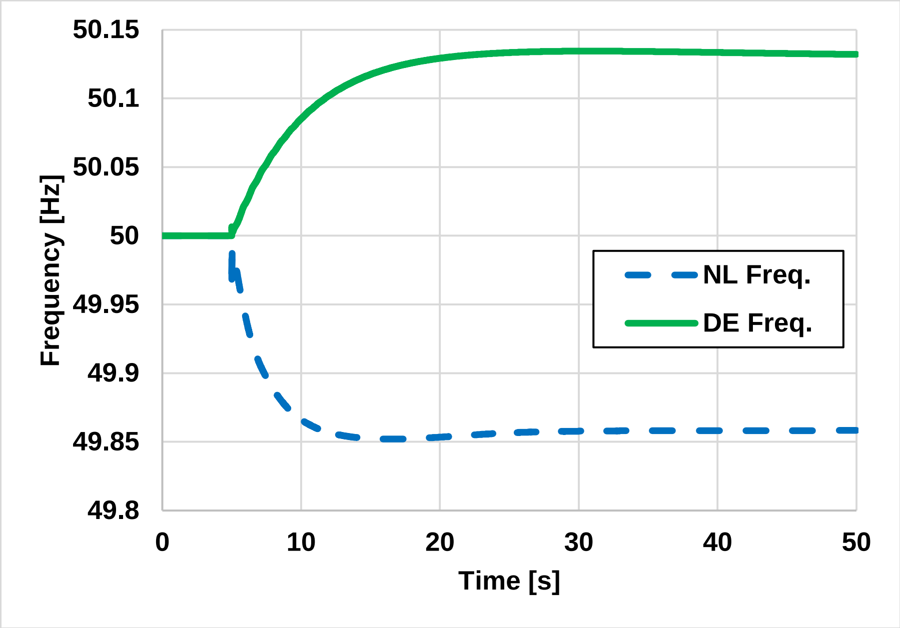

Figure 5.13. Frequency response for disconnection of the Netherlands

5.3.2. Disconnection of Denmark

The power flow between Denmark and Germany is the import of 1576 MW of active power from Germany to the Denmark and 707 MW of reactive power export from Denmark to Germany. At $(t = 5\,s)$ the lines between the Denmark and Germany will be disconnected and there will be 100 MW of FCR support by electrolyzers and fuel cells on both sides as shown in Figure 5.14.

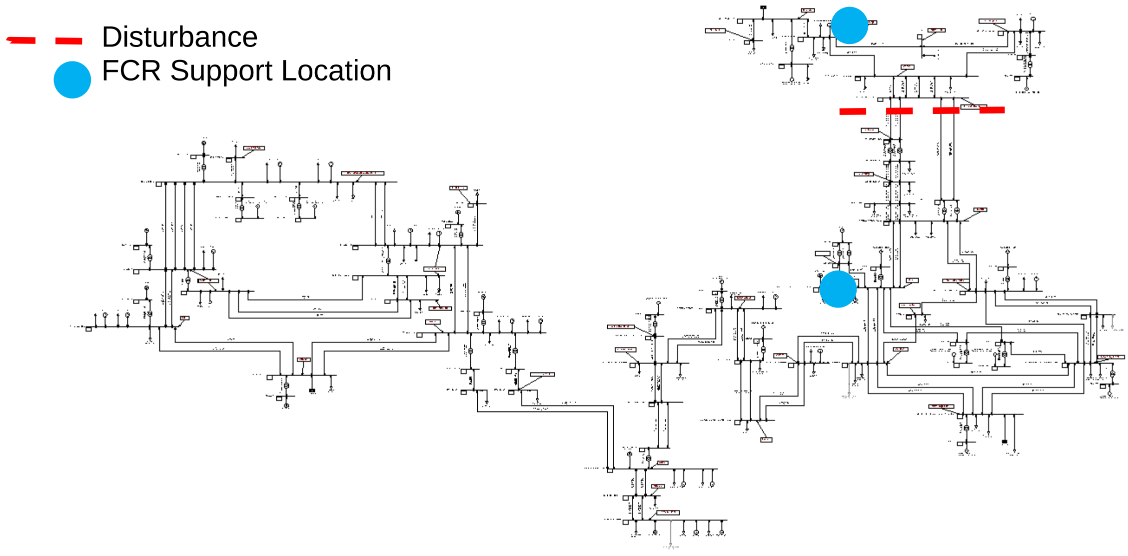

Figure 5.14. Location of the disconnection of Denmark and FCR support

The disconnection of Denmark and Germany causes the frequency of both areas to deviate with Denmark frequency falling rapidly as shown in Figure 5.15. This causes the system to operate in emergency mode which at minimum results in pole slips or load shedding or at worst cause a blackout. In this case, there is no load shedding or generation disconnection, so the system should not converge. However, PowerFactory tries to maintain system operation even when the frequency is beyond the realistic operating range. The capacity of PEM fuel cells and electrolyzers even in the foreseeable future cannot provide support for disconnection with high inter-area power flow.

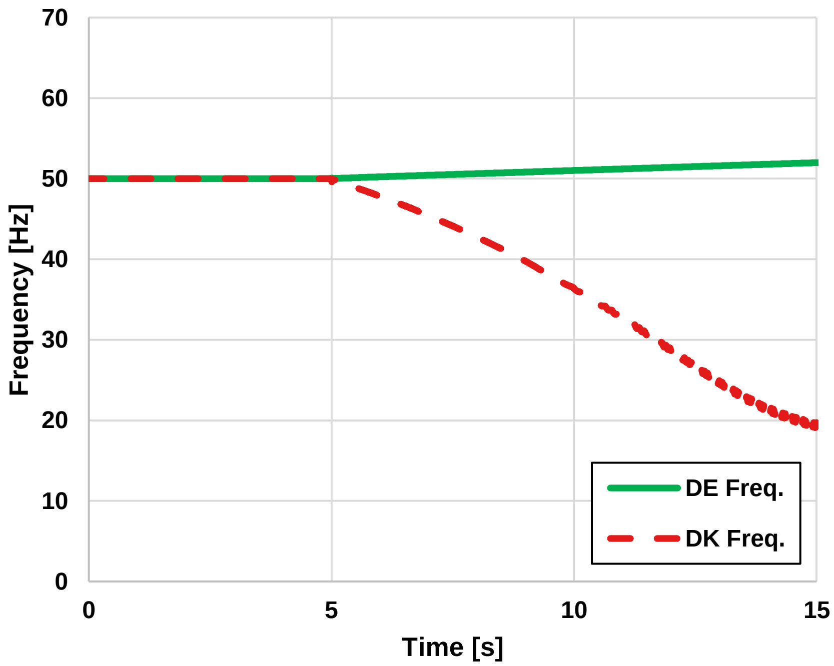

Figure 5.15. Frequency response for disconnection of Denmark

In general, PEM fuel cell and electrolyzers showed capability to effectively participate in the FCR market and to support the frequency of the power system for different system disturbances. In particular, the PEM fuel cells and electrolyzers showed improved primary frequency response due to sudden changes in power balance when compared to the synchronous generators. This is due to the PEM fuel cells and electrolyzers ability to change their operating point rapidly, in less than 1s [65, 66], compared to the slower synchronous generators.

6. Sensitivity Analysis

This chapter studies how changes in the power network and changes in the control parameters can affect the performance of the PEM fuel cell and electrolyzers in providing FCR support to the system. In all the simulations, only one parameter will be changed while all others are held constant. These sensitivities can be categorized into two categories: network conditions and control parameters. In this chapter, only PEM fuel cells and electrolyzers will contribute to the FCR except in one case where the performance of PEM technologies is compared to the synchronous generators.

The different sensitivities will be tested for one disturbance which is a connection of an 80 MW load at $(t = 5\ s)$. This causes sufficient frequency deviation that allows to study the primary frequency response in the FCR market while maintaining the deviation within the 200 mHz full bid activation frequency deviation. The FCR support will be through a 50 MW bid from the PEM fuel cell and 50 MW bid from the PEM electrolyzer which are just sufficient to contain the frequency deviation without exceeding the 200 mHz full bid activation frequency deviation. As in the previous chapter, the initial load flow is maintained the same.

6.1. Location from disturbance

To test the effect of the location of the fuel cells and electrolyzers on the frequency response, PEM fuel cells are both added to the same bus at four different locations in the network with 50 MW FCR bid for each. Only one fuel cell and electrolyzer pair will be activated and the location of the participating fuel cell and electrolyzer is changed for each simulation. Figure 6.1 shows the different locations tested and the location of the disturbance.

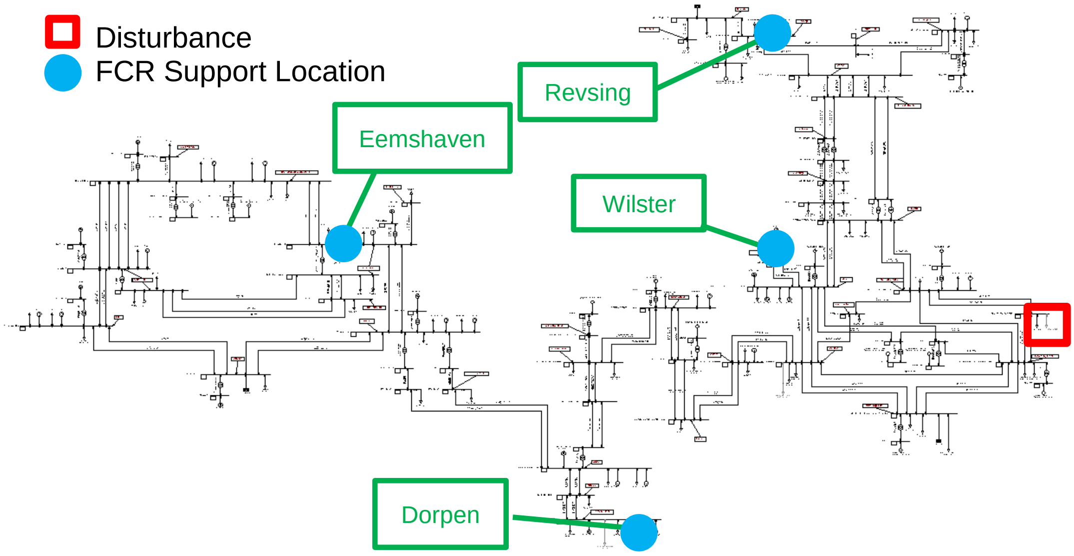

Figure 6.1. Disturbance and FCR support for location sensitivity

The results of the simulations in Figure 6.2 show that there is no difference in the frequency response when the location of the fuel cell and electrolyzer have been changed. This is expected because the driving factor for the frequency performance is the balance between generation and load demand and irrespectively from where the additional generation is coming from or where the disturbance is.

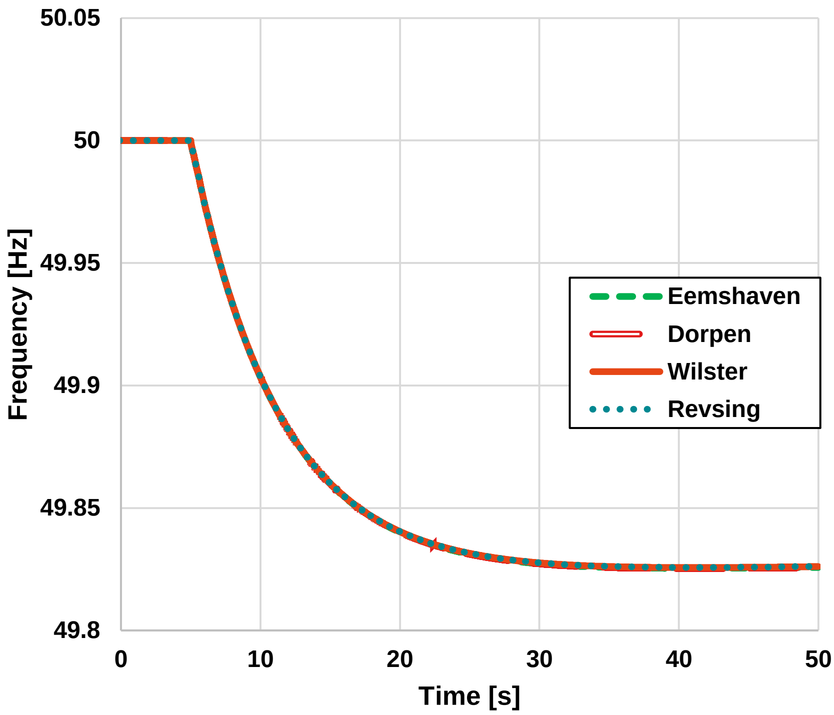

Figure 6.2. Frequency response for location sensitivity

6.2. Distribution vs. concentration

To test the effect of the concentration and the distribution of the FCR support on the frequency response of the system, the simulation will be run once with one fuel cell and one electrolyzer at the same bus with 50 MW FCR bid for each of them. Then, the same disturbance will run but with 10 fuel cells and 10 electrolyzers that each pair will be in the same bus and will have 5 MW FCR bid for each device. The layout of this test is shown in Figure 6.3.

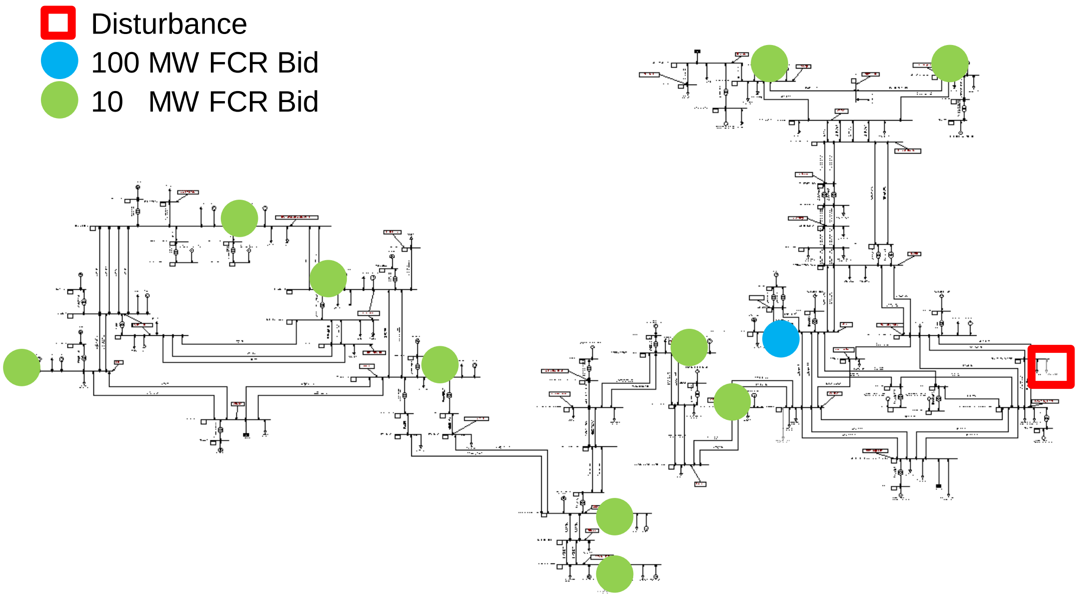

Figure 6.3. Disturbance and FCR support for distribution sensitivity

The results of the simulations in Figure 6.4 show that there is no difference in the frequency response between concentrated or distributed frequency support. This is also expected because the driving factor for the frequency response is the balance between generation and load demand and irrespectively where the additional generation is coming from one location or multiple locations.

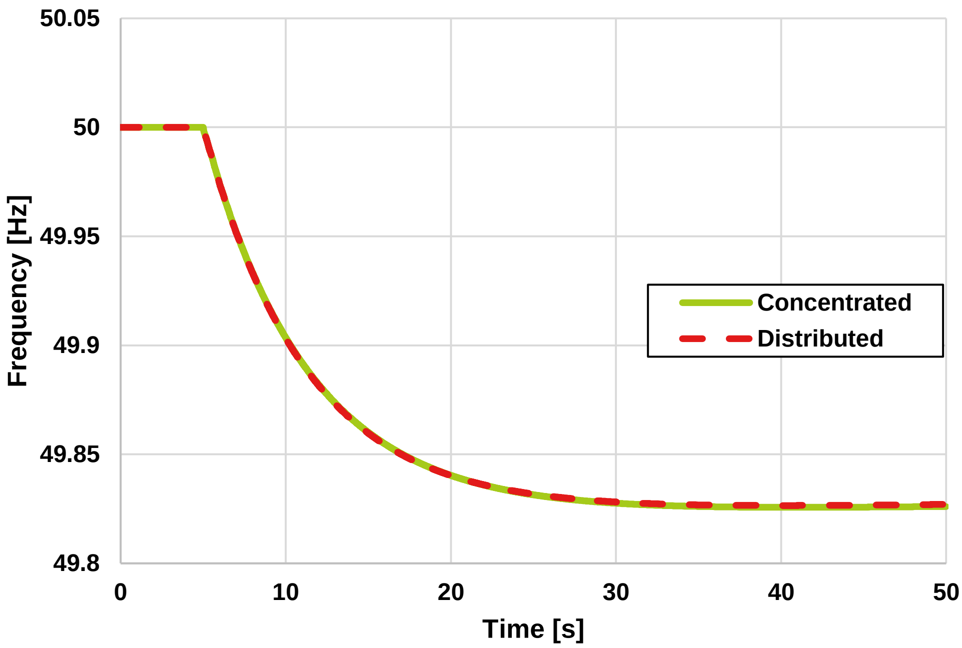

Figure 6.4. Frequency response for distribution sensitivity

6.3. Size of network

In order to evaluate the effect of changing the network size on the frequency response and the performance of the fuel cells and electrolyzers, the size of the network will be changed while maintaining the same inertia and the initial generation-load balance. The load flow in each case will be maintained by placing a constant load to represent the steady state power flow between the network and the disconnected part. The system inertia is assumed constant by adding the inertia value ***H*** of the removed generators to the generators that remain connected. The size of the network will be gradually reduced as shown in Figure 6.5. In the system the Frequency reserve is 100 MW and the disturbance applied is connecting 80 MW load at $(t = 5\,s)$.

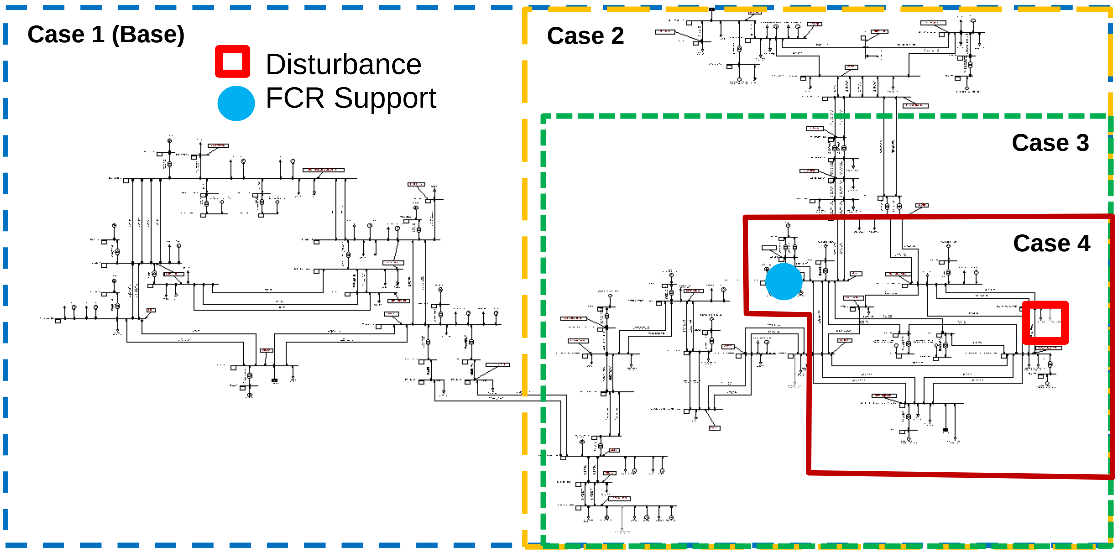

Figure 6.5. Network size change for network size sensitivity study

The resulting frequency response shown in Figure 6.6 demonstrate that reducing the size of the network while maintaining the same inertia and load flow does not affect the ability of fuel cells and electrolyzers to support the frequency and does not change the frequency response for changes in generation and loading balance.

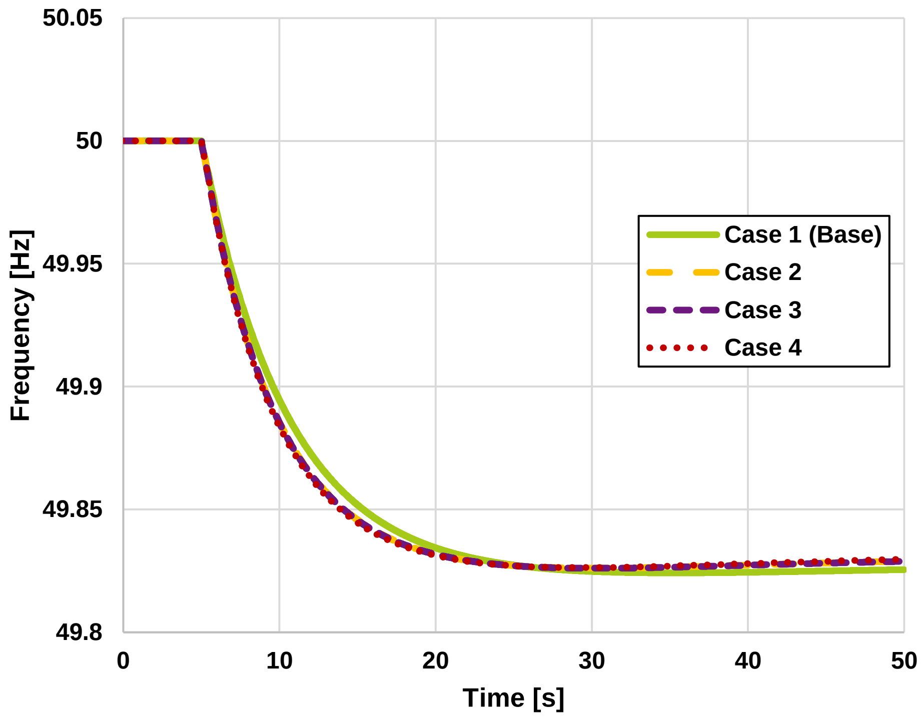

Figure 6.6. Frequency response for network size sensitivity

6.4. Reduction in inertia

This section addresses the ability of the fuel cells and electrolyzers to support the frequency with decreasing inertia. The inertia in the system is calculated by adding the inertia value ***H*** of all the synchronous generators and the external grid which sums up to 52 s. This value is considered high and it is due to the presence of 14 synchronous generators which is a relatively large number for the size of the network. The inertia in the system is decreased to simulate the expected future reduction of inertia due to phasing out of more synchronous generators and replacing them with renewable sources which in this area around the North Sea are assumed to be mainly wind generation. The inertia is decreased by reducing the inertia of all synchronous generators and the connected external grid. The synchronous generators in the system are kept working with the same power dispatch to maintain the same load flow in the network and to maintain their contribution to the reactive power generation and voltage level control in all cases. The intention here is to reduce the inertia while maintaining all other factors constant. The system will be subjected to the same disturbance as in the previous sections which is connecting an 80 MW load at $(t = 5\,s)$ and FCR support will be 50 MW by PEM fuel cell and 50 MW by PEM electrolyzer as shown in Figure 6.7. The summary of the inertia changes and the frequency nadir is shown in Table 6.1.

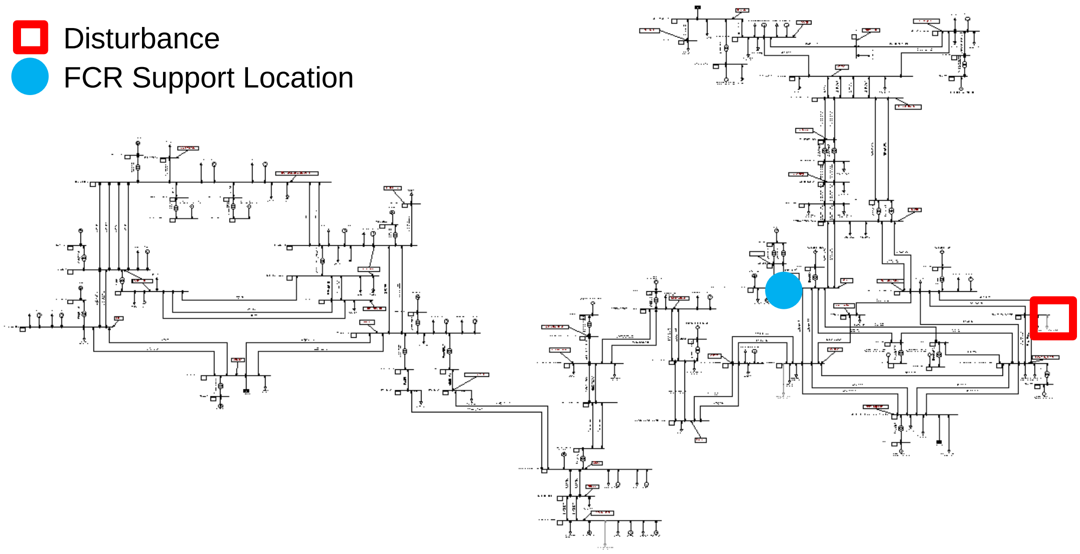

Figure 6.7. Disturbance and FCR support location for system inertia reduction

Table 6.1. Frequency response to increase in load for different system inertia values with FCR support from PEM fuel cells and electrolyzers

Nº	Case	System inertia	Nadir [Hz]	RoCoF [mHz/s]
(1)	100% Inertia (Base Case)	52 s	49.83	26.74
(2)	50% Inertia	26 s	49.83	53.41
(3)	27% Inertia	14 s	49.82	100.14
(4)	17% Inertia	9 s	49.82	166.95
(5)	11% Inertia	5.5 s	49.81	276.55

The frequency response shown in Figure 6.8 shows that in the base case the high inertia in the system controls the initial response of the system and causes the frequency deviation to be gradual thus reducing the RoCoF which is desired. However, at the same time this gradual change in frequency causes the response of the fuel cells and electrolyzers and the change in power setpoint to be gradual as well which means the fast response of these devices will not be utilized. Then, as the inertia is reduced, only the RoCof increases because the inertia still controls the frequency response for the first seconds even in cases (2) and (3). When the inertia is reduced significantly as in the cases (4) and (5), the fast response of the fuel cells and electrolyzers becomes significant and fast power injection keeps the frequency nadir close to the value of nadir obtained in case (1), with the full inertia of the system, within 5 seconds. However, the RoCoF deteriorates significantly (up to a value of 276 mHz/s for the lowest inertia) and oscillations are observed due to the reduced inertia of synchronous generators. The power output of the PEM fuel cell shown in Figure 6.9 shows that the PEM fuel cell injects fast active power according to the frequency deviation. This becomes clearer in the case of lowest inertia where the frequency deviation becomes very steep and the power output of the PEM fuel cell reaches its maximum value within the first second after the disturbance.

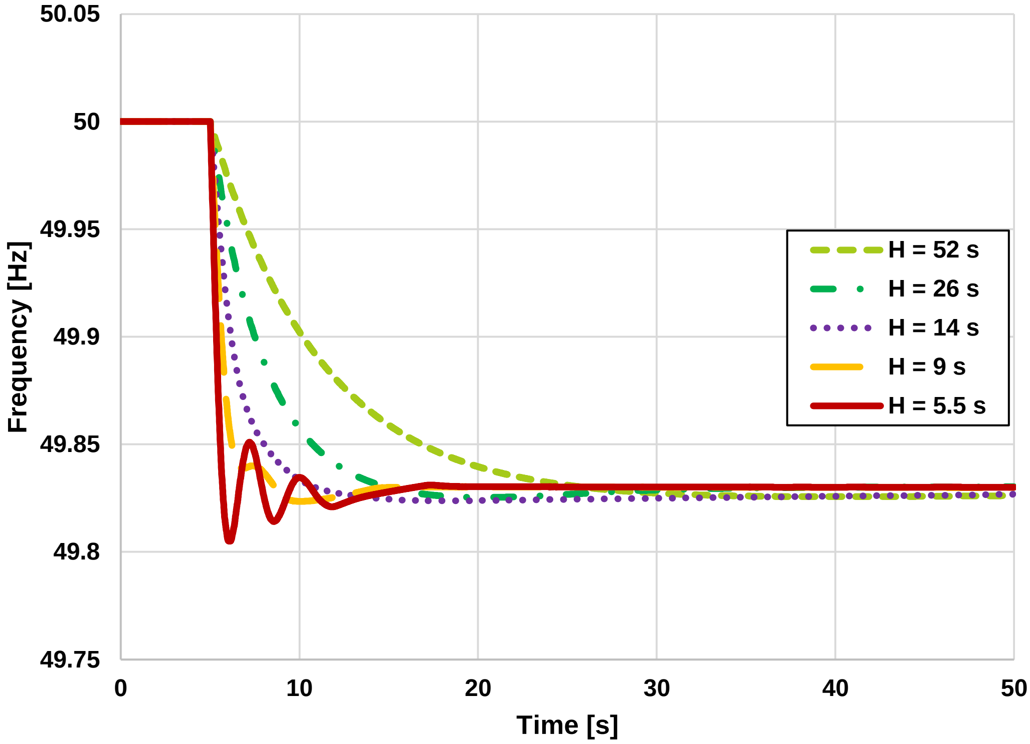

Figure 6.8. Frequency response for inertia reduction sensitivity

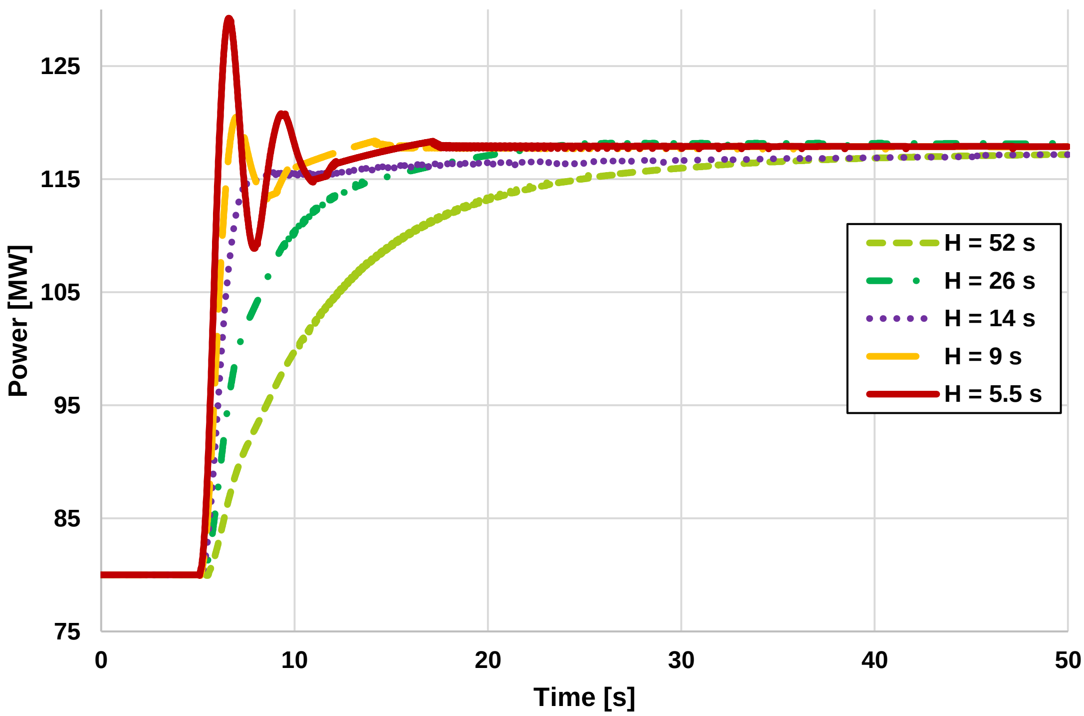

Figure 6.9. Power output by PEM fuel cell for different inertia levels

The effect of the fast power injection of the fuel cells and electrolyzers can be better observed when comparing their frequency response to the response of an equal FCR bid (100 MW) from a synchronous generator. The disturbance is simulated again for two new cases but with FCR support solely from a synchronous generator at the same bus for the full system inertia value of 52 s, Case (6), and for a reduced system inertia of 26 s, case (7). The frequency response from these new cases is compared with the frequency response for case (1) and case (2) in Table 6.2 and Figure 6.10.

Table 6.2 Comparison of frequency response for FCR support from PEM devices and synchronous generator to increase in load for two system inertia values.

Nº	Case	System inertia	FCR Support	Nadir [Hz]	RoCoF [mHz/s]
(1)	100% Inertia (Base Case)	52 s	50 MW fuel cell + 50 MW electrolyzer	49.83	26.74
(6)	100% Inertia Sync. Gen	52 s	100 MW synchronous generator	49.78	26.74
(2)	50% Inertia PEM devices	26 s	50 MW fuel cell + 50 MW electrolyzer	49.83	53.41
(7)	50% Inertia Sync. Gen	26 s	100 MW synchronous generator	49.69	53.82

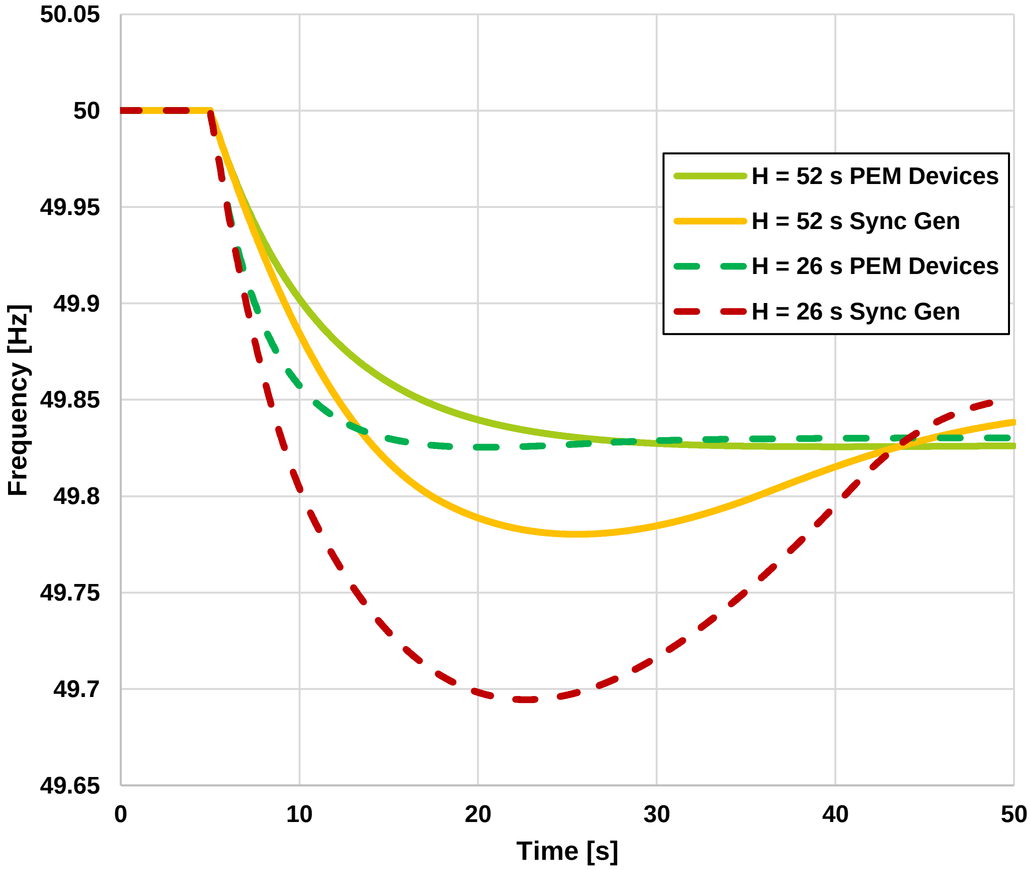

Figure 6.10. Comparison of PEM technologies and synchronous generators frequency response for inertia sensitivity

As shown in Figure 6.10, the inertia response dominates the first few seconds then the support of the FCR becomes significant gradually while the inertia's effect diminishes. This can be observed by the identical response for the PEM devices and the synchronous generator for the first two seconds after the disturbance and the divergence afterwards when the PEM devices activate their FCR bid faster than the synchronous generator. The fast power injection by the fuel cell and electrolyzer results in a smaller nadir and less sever drop in frequency. The difference in the response, mainly in frequency nadir, between the fuel cells and electrolyzers and the synchronous generators becomes more prominent as the inertia decrease as in the case of the 26 s inertia. This means that the fuel cells and electrolyzers provide faster and more effective primary frequency support to keep the nadir within acceptable value under low inertia conditions.

6.5. Increase of FCR bid value

This section addresses the effect of increasing the FCR bid capacity for PEM devices from the used value of 100 MW (50 MW for fuel cell and 50 MW for electrolyzer). For this purpose, additional fuel cells and electrolyzers will participate in the FCR market as shown in Figure 6.11. As demonstrated previously in Section 6.2 on page 54, distributing the FCR support will not affect the frequency performance and can be considered as one large FCR bid. The system will be subjected to a disturbance by connecting an 80 MW load at ($t = 5\,s$) and the total FCR bids will increase from 100 MW to 200 MW, 300 MW and 400 MW by activating more PEM devices.

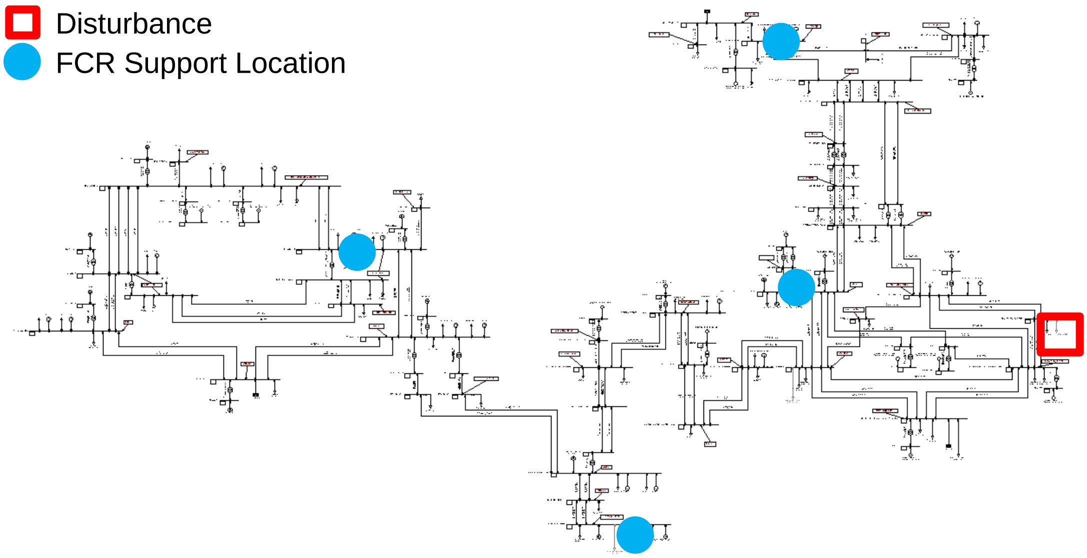

Figure 6.11. Disturbance location and FCR support locations for increasing FCR bid

The system frequency response shown in Figure 6.12 shows that increasing the FCR results in improved frequency response for the system and resulted in smaller nadir. This is expected since the same generation-load imbalance results in the same frequency deviation. However, increasing the FCR means that for the same frequency deviation value, the amount of power injected by the PEM devices is increased. For example, doubling the FCR from 100 MW to 200 MW results in doubling the power injection by the PEM devices which will result in a significantly smaller nadir. Further increasing the FCR reduces the value of the nadir but for the same generation-load imbalance of 80 MW, every addition of 100 MW to the FCR results in a smaller improvement to the nadir than the previous case.

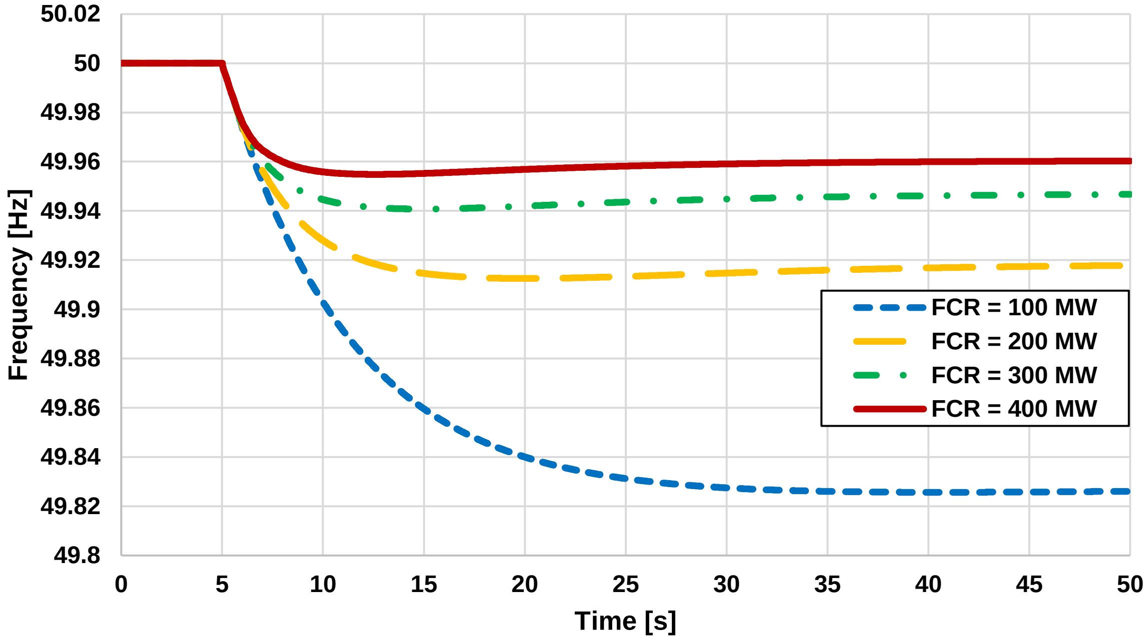

Figure 6.12. Frequency response for increasing FCR bid value

In order to further investigate how increasing the bid value can improve the response in a system with decreasing inertia. The same imbalance of 80 MW increase in load will be applied to the system at $(t = 5\ s)$. First the inertia of the system will remain at 52 s and the FCR will remain at 100 MW. Then the FCR will be increased to 400 MW while maintaining the same inertia at 52 s. After that, inertia of the system will be decreased to 5.5 s while the FCR remains 400 MW as shown in Table 6.3.

Table 6.3 Frequency response to increase in load for different FCR support from PEM fuel cells and electrolyzers at different system inertia values

Nº	**Case**	**System inertia**	**FCR Support**	**Nadir [Hz]**	**RoCoF [mHz/s]**
(1)	100% Inertia (Base Case)	52 s	50 MW fuel cell + 50 MW electrolyzer	49.83	26.86
(2)	100% Inertia, 400 FCR	52 s	200 MW fuel cells + 200 MW electrolyzers	49.95	26.48
(3)	11% Inertia, 400 FCR	5.5 s	200 MW fuel cells + 200 MW electrolyzers	49.91	185.56

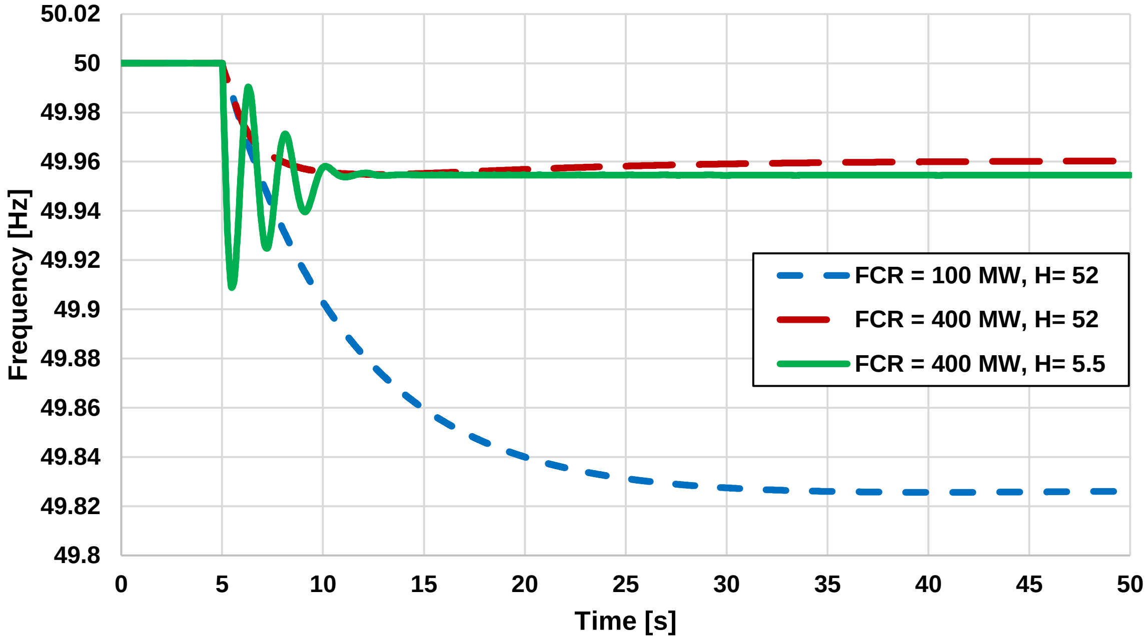

Figure 6.13. Frequency response for increasing FCR bid value with decreasing inertia

The frequency response from Figure 6.13 shows that even with minimum level of inertia, the frequency response is improved when the FCR bid value by PEM devices is increased. The the initial oscillations are due to the low inertia in the system. The results give an indication that one of the possible solutions to frequency stability in low inertia systems is the increase in primary frequency support by fast acting devices such as PEM fuel cells and electrolyzers which is effective in keeping acceptable value of nadir, but more research is needed on how to deal with deterioration of RoCoF.

6.6. Frequency droop control change

This section addresses the effect on the frequency response due to changing the droop value of the fuel cells and electrolyzers frequency control shown in Figure 3.3 on page 17 and Figure 3.12 on page 26, respectively. The droop of the frequency controller is defined by equation (6.1).

$$\Delta\mathrm{P} = \left(f - f_{ref}\right) \times \frac{\text{Bid value [MW]}}{\text{Maximum Frequency Deviation [Hz]}} \tag{6.1}$$

$$\text{droop} = \frac{1}{\text{Maximum Frequency Deviation [Hz]}} \tag{6.2}$$

The decrease in the maximum frequency deviation means increasing the frequency droop which means that more power will be injected for the same frequency deviation. The system is subjected to a sudden 80 MW increase in load at ($t = 5\,s$) and the system inertia is maintained at 52 s. Figure 6.14 shows the location of the disturbance and the FCR support by PEM fuel cell and electrolyzer.

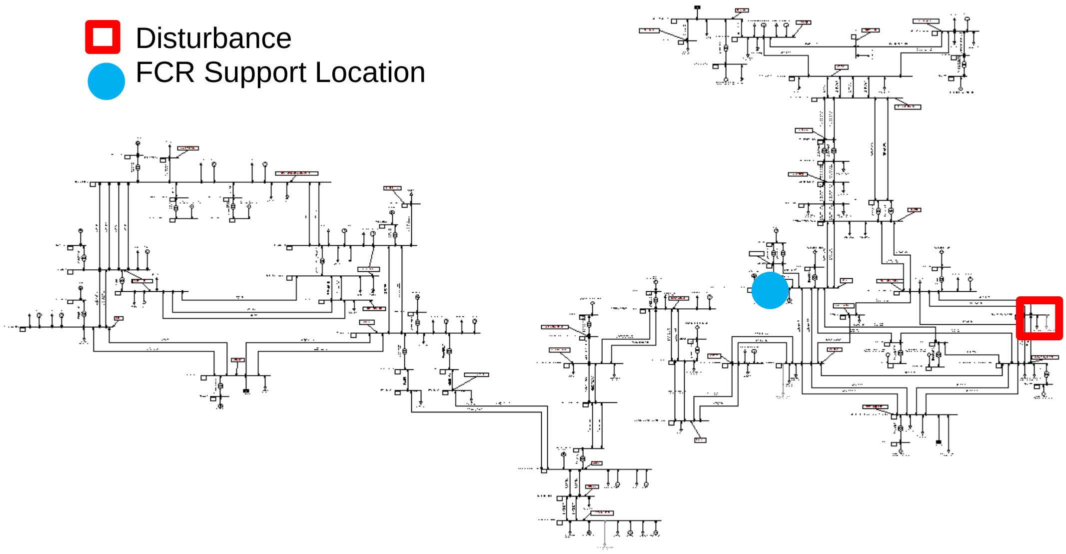

Figure 6.14. Disturbance and FCR support location for frequency droop sensitivity

The frequency response from Figure 6.15 shows that increasing the frequency droop will have identical effect to increasing the FCR bid size shown in Figure 6.12 since the output power in both cases is defined by the same equation (6.1). Similar to doubling the FCR bid value, doubling the droop value results in doubling the power injection by PEM devices for the same frequency deviation value. This indicates that another possible way to ensure acceptable nadir will be by increasing the frequency droop or in other terms narrowing the full bid frequency deviation. The effect on RoCoF remains the same, even with the higher droop for PEM fuel cells and electrolyzers.

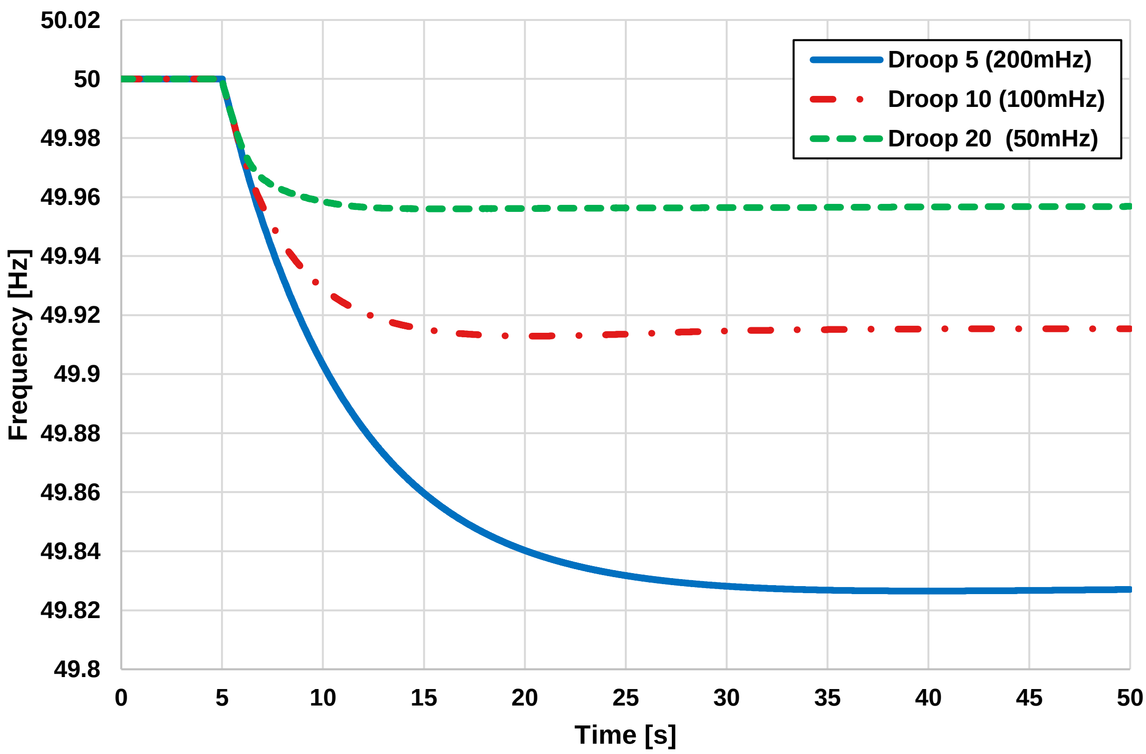

Figure 6.15. Frequency response for increasing frequency droop value

6.7. Frequency dead band

This section addresses the effect on the frequency response due to changing the dead band value of the fuel cells and electrolyzers frequency control shown in Figure 3.3 on page 17 and Figure 3.12 on page 26, respectively. The dead band value allowed by the current Dutch market regulation is 10 mHz. this value will be will be reduced to 5 mHz and 0 mHz and then increased to 20 mHz. The system is subjected to a sudden 80 MW increase in load at $(t = 5\,s)$ and the system inertia is maintained at 52 s. The location of the disturbance and the FCR support by PEM fuel cell and electrolyzer is shown in Figure 6.16.

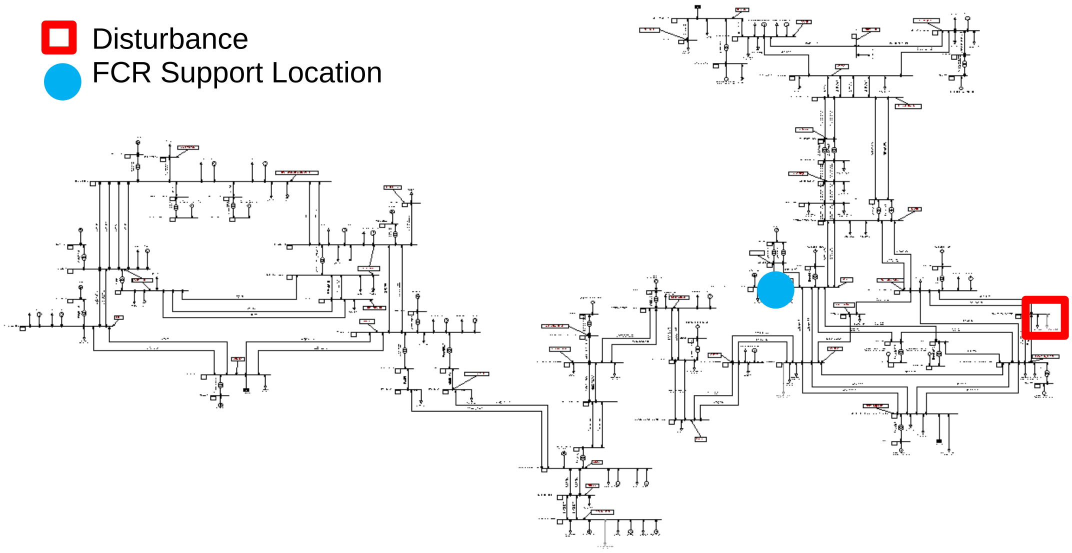

Figure 6.16. Disturbance and FCR support location for frequency dead band sensitivity

The frequency response in Figure 6.17 is the same irrespectively of the used dead band. This is expected as the inertial response by the synchronous generators in the system is dominant for the first few seconds. During these initial seconds, the frequency deviation increases beyond the dead band which means by the time the primary frequency support by the FCR becomes dominant, the frequency deviation is already significantly higher than the dead band.

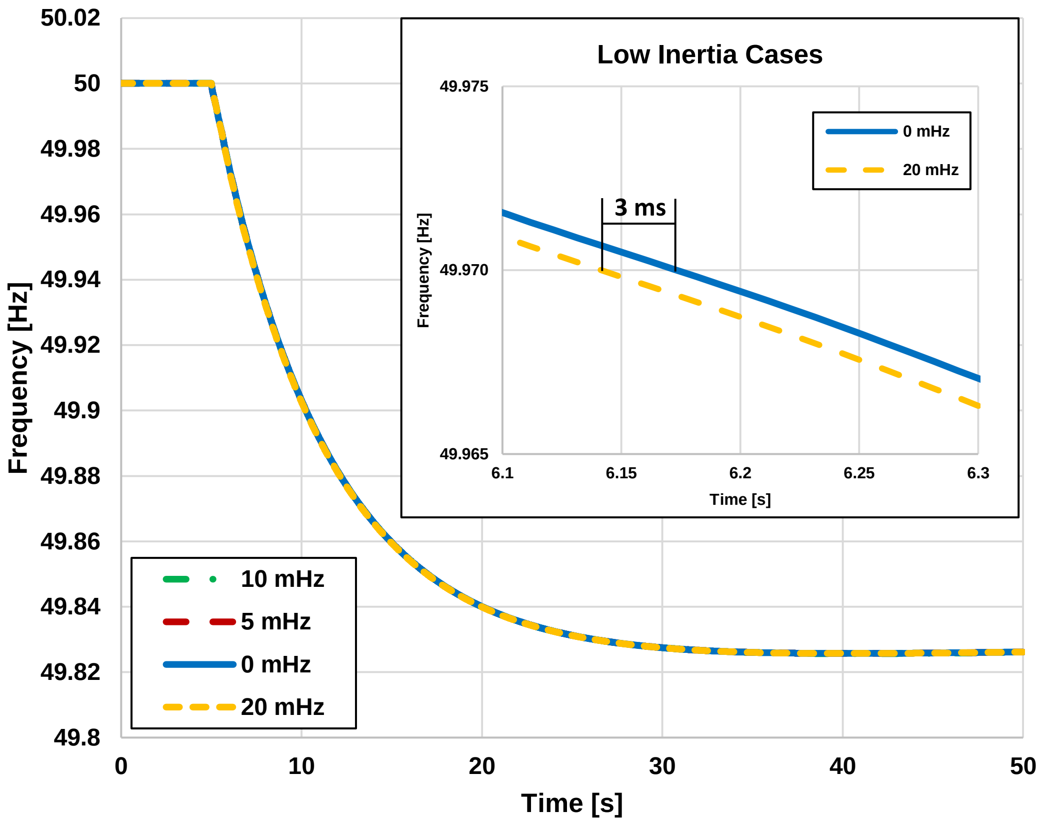

Figure 6.17. Frequency response for changing frequency dead band

The same simulation is repeated but with significantly reduced inertia from H = 52 s to H = 5.5 s and there is only a small delay of 3 ms in the response between the most extreme cases of 0 mHz dead band and 20 mHz as shown in the zoom in the embedded small plot in Figure 6.17. This delay is only present during the containment period and the steady state value remains the same. This shows that the value of the dead band does not significantly change the frequency response due to a generation-load imbalance that causes a substantial frequency deviation. Increasing the dead band beyond 20 mHz is not a realistic scenario since it will exceed 10% of the full bid activation frequency deviation mentioned in section 2.3 on page 7.

In this chapter it was demonstrated that the frequency support provided by PEM fuel cells and electrolyzers is not affected by considering different situations (e.g. operational scenarios and disturbances) in the power system. In fact, PEM technologies can provide an improved frequency response in terms of guaranteeing acceptable value of nadir when participating in FCR market in case of decreasing inertia. It is also shown that the frequency response can be improved by increasing the FCR bid value of the PEM fuel cells and electrolyzers or by increasing the frequency droop control.

7. Participation in Frequency Restoration

This chapter studies at a basic level the capability of hydrogen technologies to modify power output according to an external signal. These external signals could represent a bid activation for Frequency Restoration Reserve (FRR) or a redispatch signal from the network operator. First, the model for the frequency control needs to be modified to allow for such control signal and then the new model will be tested against few cases where the effectiveness can be tested.

7.1. Model modification

The model for the fuel cell and electrolyzer is slightly modified to allow for the provision of an external signal to increase or decrease the set point for active power. This modification is done to the frequency controller, as shown in Figure 7.1, which defines the power reference for the dynamic model.

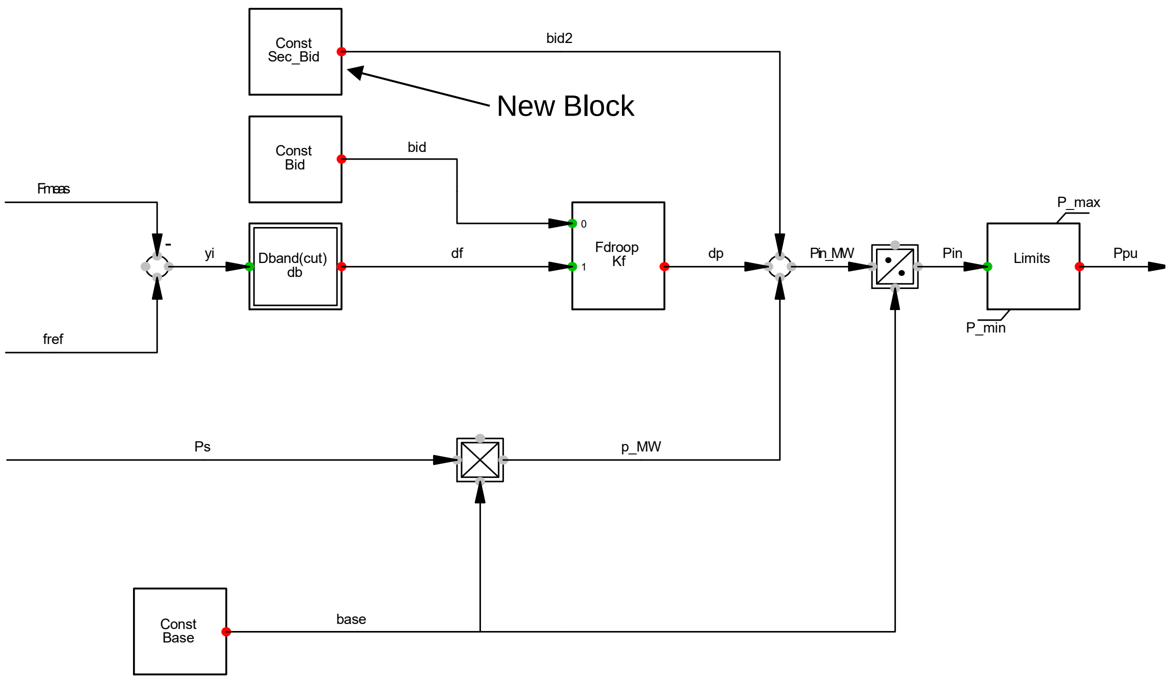

Figure 7.1. Modified frequency control for FRR

Here, a new constant signal “Sec_Bid” is added to the model to represent the FRR bid by the PEM fuel cell or electrolyzer. This signal is added to the sum of the reference power and the power for frequency containment to give the power set point for the device.

The FRR bid is activated through an external signal by the system operator. This activation signal will be simulated by modifying the constant value “Sec_Bid” through a parameter event programmed in PowerFactory. The activation of this signal will be only after the frequency change is contained and new steady state frequency is reached.

7.2. Assessment for generation-load imbalance

This modified model is tested on the same network for a decrease in wind generation of 40 MW at $(t = 5\,s)$ and FCR bid of 50 MW and FRR activation signal of 40 MW at $(t = 200\,s)$. Figure 7.2 shows the location of the disturbance and the frequency support.

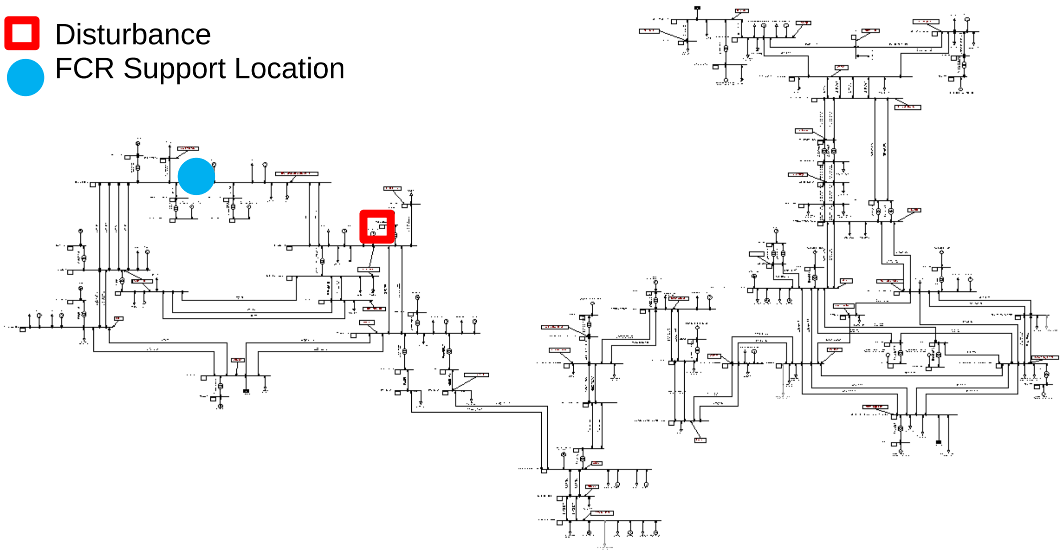

Figure 7.2. disturbance and PEM device locations for secondary frequency support

The frequency response shown in Figure 7.3. and power output in Figure 7.4 show that after the FRR bid is activated at 200 seconds, the frequency starts increasing and the FCR support decreases until the value is within the 10 mHz dead band. At that time, the FCR support is stopped before the frequency is restored to the nominal 50 Hz. The frequency starts to fall again until the FCR is activated when the limit of the dead band is reached at a frequency of 49.99 Hz and more power from the FCR is injected into the system to maintain the frequency within the dead band limits.

The dead band in FCR control works to prevent the activation of the bid for small oscillations or noise in the system frequency. However, in the case of frequency restoration, the FCR bid is deactivated and no action will be taken by the FCR control as long as the frequency remain between 49.99 Hz and 50.01 Hz. It is also noticeable that the inertia of the system resists the change in frequency in both directions and results in similar slope for both the increase and the decrease of frequency.

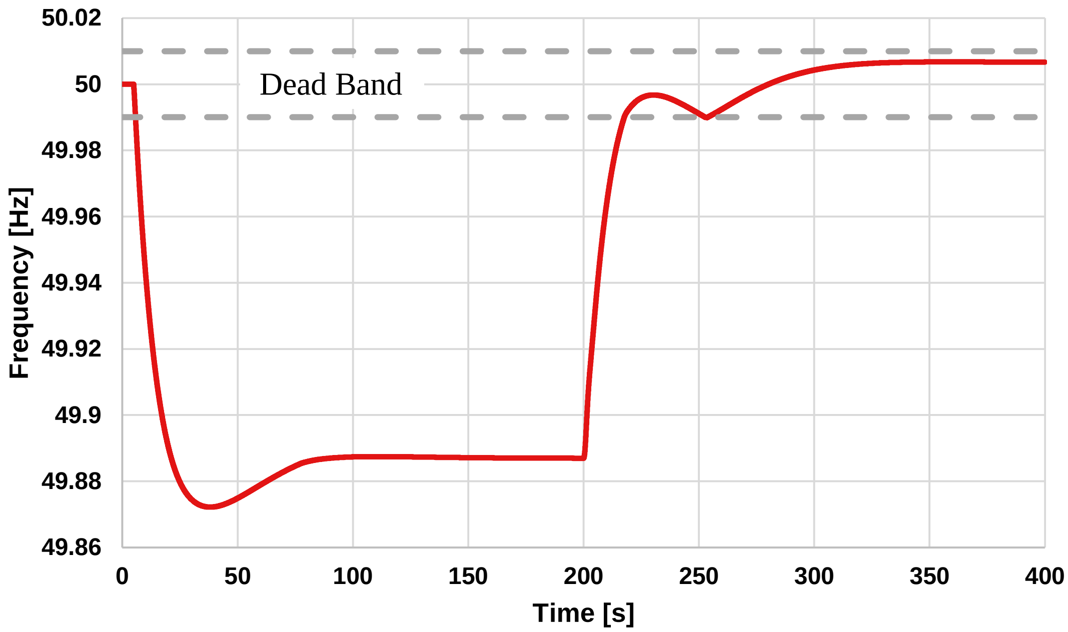

Figure 7.3. Frequency response for combined FCR and FRR support

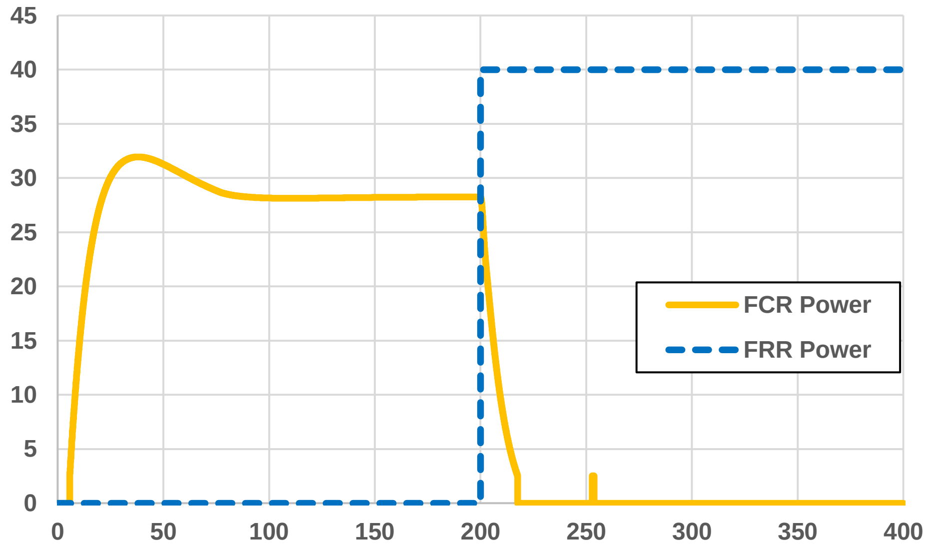

Figure 7.4. Power output by FCR and FRR control

This simulation showed that with small modification in the model, the PEM fuel cells and electrolyzer are capable of providing both primary and secondary frequency support and can participate effectively in the FCR and FRR markets. The PEM fuel cell and electrolyzer can continue to provide FCR and FRR support as long as it is needed given that the power set point remains within the allowable power range of 20-100% of their rated power and there is sufficient storage capacity to absorb the hydrogen produced by the electrolyzer or supply hydrogen fuel to the fuel cell.

8. Limitations of Hydrogen PEM Devices in Grid Applications

PEM devices show great promise in grid support applications but there is no widespread use of it. This is due to several reasons which are both technical and economics. These have to do mainly with the high cost of material and the high cost of hydrogen. More details will be given in the following sections.

8.1. High cost of PEM technology

Since the reactions that happen at the PEM fuel cell and electrolyzer happen in relatively low temperatures below 100°C, a platinum catalyst is needed in the anode and cathode to breakdown the molecules for hydrogen and oxygen gases [27]. The high cost of platinum catalyst increases the capital cost and initial investment in PEM fuel cells and electrolyzers which makes them financially unfeasible when compared to other technologies especially at the large scale. However, establishing a proper business model for salvaging the platinum at the end of life for PEM stacks can offset a significant part of the initial investment and reduce the life cycle cost of fuel cells and electrolyzers [67].

8.2. High cost of hydrogen

The high cost of hydrogen is a large obstacle when it comes to wide spread use of hydrogen fuel cells. The energy in one kilogram of hydrogen is almost equivalent to the energy in one gallon of gasoline however the cost of hydrogen is nearly double if it is created by natural gas reforming and it is more than five times the cost when hydrogen is generated through electrolysis [48]. It is possible that the increase in renewable energy sources will decrease the cost of generation of hydrogen through electrolysis especially in the case of negative prices which will benefit flexible loads such as the PEM electrolyzer. Also, the upcoming changes in the FCR market regulations will reduce the supplier bid commitment to 4 hours slots with daily auction will improve the suppliers' estimations of available capacity, increase their flexibility and improving their profits [24].

8.3. Small scale

The largest PEM fuel cell plant is 2 MW and it is located at a chlor-alkali plant where hydrogen is a by-product [68]. While the largest PEM electrolyzer project is planned to be 10 MW located within a refinery to generate hydrogen for refining use [69]. This shows that at this time, PEM technologies are used as auxiliary systems to increase the efficiency of other industrial processes. If these capacities are compared to the requirements of the ancillary services market, these plants cannot compete with other generators due to their low capacity.

In general PEM fuel cells and electrolyzers are still in early commercialization phase and there will be a long period before the technology is competitive with current methods of hydrogen generation or power generation. However, research in PEM technologies is increasing and the funding is increasing as well.

8.4. Opportunities for PEM technologies

The main advantage of PEM fuel cells and electrolyzers when providing frequency support to the power system is their capability of fast response and fast start-up time. This enables them to be very effective in arresting frequency change and containing the deviations (i.e. frequency nadir) especially in power systems with decreased inertia as expected in the future. In addition, the possibility of more strict requirements on bid activation and response times in the FCR market will motivate more participation of faster technologies such as PEM fuel cells and electrolyzers in the ancillary services market [24].

Mitigation of deterioration of RoCoF requires further investigation, specially about possible use of Modular Multilevel Converters (MMC) for fuel cells and electrolysers to interface with the grid, as well as adding new controls for inertia emulation or enhanced fast active power frequency injection to mitigate RoCoF.

9. Conclusions

The continuously growing share of renewable energy sources and their variable and intermittent generation profile poses several challenges to the power system. One of which, is maintaining generation-load balance and frequency stability. The system operators utilize the ancillary services market procure reserves for frequency containment and frequency restoration among other services.

Hydrogen as an energy carrier has the advantage of storage for long and short durations which can be beneficial to the power system. The power-to-gas and gas-to-power concepts represented by electrolyzers and hydrogen fuel cells enable the synergy between the generation of hydrogen and the consumption of electricity and vice versa. Exploiting this interplay has the potential to manage the variation in generation and caused by the renewable energy sources. Proton exchange membrane (PEM) fuel cells and electrolyzers have the potential to be the link that enable the coupling of these two sectors.

It is crucial to understand how PEM fuel cells combined with electrolyzers may participate in the ancillary services market and how they can impact the frequency stability of the power system. To accomplish that, it is important to perform simulations using reliable models that reflect the dynamic behavior of the PEM devices as well as provide the necessary controls to connect to the grid and participate in the ancillary services market. This thesis has thoroughly investigated the benefits of using power-to-gas and gas-to-power conversion to support the frequency stability of electrical power systems through addressing the following research questions:

1. How can hydrogen PEM fuel cells and electrolyzers be represented in frequency stability studies?

While the current literature offers different models for PEM fuel cells and electrolyzers in that reflect different study requirements there are no comprehensive generic models that can be used for power system frequency stability studies. This thesis develops a generic model for grid-connected PEM fuel cells and electrolyzers using DIgSILENT PowerFactory. The model provides frequency control using the product specifications for the FCR market and also reflects the dynamic behaviour of the PEM fuel cells and electrolyzers DC circuits based on literature models. The dynamic model for the PEM fuel cell shows close resemblance to the literature dynamic models in the linear range. The generic models also reflect the desirable features of fast response and separate active and reactive power control. The models can be expanded in the future to include voltage support capability.

2. How do hydrogen PEM fuel cells and electrolyzers perform when providing ancillary services for active power-frequency support?

The PEM fuel cells and electrolyzers comply with the technical requirements for frequency support in the ancillary services market. Namely, the Frequency Containment Reserve (FCR) and the automatic Frequency Restoration Reserve (aFRR). The developed test network is was used to evaluate the performance of the PEM devices for active power imbalance, line outage and disconnection between areas. The PEM fuel cells and electrolyzers showed that they can provide the necessary active power-frequency support to the power system in all these disturbances. More specifically, for the same generation-load imbalance and the same FCR bid capacity, the PEM fuel cells and electrolyzers provide more effective active power frequency support when compared to conventional synchronous generators. This is observed in a lower value of frequency nadir and reduction in post-disturbance frequency oscillations. The PEM fuel cell model was expanded to provide secondary frequency support and participate in the aFRR market. The studied scenario showed that the PEM fuel cell was able to contain the initial frequency deviation and restore the frequency to acceptable range around its nominal value thus showing effective participation in both the FCR and aFRR markets.

3. How can changes in the transmission network and the control parameters affect the performance of PEM hydrogen technologies.

Sensitivity analysis was performed to assess how changes in the network can affect the performance of PEM fuel cells and electrolyzers. The network parameters and layout will change under different scenarios while the network is subjected to the same disturbance and the frequency response will be measured and compared for the different scenarios. It was found that while maintaining other things constant, the size of the network, the location of the FCR support by PEM devices relative to the disturbance and the distribution of the FCR support do not affect the performance of the PEM devices to support the system frequency stability.

It was also found that reduction in the inertia of the grid results in increased RoCoF but does not affect the frequency nadir when the FCR support is provided by the PEM fuel cells and electrolyzers. When compared to the synchronous generators under decreasing inertia levels and for the same FCR bid value, the PEM devices significantly out perform the synchronous generator both in terms of frequency nadir and post-disturbance frequency oscillations. The RoCoF remains largely the same and does not improve with the PEM devices.

Sensitivity analysis was also performed to assess how changes in the control parameters of the PEM fuel cells and electrolyzers can affect their performance in frequency support. The control parameters will change under different scenarios while the network is subjected to the same disturbance and the frequency response will be measured and compared for the different scenarios. It was found that increasing the FCR bid size improves the frequency response in terms of smaller frequency nadir. Also, increasing the frequency droop (i.e. reducing the full bid frequency deviation) improves the frequency response as well in the form of smaller nadir. Changing the frequency dead-band however, does not have significant effect on the performance. The RoCoF remains unaffected by the change in control parameters of the PEM devices.

4. What are the technical and other challenges that limit the use of hydrogen based ancillary services for active power frequency support?

The main obstacles facing wide-spread use of PEM fuel cells and electrolyzers is cost both capital and operational. The use of platinum catalyst in the electrodes increases the cost of the initial investment and makes PEM devices unattractive when compared to other technologies especially at the large scale. Also, the high cost of hydrogen production through both gas reformers and electrolyzers makes the use of hydrogen fuel cells in grid-connected applications financially unattractive. In addition, the limited capacity of commercially available PEM fuel cells and electrolyzers limits its use to small specialized applications.

PEM devices have the advantage of fast response which makes them attractive for other applications in addition to power system frequency support such as in fuel cell electric vehicle which benefit from the fuel cell ability to rapidly change the power output. Also, changes in the ancillary services market that favour fast acting technologies may enable more participation of PEM fuel cells and electrolyzers in the ancillary services. PEM technology is still in the early commercialization phase but there is a steady growth in research investment which should enable the technology to become more competitive in the future.

9.1. Thesis Contributions

In this thesis generic PEM fuel cell and electrolyzer dynamic PowerFactor models have been developed for frequency stability studies. The model extends beyond the current-voltage models found in the literature by adding frequency control and power control to PEM devices enabling them to be connected to the power system and participate in the FCR market. This model can be used by other researchers to perform other types of stability studies or frequency studies in other simulation platforms.

As part of this thesis, a translation and reduction were done on part of the interconnected European network. This part represents the 380-400 kV network of North Netherlands, North-West Germany and South Denmark. This network represents both sides of COBRAcable and will be also be used for future studies related to it.

Also, this thesis demonstrated that it is feasible for PEM fuel cells and electrolyzers to support the frequency stability in the system and that they are in theory capable of participating effectively in the FCR market in its current setup. It was also shown that PEM fuel cells and electrolyzers are capable of frequency restoration and can participate effectively in the current FRR market.

Finally, the thesis performed sensitivity analysis on how modifications in the network and the control parameters may affect the ability of PEM electrolyzers and fuel cells to support the frequency stability in the power system. It was demonstrated that the frequency response is not affected by different operational scenarios in the power system. Further, PEM technologies can provide an improved frequency response compared to synchronous generators in terms of lower nadir in case of decreasing inertia. It was also shown that the frequency response can be improved by increasing the FCR bid value of the PEM fuel cells and electrolyzers or by increasing the frequency droop control.

9.2. Further Research

Future research can be categorized into two categories: modelling oriented and further studies.

9.2.1. **Additional models**

This thesis has developed an RMS model in PowerFactory to assess the fuel cell and electrolyzer effectiveness in frequency stability study. Further modelling can include developing an Electromagnetic Transients (EMT) model to study PEM fuel cells similar to the EMT model for the PEM electrolyzers developed by [54] in Real Time Digital Simulator (RTDS). The EMT model can be used to study the behavior under fault conditions, lightning and switching. This will help develop a comprehensive understanding of the behavior of PEM devices in the power system at different time scales.

Further, the same equations and methodology used to develop the dynamic model for PEM fuel cells and electrolyzers can be used to develop or translate the model into other simulation platforms to verify the findings of this research or to start new research that involves the dynamics of the PEM fuel cells and electrolyzers.

9.2.2. **Further studies**

As mentioned previously, the focus of this thesis is on the frequency support capability of grid connected PEM fuel cells and electrolyzers. However, the same developed model can be used to study the PEM fuel cells and electrolyzers in other stability studies such as voltage support and stability.

It is also possible to develop dynamic models for other types fuel cells and electrolyzers in order to understand how the different technologies can affect the response of the devices and how they differ in their ability to provide frequency support to the power system.

The most important study in this field is developing a demonstration project by using Real Time Digital Simulator (RTDS) for hardware-in-the-loop testing where PEM fuel cells and electrolyzers participate in the FCR market and support the system frequency stability. More insight can be found about the performance and limitations of these devices in a real-life connected system.

Bibliography

[1] S. Martinez Romero and W. Hughes, "Bringing Variable Renewable Energy Up To Scale Options for Grid Integration Using Natural Gas and Energy Storage," Energy Sector Management Assistance Program, The World Bank, Washington DC, USA, Tech. Rep. 006/15, 2014.

[2] United Nations Framework Convention on Climate Change. *"The Paris Agreement". 2018.* [Online]. Available: https://unfccc.int/process-and-meetings/the-paris-agreement/the-paris-agreement

[3] J. Töpler and J. Lehmann, *Hydrogen and fuel cell: technologies and market perspectives*. Springer, 2015.

[4] D. Fraile, J. Lanoix, P. Maio, A. Rangel, and A. Torres, "Overview of the market segmentation for hydrogen across potential customer groups, based on key application areas," CertifHy, Deliverable No. 1.2, Jun. 2015.

[5] Fuel Cell Technologies Office, "State of the States: Fuel Cells in America 2016 7th Edition," U.S. Department of Energy, DOE/EE-1493, Nov. 2016, .[online]. Available: https://www.energy.gov/eere/fuelcells/downloads/state-states-fuel-cells-america-2016.

[6] "Toyota opens up its patents to boost FCEV industry collaboration," *Fuel Cells Bulletin*, vol. 2015, no. 1, pp. 9-10, 2015/01/01/ 2015.

[7] A. Alaswad, A. Palumbo, M. Dassisti, and A. G. Olabi, "Fuel Cell Technologies, Applications, and State of the Art. A Reference Guide," in *Reference Module in Materials Science and Materials Engineering*: Elsevier, 2016.

[8] J. Barton and R. Gammon, "The production of hydrogen fuel from renewable sources and its role in grid operations," *Journal of Power Sources*, vol. 195, no. 24, pp. 8222-8235, Dec. 2010.

[9] P. Hoffmann, *Tomorrow's energy: hydrogen, fuel cells, and the prospects for a cleaner planet*. MIT press, 2012.

[10] D. Stolten, R. C. Samsun, and N. Garland, *Fuel cells: data, facts, and figures*. John Wiley & Sons, 2016.

[11] S. Cordiner *et al.*, "Fuel cell based Hybrid Renewable Energy Systems for off-grid telecom stations: Data analysis from on field demonstration tests," *Applied energy*, vol. 192, pp. 508-518, Apr. 2017.

[12] S. Bennoua, A. Le Duigou, M.-M. Quéméré, and S. Dautremont, "Role of hydrogen in resolving electricity grid issues," *international journal of hydrogen energy*, vol. 40, no. 23, pp. 7231-7245, Jun. 2015.

[13] *Power to Gas – Overview*.

[14] V. Garcia Suarez, J. Rueda Torres, A. Tuinema, A. Perilla Guerra, and M. van der Meijden, "Integration of Power-to-Gas Conversion into Dutch Electrical Ancillary Services Markets," presented at the ENERDAY 2018, Dresden, Germany, 2018.

[15] J. Morren, S. W. De Haan, and J. Ferreira, "Primary power/frequency control with wind turbines and fuel cells," in *Power Engineering Society General Meeting, 2006. IEEE*, 2006, p. 8 pp.

[16] US Department of Energy. *"Electric Market and Utility Operation Terminology". 2011.* [online]. Available: https://www.energy.gov/sites/prod/files/2014/01/f7/50169.pdf

[17] A. M. Pirbazari, "Ancillary services definitions, markets and practices in the world," in *2010 IEEE/PES Transmission and Distribution Conference and Exposition: Latin America (T&D-LA)*, 2010, pp. 32-36.

[18] P. Kundur *et al.*, "Definition and classification of power system stability IEEE/CIGRE joint task force on stability terms and definitions," *IEEE Transactions on Power Systems*, vol. 19, no. 3, pp. 1387-1401, 2004.

[19] J. Aho *et al.*, "Tutorial of Wind Turbine Control for Supporting Grid Frequency through Active Power Control," presented at the *American Control Conference (ACC)*, Montreal, QC, 2012.

[20] J. J. Grainger, W. D. Stevenson, and G. W. Chang, *Power system analysis*. McGraw-Hill New York, 1994.

[21] TenneT Holding B.V. *"Productspecificatie FCR". 2015.* [online]. Available: https://www.tennet.eu/fileadmin/user_upload/Bijlage_B_-_Productspecifications_FCR_ENG.pdf

[22] TenneT Holding B.V. *"Productinformation aFRR (Regulating power)". 2018.* [online]. Available: https://www.tennet.eu/fileadmin/user_upload/Company/Publications/Technical_Publications/Dutch/Product_information_aFRR_-regulating_power-_16-01-2018.pdf

[23] Frequency Containment Reserve (FCR) Cooperation. *"Proposal for the establishment of common and harmonised rules and processes for the exchange and procurement of Frequency Containment Reserve (FCR) in accordance with Art. 33 of COMMISSION REGULATION (EU) 2017/2195 establishing a guideline on electricity balancing". 2018.* [online]. Available: https://consultations.entsoe.eu/markets/draft-proposal-for-fcr-cooperation-market-design/supporting_documents/FCR%20Draft%20Proposal.pdf

[24] V. Garcia Suarez, "Exploitation of Power-to-Gas for Ancillary Services Provision (within the Context of Synergy Action TSO 2020)," M.S. Thesis, EEMCS Faculty, TU Delft, Delft, Netherlands, 2018.

[25] P. Breeze, "The Fundamentals of Fuel Cell Operation," in *Fuel Cells*: Academic Press, 2017, pp. 11-21.

[26] P. Breeze, "The Proton Exchange Membrane Fuel Cell," in *Fuel Cells*: Academic Press, 2017, pp. 33-43.

[27] I. EG&G Technical Services, *Fuel Cell Handbook (Seventh Edition)*. Morgantown, WV: U.S. Department of Energy Office of Fossil Energy National Energy Technology Laboratory, 2004.

[28] P. Breeze, "The Alkaline Fuel Cell," in *Fuel Cells*: Academic Press, 2017, pp. 23-32.

[29] P. Breeze, "The Phosphoric Acid Fuel Cell," in *Fuel Cells*: Academic Press, 2017, pp. 45-51.

[30] P. Breeze, "The Molten Carbonate Fuel Cell," in *Fuel Cells*: Academic Press, 2017, pp. 53-62.

[31] P. Breeze, "The Solid Oxide Fuel Cell," in *Fuel Cells*: Academic Press, 2017, pp. 63-73.

[32] J. C. Amphlett, R. F. Mann, B. A. Peppley, P. R. Roberge, and A. Rodrigues, "A model predicting transient responses of proton exchange membrane fuel cells," *Journal of Power Sources*, vol. 61, no. 1, pp. 183-188, Jul. 1996.

[33] C. Wang, M. H. Nehrir, and S. R. Shaw, "Dynamic models and model validation for PEM fuel cells using electrical circuits," *IEEE transactions on energy conversion*, vol. 20, no. 2, pp. 442-451, Jun. 2005.

[34] J. Andujar, F. Segura, and M. Vasallo, "A suitable model plant for control of the set fuel cell−DC/DC converter," *Renewable Energy*, vol. 33, no. 4, pp. 813-826, Apr. 2008.

[35] I. San Martín, A. Ursúa, and P. Sanchis, "Modelling of PEM fuel cell performance: Steady-state and dynamic experimental validation," *Energies*, vol. 7, no. 2, pp. 670-700, Feb. 2014.

[36] Y. Hou, Z. Yang, and G. Wan, "An improved dynamic voltage model of PEM fuel cell stack," *international journal of hydrogen energy*, vol. 35, no. 20, pp. 11154-11160, Oct. 2010.

[37] X. Kong, A. M. Khambadkone, and S. K. Thum, "A hybrid model with combined steady-state and dynamic characteristics of PEMFC fuel cell stack," in *Industry Applications Conference, 2005. Fourtieth IAS Annual Meeting. Conference Record of the 2005*, Oct. 2005, vol. 3, pp. 1618-1625.

[38] M. V. Moreira and G. E. Da Silva, "A practical model for evaluating the performance of proton exchange membrane fuel cells," *Renewable Energy,* vol. 34, no. 7, pp. 1734-1741, Jul. 2009.

[39] M. Soltani and S. M. T. Bathaee, "Development of an empirical dynamic model for a Nexa PEM fuel cell power module," *Energy Conversion and Management,* vol. 51, no. 12, pp. 2492-2500, Dec. 2010.

[40] C. Restrepo, T. Konjedic, A. Garces, J. Calvente, and R. Giral, "Identification of a proton-exchange membrane fuel cell's model parameters by means of an evolution strategy," *IEEE Transactions on Industrial Informatics,* vol. 11, no. 2, pp. 548-559, Apr. 2015.

[41] P. Gabrielli, B. Flamm, A. Eichler, M. Gazzani, J. Lygeros, and M. Mazzotti, "Modeling for optimal operation of PEM fuel cells and electrolyzers," in *Environment and Electrical Engineering (EEEIC), 2016 IEEE 16th International Conference on*, Jun. 2016, pp. 1-7.

[42] H.-i. Kim, C. Y. Cho, J. H. Nam, D. Shin, and T.-Y. Chung, "A simple dynamic model for polymer electrolyte membrane fuel cell (PEMFC) power modules: Parameter estimation and model prediction," *international journal of hydrogen energy,* vol. 35, no. 8, pp. 3656-3663, Apr. 2010.

[43] *Nexa^{TM} Power Module User's Manual*. Ballard Power Systems Inc., 2003.

[44] J. Laramie and A. Dicks, *Fuel cell systems explained*. New York, NY: John Wiley and Sons, 2003.

[45] R. O'hayre, S.-W. Cha, F. B. Prinz, and W. Colella, *Fuel cell fundamentals*. John Wiley & Sons, 2016.

[46] DIgSILENT GmbH, *DIgSILENT PowerFactory 2016 User Manual*. Gomaringen, Germany: DIgSILENT GmbH, Mar. 2016.

[47] T. Smolinka, E. T. Ojong, and J. Garche, "Hydrogen Production from Renewable Energies—Electrolyzer Technologies," in *Electrochemical Energy Storage for Renewable Sources and Grid Balancing,* Amsterdam: Elsevier, 2015, pp. 103-128.

[48] R. B. Gupta, *Hydrogen fuel: production, transport, and storage*. CRC press, 2008.

[49] F. Aouali, M. Becherif, H. Ramadan, M. Emziane, A. Khellaf, and K. Mohammedi, "Analytical modelling and experimental validation of proton exchange membrane electrolyser for hydrogen production," *International Journal of Hydrogen Energy,* vol. 42, no. 2, pp. 1366-1374, Jan. 2017.

[50] R. García-Valverde, N. Espinosa, and A. Urbina, "Simple PEM water electrolyser model and experimental validation," *international journal of hydrogen energy,* vol. 37, no. 2, pp. 1927-1938, Jan. 2012.

[51] A. Awasthi, K. Scott, and S. Basu, "Dynamic modeling and simulation of a proton exchange membrane electrolyzer for hydrogen production," *International journal of hydrogen energy,* vol. 36, no. 22, pp. 14779-14786, Nov. 2011.

[52] M. Lebbal and S. Lecœuche, "Identification and monitoring of a PEM electrolyser based on dynamical modelling," *International journal of hydrogen energy,* vol. 34, no. 14, pp. 5992-5999, Jul. 2009.

[53] Z. Abdin, C. Webb, and E. M. Gray, "Modelling and simulation of a proton exchange membrane (PEM) electrolyser cell," *International Journal of Hydrogen Energy,* vol. 40, no. 39, pp. 13243-13257, Oct. 2015.

[54] P. Ayivor, "Feasibility Of Demand Side Response From Electrolyzers To Support Power System Stability," M.S. Thesis, EEMCS Faculty, TU Delft, Delft, Netherlands, 2018.

[55] ENTSO-E. *"ENTSO-E Transmission System Map". 2018* [online]. Available: https://www.entsoe.eu/data/map/

[56] TenneT Holding B.V. *"Nederlands Transportnet". 2017.* [online]. Available: https://www.tennet.eu/fileadmin/user_upload/Company/Publications/Gridmaps/NL/netkaart_extern-2017.pdf

[57] TenneT Holding B.V. *"Gridmap Germany". 2018.* [online]. Available: https://www.tennet.eu/fileadmin/user_upload/Company/Publications/Gridmaps/ENG/Gridmap_Germany_ENG.pdf

[58] Flosm. *"Stromnetzkarte auf Basis von OSM-Daten". 2018.* [online]. Available: http://www.flosm.de/html/Stromnetz.html

[59] Geoportal.de. *"Karten". 2018* [online]. Available: http://www.geoportal.de/DE/Geoportal/Karten/karten.html;jsessionid=2E448B7BA6B6842FC2D675A9B89C4C51?lang=de&wmcid=113

[60] Energy Charts. *"Map of Power Plants". 2018.* [online]. Available: https://www.energy-charts.de/osm.htm?country=DE

[61] Energinet. *"TRANSMISSION SYSTEM DATA". 2018.* [online]. Available: https://en.energinet.dk/Electricity/Energy-data/System-data

[62] TenneT Holding B.V. *"Offshore projects Germany". 2018.* [online]. Available: https://www.tennet.eu/index.php?id=2130&L=0

[63] P. Fairley, "Germany jump-starts the supergrid," *IEEE Spectrum*, vol. 50, no. 5, pp. 36-41, May 2013.

[64] P. Kundur, N. J. Balu, and M. G. Lauby, *Power system stability and control*. McGraw-hill New York, 1994.

[65] K. Nikiforow, J. Pennanen, J. Ihonen, S. Uski, and P. Koski, "Power ramp rate capabilities of a 5 kW proton exchange membrane fuel cell system with discrete ejector control," *Journal of Power Sources*, vol. 381, pp. 30-37, Mar. 2018.

[66] J. Eichman, K. Harrison, and M. Peters, "Novel electrolyzer applications: providing more than just hydrogen," National Renewable Energy Laboratory (NREL) Golden, CO.NREL/TP-5400-61758, Sep. 2014.

[67] P. C. Ghosh, "High platinum cost: obstacle or blessing for commercialization of low-temperature fuel cell technologies," *Clean Technologies and Environmental Policy*, vol. 19, no. 2, pp. 595-601, Mar. 2017.

[68] S. Barrett. *"Dutch partners deliver first 2 MW PEM fuel cell plant in China". Mar. 2017.* [online]. Available: http://www.renewableenergyfocus.com/view/45502/dutch-partners-deliver-first-2-mw-pem-fuel-cell-plant-in-china/

[69] Financial Times. *"Largest Hydrogen Electrolysis in Shell Refinery". Jan. 2018.* [online]. Available: https://markets.ft.com/data/announce/detail?dockey=1323-13501460-5UJRPTCHJ6GH6TO7PQL0PMFP0F

Appendix I – Control Parameters

1. Synchronous Generator

1.1. Typical value of Synchronous Generator Settings (6^{th} order subtransient model)

Parameter	Units	Value
H	s	3
Rotor Type		Round Rotor
Xl	p.u.	0.15
xd	p.u.	2
xq	p.u.	1.8
xd’	p.u.	0.35
xq’	p.u.	0.5
xd”	p.u.	0.25
xq”	p.u.	0.25
x2	p.u.	0.2
x0	p.u.	0.1
Td0’	s	5.1428
Tq0’	s	2.16
Td0”	s	0.042
Tq0”	s	0.0833

1.2. Governor

Parameter	Discerption	Units	Value
dfmax	Full bid frequency deviation	Hz	0.200
Bid	FCR Bid Value	MW	varies
A	Scale Factor		1
R	Permanent Droop	p.u.	0.3579
T2	Numerator Time constant	s	6
T3	Reheater time constant	s	14
Dt	Turbine damping coefficient	s	0
T1	Steam bowl time constant	s	0.5
Trate	Base for power values = Turbine rated power		0
FCR	Participation in FCR market 1: yes / 0: no		0
V_min	Minimum valve position	p.u.	0
V_max	Maximum valve position	p.u.	1

1.3. Exciter

Parameter	Discerption	Units	Value
TaTb	Filter derivative time constant	s	0.3
Tb	Filter delay time	s	10
PSSon	PSS signal 1: on/0: off		1
K	Controller gain		40
Te	Exciter time constant	s	0.5
Emin	Controller minimum output	p.u.	0
Emax	Controller maximum output	p.u.	4

1.4. Power System Stabilizer

Parameter	Discerption	Units	Value
T1	1st lead-lag numerator time constant	s	0.08
T2	1st lead-lag denominator time constant	s	0.015
T3	2nd lead-lag numerator time constant	s	0.08
T4	2nd lead-lag denominator time constant	s	0.015
Tw	Washout time constant	s	10.
Kpss	PSS gain		0.5
Vpssmin	Minimum value of Vpss	p.u.	-0.05
Vpssmax	Maximum Value of Vpss	p.u.	0.05

2. PEM Fuel Cell

2.1. Static Generator Settings

Parameter	Value
Technology	3PH
Plant Category	Fuel Cell
Parallel Units	1
Local Controller	Const. Q

2.2. Frequency Control

Parameter	Discerption	Units	Value
db	Dead band	Hz	0.01
Kf	Frequency gain (droop)	Hz^{-1}	5
Bid	FCR bid value	MW	5 or 50
Base	Fuel cell rated power	MW	20 or 150
P_min	Minimum allowable power output	p.u.	0.2
P_max	Maximum allowable power output	p.u.	1

2.3. Power Control

Parameter	Discerption	Units	Value
Kpp	P proportional gain		0.05
Kip	P integral gain		5
Kpq	Q proportional gain		0.05
Kiq	Q integral gain		5
dbp	P dead band	p.u.	0.01
dbq	Q dead band	p.u.	0.01

2.4. Current Control

Parameter	Discerption	Units	Value
Kpd	id proportional gain		15
Kid	id integral gain		2
Kpq	iq proportional gain		15
Kiq	iq integral gain		2
Td	id delay time constant	s	0.01
Tbd	id lead-lag numerator time constant	s	0.1
Tad	id lead-lag denominator time constant	s	10
dbp	id dead band	p.u.	0.01
Tq	iq delay time constant	s	0.01
Tbq	iq lead-lag numerator time constant	s	0.1
Taq	iq lead-lag denominator time constant	s	10
id_min	id minimum allowable value	p.u.	0.2
id_max	id maximum allowable value	p.u.	1
iq_min	iq minimum allowable value	p.u.	-1
iq_max	iq maximum allowable value	p.u.	1

3. PEM Electrolyzer

3.1. General Load Settings

Parameter	Value
Input Mode	P, Q
Balanced/Unbalanced	Balanced
Scaling Factor	1

3.2. Frequency Control

Parameter	Discerption	Units	Value
db	Dead band	Hz	0.01
Kf	Frequency gain (droop)	Hz^{-1}	-5
T	Dynamic delay constant	s	0.1
Bid	FCR bid value	MW	5 or 50
Base	Electrolyzer rated power	MW	20 or 150
P_min	Minimum allowable power output	p.u.	0.2
P_max	Maximum allowable power output	p.u.	1

3.3. Power Control

Parameter	Discerption	Units	Value
Kpp	P proportional gain		8
Kip	P integral gain		10
Kpq	lead-lag numerator time constant	s	0.2
Kiq	lead-lag denominator time constant	s	2
Base	Electrolyzer rated power	MW	20 or 150
P_min	Minimum allowable power input	p.u.	0.2
P_max	Maximum allowable power input	p.u.	1

4. External Grid Settings

Parameter	Units	Value
Bus Type		SL
Acceleration time constant (H)	s	5
Secondary Frequency Bias	MW/Hz	0